Micro Propulsion Systems

Development of a LaB_6 Cathode for Micro Electric Thrusters.

T.G.E. van 't Klooster 4163397

Literature Study Report

Airbus Defence and Space GmbH

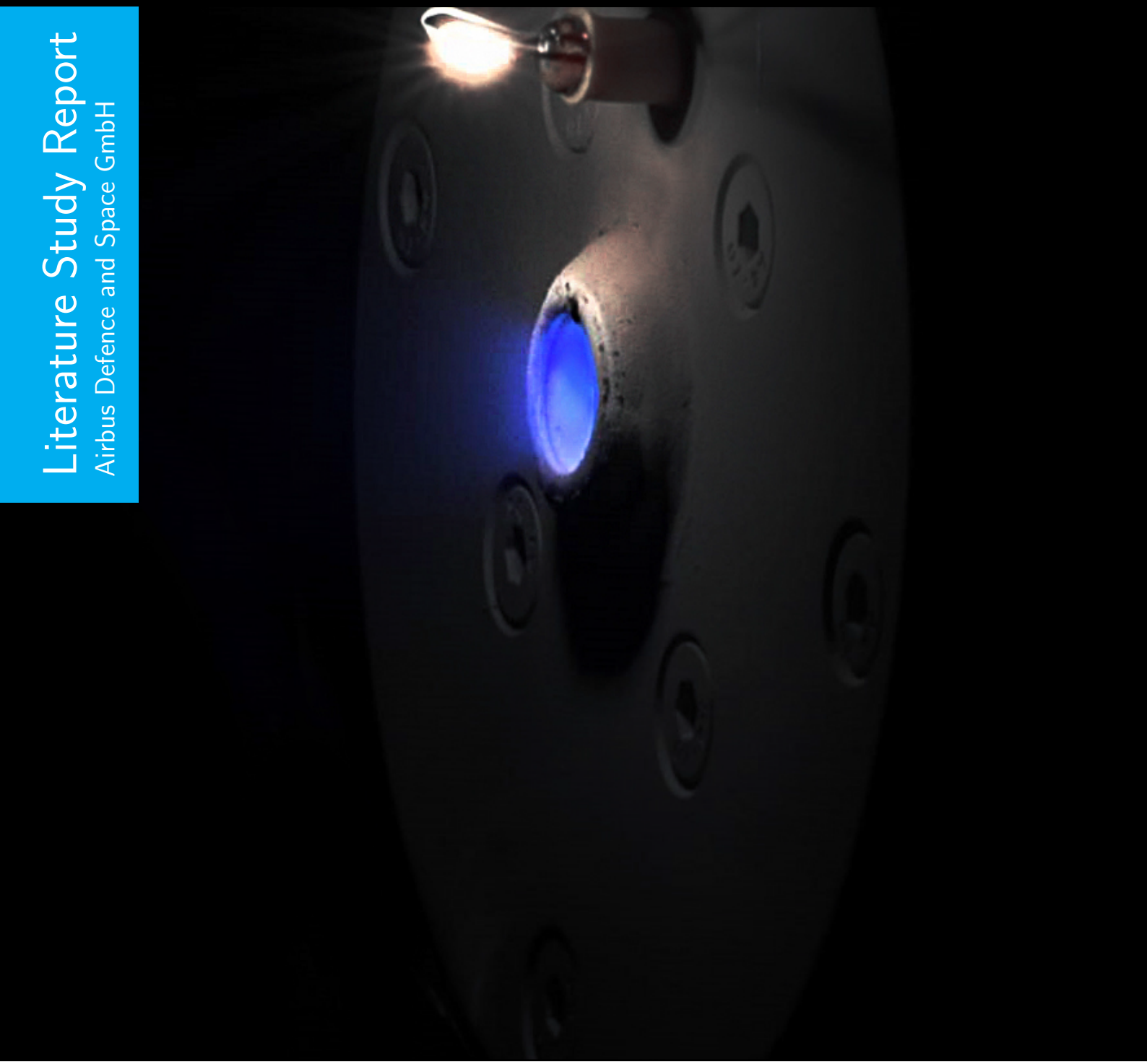

TU Delft Delft University of Technology

Aerospace Engineering

December 14, 2017

MICRO PROPULSION

DEVELOPMENT OF A LaB_6 CATHODE

by

T.G.E. van 't Klooster

as part of the

AE4020 Literature Study

in MSc. Aerospace Engineering

at Delft University of Technology

Author:	Thomas van 't Klooster	tgevantklooster@gmail.com
Supervisors:	Dr. Franz Georg Hey	franz.hey@airbus.com
	Max Vaupel	max.vaupel@airbus.com
Professor:	Dr. Angelo Cervone	a.cervone@tudelft.nl

TU Delft Delft University of Technology

AIRBUS

VERSION CONTROL

Version	Date	Changes
1.0	09-10-2017	Creation of draft version
1.1	02-11-2017	Updated: Structure of report Added: Literature Study, Market Survey
1.2	09-11-2017	Updated: Layout style of report Added: Fundamentals, Experimental Setup
1.3	17-11-2017	Updated: Literature Study, Market Survey Added: Additional Micro Propulsion Systems
1.4	20-11-2017	Updated: Propellant compatibility
1.5	24-11-2017	Updated: Market Survey
1.6	27-11-2017	Updated: Small updates and adaptions
1.7	14-12-2017	Updated: Comments and revision incorporated

PREFACE

This is the literature study report written by Thomas van 't Klooster for the AE5810 Thesis programme of the Master of Science of Aerospace Engineering at Delft University of Technology. The literature study consists out of a two month period that is performed full-time, prior to the main thesis work which lasts six months. Afterwards, the Master Thesis Graduation will commence.

I would like to express my gratitude to my supervisors Franz Georg Hey and Max Vaupel, Professor Angelo Cervone and my propulsion engineering colleague Jonathan Bach for their assistance and tutoring. Next to that, I would like to thank the whole team at Airbus for having a very interesting and educative Literature Study period. Finally, I would like to thank the Delft University of Technology, particularly the faculty of Aerospace Engineering, for putting available their facilities and resources.

Thomas van 't Klooster, Airbus, Advanced Projects, Immenstaad am Bodensee, Germany

January 15, 2018

SUMMARY

There is a trend in the miniaturisation of satellites. They not only become smaller, but lighter and more powerful as well. A large growth in the nano-satellite sector is present in the form of CubeSats. These milk carton size satellites use commercial of the shelf components in order to keep the costs low and to allow for technology demonstrations for future larger space missions. In order to increase their current mission lifetime from 1 - 2 years, electric micro propulsion systems are being developed. These systems are able to provide sufficient velocity increments in order to provide the CubeSat with the required orbit elevation.

Electric micro propulsion systems make use of the Coulomb force to accelerate charged particles. The method is to inject an propellant gas such as xenon into a cylindrical discharge chamber. The propellant is ionised by means of electron bombardment. The electrons that are required in order to do so are pulled from the cathode into the thruster system. Inside the discharge chamber they experience an electromagnetic field, where the resulting Lorentz force makes them gyrate in the projection plane that is perpendicular to the magnetic field lines. As the propellant is inserted in the discharge chamber, a neutral gas pressure builds up. Next, the electrons that are emitted from the cathode are colliding with the neutral gas particles, which causes them to be ionised. These charged particles get accelerated out of the discharge chamber by the electrostatic field in order to create the required thrust. The goal is to develop an affordable, low complexity and efficient cathode for a high performance micro propulsion system that can be used on small satellites. In the future, the whole system can be miniaturised in order to realise an electric thruster system that can be implemented on CubeSats in order to expand their mission lifetime.

The micro High Efficiency Multistage Plasma Thruster has a mass flow of 0.1 sccm. In order to generate a thrust of 86 μN, it uses a anode voltage and anode current of 1300 V and 5.8 mA respectively. The power to thrust ratio is equal to 87.7 W/mN and the specific impulse that is achieved equals 897 s, dependent on the applied settings. The divergence efficiency ranges from 57 - 67 % and the total system efficiency is currently equal to 5.5 %. This total efficiency needs to be improved in the subsequent iterations of the design.

NOMENCLATURE

Abbreviation	Description
AIAA	American Institute of Aeronautics and Astronautics
AOCS	Attitude Orbit and Control System
ARCS	Austrian Research Centres Seibersdorf
CD&H	Command and Data Handling
CO2	Carbon dioxide
CFRP	Carbon Fibre Reinforced Polymer
COTS	Commercial-Off-The-Shelf
CNES	Centre national d'études spatiales
CTE	Coefficient of Thermal Expansion
DLR	Deutsches Zentrum für Luft- und Raumfahrt
EGSE	Electrical Ground Support Equipment
EOL	End of Life
ESA	European Space Agency
ESD	Electro Static Discharge
GL	Thermal Conductance
GN2	Gaseous Nitrogen
HET	Hall Effect Thruster
IR	Infrared
LED	Light Emitting Diode
LN2	Liquid Nitrogen
LEO	Low Earth Orbit
LOX	Liquid Oxygen
LT	Local Time
MAI	Manufacturing, Assembly & Integration
MGSE	Mechanical Ground Support Equipment
MiXI	Miniature Xenon Ion Thruster
MIT	Massachusetts Institute of Technology
MLI	Multi Layer Insulation
MRIT	Miniature Radio Frequency Thruster
NASA	National Aeronautics and Space Administration
PAN	Polyacrylonitrile
PCB	Printed Circuit Board
PEEK	Polyether ether ketone
POM	Polyoxymethylene
PPE	Polyphenylene ether
PPT	Pulsed Plasma Thruster
PPU	Power Processing Unit
PTFE	Polytetrafluorethylene
PVC	Polyvinylchloride
RF	Radio Frequency
RIT	Radio frequency Ion Thruster
RPA	Retarding Potential Analyser
SSD	Sample Standard Deviation
USA	United States of America
TED	Thales Electron Device
TPF	Terrestrial Planet Finder
TRL	Technology Readiness Level

LIST OF SYMBOLS

Symbol	Description	Unit
A	Area	[m^2]
A	Richardson constant	[-]
B	Magnetic Field Strength	[T]
C_{ij}	Thermal Conductance	[W/K]
eV	Electronvolt	[J]
E	Young's modulus	[GPa]
F	Force	[N]
f	Frequency	[Hz]
g_0	Sea-level gravity	[m/s^2]
h	Height	[m]
I	Moment of Inertia/Second Moment of Inertia	[m^4]
I_{xx}	Mass moment of Inertia around x-axis	[kg m^2]
I_{yy}	Mass moment of Inertia around y-axis	[kg m^2]
J	Emitted current	[A/m^2]
j	Safety factor	[-]
k	Boltzmann constant	[J/K]
k	Thermal conductivity	[W/(m·K)]
L	Length	[m]
M_w	Molecular weight	[u]
m	Mass	[kg]
n	Number of mols	[-]
P	Pressure	[Pa]
P	Power	[W]
P_a	Ambient pressure	[Pa]
$PTTR$	Power to Thrust Ratio	[W/mN]
q	Particle charge	[C]
R	Resistance	[Ω]
R	Gas constant	[J/(K·mol)]
R_L	Lamor Radius	[m]
R_m	Mirror ratio	[-]
r	Radius	[m]
$sccm$	Standard Cubic Centimetre per Minute	[cm^3/min]
T	Temperature	[K]
T	Torque	[Nm]
t	Thickness	[m]
t	Time	[s]
U	Voltage	[V]
V	Volume	[m^3]
v	Velocity	[m/s]
w	Width	[m]
δ	Displacement	[mm]
θ	Deflection angle	[deg]
Θ_m	Pitch angle	[deg]
μ	Mean	[-]
μ_E	Gravitational parameter Earth	[m^3/s^2]
ρ	Density	[kg/m^3]
σ	Sample Standard Deviation	[-]

CONTENTS

LIST OF TABLES

LIST OF FIGURES

1

INTRODUCTION

The small satellite market is growing and it is growing fast [18]. One of the largest contributors to this growth is due to the fact that more and more CubeSats are being launched. These satellites are becoming more powerful and capable of replacing larger satellites. Moreover, there is more space available for these CubeSats to be launched by piggybacking on various larger satellite launchers, that do not have bigger satellites to place in their launch bays. In this manner, many CubeSats can be put into orbit a relatively short time. A recent example of this is the successful launch[1] of the Indian Polar Satellite Launch Vehicle (PSLV) in February 2017, which carried 101 CubeSats.

The CubeSats are not only getting more powerful instruments, sensors and electronics, but they are also being equipped with electric / micro propulsion systems in order to allow for orbit keeping. These systems require and dissipate a lot of power, which needs to be evacuated to space in the form of heat. This is possible, for both small satellites as well as CubeSats, using foldable and flexible radiator panels that are connected using flexible thermal straps. Electric propulsion systems are not only used for orbit keeping, but also for future interplanetary missions and orbit raising manoeuvres. The main goal of the micro propulsion system (μN thrust range) that is currently being developed at Airbus is to realise a low complexity, affordable and efficient successfully operating cathode. In this manner, the system can be miniaturised in the future and in that way implemented in CubeSats. The current Technology Readiness Level (TRL) of the to be developed micro propulsion system that uses a thermionic cathode is level 4. This means that it has been tested on a component level in a laboratory environment (i.e. vacuum chamber). It is common practice for space (sub)systems and components to be organised around the National Aeronautics and Space Administration (NASA)-originated Technology Readiness Ladder in order to quantify the readiness of all new developments for flight in space. It consists out of nine levels that can be seen in Figure 1.1.

The purpose of this report is to analyse the research that has been performed on electric micro propulsion systems. This involves a focus on the cathode system in particular, with the used materials and their characteristics. In addition to that, compatibility with the alternative propellant iodine is investigated. The approach that is followed includes performing research on experimental models, tests, analyses, their discussions and conclusions. The goal of this literature study report is to establish a clear overview that concerns these aspects on the electric micro propulsion system, with the cathode as main objective of interest.

First, the research questions, aim and objectives are discussed in Chapter 2. Next to that, Chapter 3 elaborates on the fundamentals of electric propulsion with the focus on micro propulsion systems. Subsequently, Chapter 4 gives the background information on the topic and evaluates the research questions. Afterwards, a market survey is performed in Chapter 5. Furthermore, the experimental setup will be treated in Chapter 6. Finally, conclusions and interesting recommendations are given in Chapter 7.

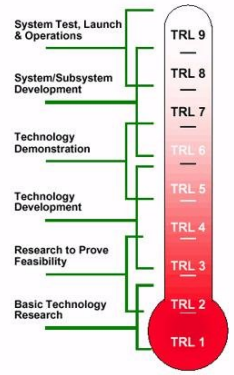

Figure 1.1: Technology Readiness Levels [13]

[1] https://www.isispace.nl/dutch-nanosatellite-company-gets-101-cubesats-launched-recordbreaking-pslv-launch/ | Visited on 09 November 2017

2

RESEARCH QUESTIONS, AIMS AND OBJECTIVES

In order to elaborate on the research questions, aim and objectives, this chapter is divided in four parts. First, Section 2.1 will elaborate on the research questions. Afterwards, Section 2.2 will deal with the research aim. Subsequently, the research objectives are discussed in Section 2.3. Finally, Section 2.4 gives an illustration of the research framework.

2.1. RESEARCH QUESTIONS

The research questions concern the main topics of the research to be solved and focus on the sources the researcher needs in order to establish the research perspective. The research questions consist out of central questions (that are combined with the research framework in Section 2.4) and different level sub-questions that follow from these central research questions. First, the research questions for the literature study period will be treated in Section 2.1.1. Afterwards, the intended research questions for the main thesis project are described in Section 2.1.2.

2.1.1. LITERATURE STUDY

In the literature study period, the main goal is to evaluate what research has been performed in the field of micro propulsion (μN thrust range, up to 10 mN) so far, at what level the technology is available on the market and what the position of Airbus is with respect to this market. Therefore, in discussion with supervisors Franz Georg Hey and Max Vaupel the following research questions for the literature study period are defined. The research questions under 1. are evaluated in Chapter 4, whereas the ones under 2., 3. and 4. are treated in Chapter 5.

1. What research has been performed in the field of micro propulsion engineering for low thrust (up to 10 mN) satellite missions?
   (a) What kind of cathodes have been used for electric propulsion in space up to know?
   (b) Which materials have been used for these neutralisers and what are their properties?
   (c) Are there any new materials in the focus of the current research?
   (d) How are the different neutraliser materials being handled with respect to poisoning?
   (e) Are the neutraliser materials compatible with different type of propellants?
   (f) Is the neutraliser compatible with iodine as a propellant?
2. What technology in the field of micro propulsion engineering for space systems is available on the market?
3. What is the position of Airbus on the market with respect to micro propulsion applications for space systems?
4. What type of cathode should be used to realise the electric thruster system as a whole?

2.1.2. THESIS PROJECT

The goal of the research questions is to provide an adequate steering function, so that more sub-questions can follow from them. Then, lower level questions can be solved and provide answers to the higher level research questions. In addition to that, they need to be useful, realistic, feasible, clear and informative. The thesis research questions are defined below [46].

1. What criteria are relevant for assessing the performance of various types of cathodes for micro propulsion systems?
2. What is the value and quality of the different types of cathodes in view of the assessment criteria?

3. What do we learn from comparing results from the analyses and results of the different types of cathodes in order to establish recommendations on how to develop an efficient cathode for micro propulsion systems?

The first central research question provides, together with the research framework in Section 2.4, an adequate steering function. It makes clear what theories need to be studied in order to establish the assessment criteria. These criteria will in turn give a research perspective. The second central research question cannot be answered before the first one is. The answer of the second research question will provide sufficient information in order to be able to answer the third research question. From the third question it is clear that it cannot be answered before having answered the second question. The answer of the third central research question is able to ascertain whether the objective of the thesis project has been achieved and if so, to what extent.

2.2. RESEARCH AIM

This section discusses the general research aim of the research. The goal of the thesis project is contribute to scientific research by evaluating the adequacy of multiple thermionic cathode solutions for micro propulsion systems for space systems. Eventually, the objective of the thesis research is to design, manufacture and test a light weight and high performance (both propulsive as well as mechanical) thermionic cathode for a micro electric thruster.

2.3. RESEARCH OBJECTIVES

This section will discuss the research objectives. For the literature study period of the first two months starting from 04 October 2017, the goal is to define the research area. This will be done by reviewing the work that has already been carried out by other academics in the area of micro propulsion. Simultaneously, the industry best practice in this field of propulsion engineering will be benchmarked. In this manner, the areas that are relevant for the research can be identified. Furthermore, the current understanding alongside with any opposing views will be addressed. These items will be shortly discussed below.

- **Review the academic research performed on micro propulsion -** One of the first actions to be performed in the literature study involves reviewing the academic research that has been performed on the topic. In this manner, it can be made sure what fields of the topic remain interested to perform research on and what field are not (i.e. have been studied and concluded for a large part already).
- **Benchmark the current industry developments -** In addition to the academic research, industry developments need to be investigated as well. This involves both the European as well as the non-European companies that are developing electric propulsion systems. These are addressed in Chapter 4.
- **Address current understanding alongside opposing views -** This part will be up for discussion at the start of the literature study at 04 October 2017 at Airbus in Germany. The goal is to discuss the topic with supervisors Franz Georg Hey, PhD student Max Vaupel and other colleagues in order to gather different opinions and views on the field of micro propulsion engineering.

In the next part, the MSc thesis project context will be shortly described. Afterwards, the research objective that contains the research goals which follow from the project context is discussed.

Project Context
The development of technologies in electric and micro propulsion systems will not only allow for orbit keeping and interplanetary missions, but also for cost efficient orbit raising manoeuvres. The second generation of ESA's Galileo satellite system is planning to use this technology in order to performed required orbit insertion. In this manner the costs of a launch to a GTO[1] can be strongly diminished by performing orbit raising from LEO[2] to GTO or other high elliptic orbits using electric propulsion [47].

Research Objective
The research objective of the MSc Thesis Literature Study is to further develop a cathode for micro propulsion systems, by comparing the propulsion, thermal and mechanical performance of different thermionic cathodes made from different materials. The research will consist out of a practical oriented approach. The current aim is that the thermionic cathode shall be made from LaB_6 (i.e. lanthanum hexaboride) and this needs to be tested for. This material has a low work function and has one of the highest electron emissivities, which will be discussed later in more detail. Based on the exploration of the project context, the practice oriented research will be of the engineering design type. The following five steps describe the practice oriented research [46].

[1] Geostationary Transfer Orbit
[2] Low Earth Orbit

1. **Problem Analysis -** In the first phase, the *problem analysis*, the problem is brought to the attention of the stakeholders. The goal of this is to bring the problem into the open such that it becomes transparent and can be discussed by all stakeholders. This involves the discussion of the to be developed technology and for what reasons this development is necessary. It is made clear what the problem involves, why it is a problem and whose task it is to solve it and to which extent.
2. **Diagnosis -** Next, as the problem has been identified and acknowledged by all stakeholders, the *diagnostic phase* follows. In this phase, the background and the causes of the identified problem will be examined. In addition to that, the goal is to find a solution that contains certain courses of action that need to be taken in order to solve the posed problem.
3. **Design -** Subsequently, as the problem analysis an the diagnosis are made, an intervention plan needs to developed in order to find a solution for the posed problem. Considering the micro propulsion topic, this involves the design of a cathode that will be able to let the micro propulsion system realise the required thrust of up to 200 μN [48].
4. **Intervention/change -** In this phase a course of intervention or change will be set in motion in order to solve the problem. This involves carrying out the set plan or design for the problem statement. As with many engineering problems, new problems will arise during the design and analysis. These need to be reported and documented consistently.
5. **Evaluation -** The last phase of the practice oriented research consists out of the evaluation part. In this phase, it will be verified whether the implemented changes to the problem actually solve the posed problem. As mentioned in the previous steps, often new problems occur during the analysis which cause the posed problem to be only partially solved in many cases. If this holds, then the five steps described in this section need to be repeated from step one. Therefore, this whole process is described as an intervention cycle [46].

2.4. RESEARCH FRAMEWORK

In this part a schematic presentation of the research framework is given. It can be seen in Figure 2.1. The research framework gives an overview of the subsequent steps that need to be taken during the research. As an initial step, four implementations of the conceptual model that will be analysed (A, B, C and D) are established.

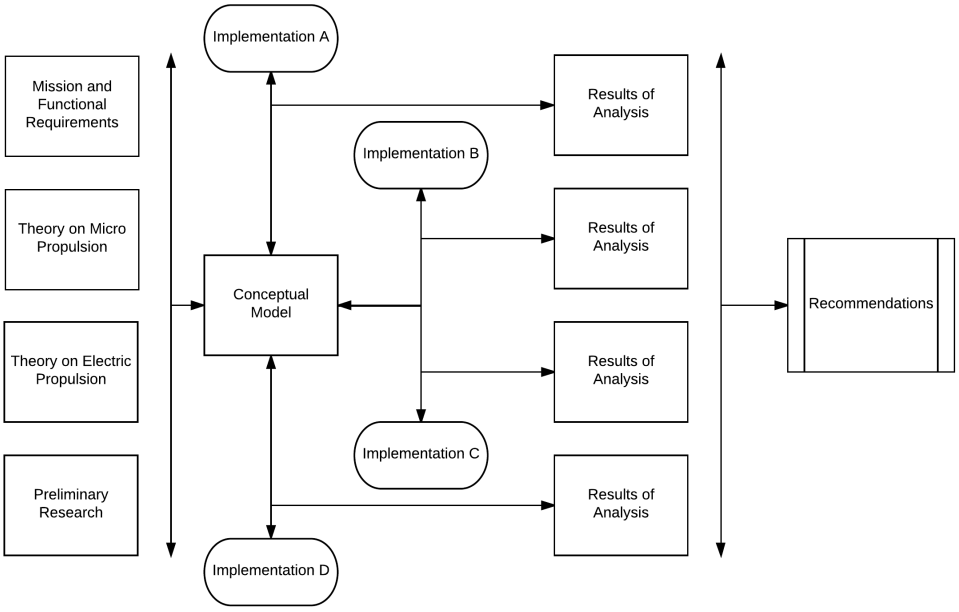

Figure 2.1: Thesis Project Research Framework

3

FUNDAMENTALS

This chapter will elaborate on the fundamentals that apply to micro propulsion systems. First, the general principle in order to create thrust by means of electric propulsion is discussed in Section 3.1. Next to that, the principle of thermionic emission for thermionic cathodes is treated in Section 3.2. In addition to that, an important aspect of electron emission, namely the Child-Langmuir law is dealt with in Section 3.3. Furthermore, the principle of the high efficiency multistage plasma thruster is discussed in Section 3.4.

3.1. MICRO ELECTRIC PROPULSION

In electric propulsion the mass that is accelerated and ejected from the spacecraft consists out of charged particles. Whereas in chemical propulsion the achievable exhaust velocities that can be reached are about 3 to 4 km/s, in electrical propulsion they can be as high as 100 km/s [49]. This is due to the fact that the energy source is decoupled from the propellant. In electric propulsion, the acceleration of the propellant particles is realised by an external power source. In general, electricity is used in order to increase the propellant exhaust velocity. Many different figures can be used in order to characterise electric thrusters. However, the main ones of interest for mission analysts and space engineers are thrust, specific impulse and total efficiency that can all relate the performance of the thruster to the delivered mass and change of the spacecraft's velocity during the thrust periods.

In electric thrusters where an applied electric field is used in order to accelerate the ionised propellant particles, the thrust that is produced is proportional to the velocity of an ionised particle. This velocity is described by Equation (3.1). In this equation, q_i is the particle charge, m_i is the ion mass and U_B is the beam potential. Next to that, the mass flow can be described by Equation (3.2), where I_B is the ion beam current. Combining these two equations with Newton's 2nd law in Equation (3.3), the Equation for the thrust can be derived and is given in Equation (3.4) [20, 49].

$$v_i = \sqrt{\frac{2q_i \cdot U_B}{m_i}} \tag{3.1}$$

$$\dot{m} = I_B \cdot \frac{m_i}{q_i} \tag{3.2}$$

$$F = \dot{m} \cdot v \tag{3.3}$$

$$F_T = I_B \sqrt{\frac{2m_i \cdot U_B}{q_i}} \tag{3.4}$$

Furthermore, in order to compare different thruster technologies and models, the standardised figure of specific impulse I_{sp} has been introduced. It describes the propellant efficiency of a thruster and is defined as the thrust divided by the mass flow of the propellant times the gravitational constant. This is evaluated in Equation (3.7). In this equation, γ equals the beam divergence correction factor for the thrust directional velocity and η_m is equal to the mass efficiency correction factor. The first term, γ, takes into account that not all ions that leave the thruster have a velocity that is completely parallel to the thrust direction. It can be determined by using the cosine of the average divergence half beam angle θ in Equation (3.5). The other term, η_m, is used since not all propellant particles in electric thrusters are ionised and therefore it is required to determine the propellant mass utilisation efficiency. This is determined by Equation (3.6) [20].

$$\gamma = \cos(\theta) \tag{3.5}$$

$$\eta_m = \frac{I_B}{\dot{m}} \cdot \frac{m_i}{q_i} \cdot \tag{3.6}$$

$$I_{sp} = \frac{F_T}{\dot{m} \cdot g_0} = \frac{\gamma \cdot \eta_m}{g_0} \sqrt{\frac{2q_i \cdot U_B}{m_i}} \tag{3.7}$$

It can be seen that if the thrust is kept constant and the mass flow is decreased, then the specific impulse increases. One way of realising this is by increasing the exhaust velocity of the propellant particles. The exhaust velocity depends on the energy source of the propulsion system. Electric thrusters are able to realise various exhaust speeds

and have operating specific impulses in the range of 1000 to 8000 s. Chemical propulsion systems on the other hand, have lower specific impulses up to 500 s [49, 50].

In the next part, electrical parameters are introduced in order to describe the thrust and specific impulse. The anode current can be evaluated by using the supplied power, in order to obtain the beam current I_B in Equation (3.8), where η_d equals the discharge efficiency. The discharge efficiency describes how the anode current can be transferred into the current of the beam. It is given by Equation (3.9). Together with the overall thruster power in Equation (3.10) that is only dependent on the anode current I_A and the anode voltage U_A, the electrical efficiency of the system is defined by the discharge efficiency η_d and the acceleration efficiency η_v in Equation (3.11).

$$I_B = I_A \cdot \eta_d \quad (3.8) \qquad \eta_d = \frac{I_B}{I_A} \quad (3.9) \qquad P_T = U_A \cdot I_A \quad (3.10) \qquad \eta_e = \eta_d \cdot \eta_v \quad (3.11)$$

With Equation (3.11), the beam divergence correction factor γ and the mass efficiency correction factor η_m, the total thruster efficiency can be described. It is given by Equation (3.12). On the other hand, the total efficiency of the thruster system can be determined by using the thrust, which can be obtained via direct thrust measurements. In this case, Equation (3.13) can be used.

$$\eta_T = \gamma^2 \cdot \eta_e \cdot \eta_m \quad (3.12) \qquad \eta_T = \frac{P_{jet}}{P_{el}} = \frac{\dot{m} \cdot v_e^2}{2P_{el}} = \frac{F_T^2}{2\dot{m} \cdot P_T} \quad (3.13)$$

Next to that, the Power To Thrust Ratio (PTTR) is a common used figure in order to describe the thruster performance. With this parameter one is able to make an easy distinction between various electric thrusters. It defines the overall external required power per thrust and is given by Equation (3.14). In most cases the PTTR is required to be low because of the limited amount of power that is available on a spacecraft. For the radio frequency ion thrusters such as ArianeGroup's RIT (discussed in Section 5.1.2), the PTTR is around 33 W/mN. Colloid thrusters (discussed in Section 5.1.3) have a PTTR in the range of 4 - 10 W/mN. Next to that, field emission electric propulsion (FEEP) systems (discussed in Section 5.1.4) have a PTTR in the range of 70 W/mN. Furthermore, high efficiency multistage plasma thrusters (μHEMPT; discussed in Section 5.1.5) have a PTTR in the range of 20 - 30 W/mN [20, 51].

$$PTTR = \frac{P_{el}}{F_T} \quad (3.14)$$

In general, the required power for a thruster system will increase in order to achieve a higher specific impulse for a certain amount of thrust. As can be seen by Equation (3.7), the specific impulse increases for lighter propellant particles (as m_i gets lower). Therefore, in order to obtain a certain amount of thrust with little power (that is available from the spacecraft), it is desired to use propellants with heavy particles that are thus able to produce as much thrust as possible with the power that is available. Hence, the propellant xenon is used in many systems, since it can by ionised easily and it has a large atomic mass. The PTTR can be determined by both measuring the thrust produced by the thruster and the power that is used in order to obtain it. In this manner, losses are directly taken into account. In parallel, the specific impulse can be evaluated by using the corresponding input mass flow $\dot{m}$.

Charged Particle Acceleration

Now that the important parameters in order to characterise electric thrusters have been discussed, the principle of accelerating charged particles in an electric field will be treated. The charged particles are generated by a propellant that is fed into a discharge chamber. In here, the propellant particles are bombarded by electrons. Due to these particle collisions, the propellant particles get their electrons knocked of and this causes them to become positively charged. The neutral gas particles get separated into positively charged ions and electrons so that a plasma is formed. The charged particles inside the plasma are able to move due to the electric and magnetic fields that exist due to the particles themselves and due to the applied electrical and/or magnetic field. These motions of the charged particles are characterised by the Maxwell equations and the Lorentz force. The Maxwell equations are used within the electric thruster in order to characterise the electric and magnetic field properties. The Lorentz force determines the path of the charged particle that it follows through these electric and magnetic fields. It is given by Equation (3.15).

$$\vec{F}_L = q \cdot \left(\vec{E} + \vec{v} \times \vec{B}\right) \quad (3.15)$$

These paths describe a helical motion since the Lorentz force acts perpendicular to the velocity vector of a charged particle and the magnetic field lines. This can be seen in Figure 3.1. The heading of the path depends on the charge of the particle. This is illustrated in Figure 3.2, which illustrates a positively charged particle $q+$ that experiences a helical motion in a magnetic field. Its velocity component that is parallel to the magnetic field $\vec{B}$ remains constant. By equating the centripetal force from Equation (3.16) and the Lorentz force from Equation (3.17), the radius of the helical path of the charged particle can be found. This radius is also called the Lamor radius [20].

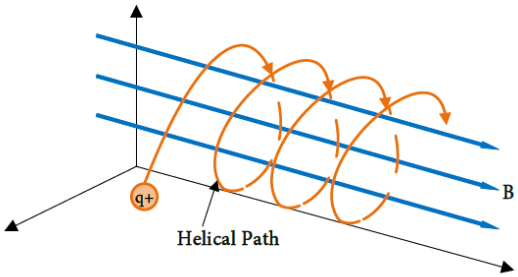

Figure 3.1: Helical Path Positively Charged Particle in a Magnetic Field [7]

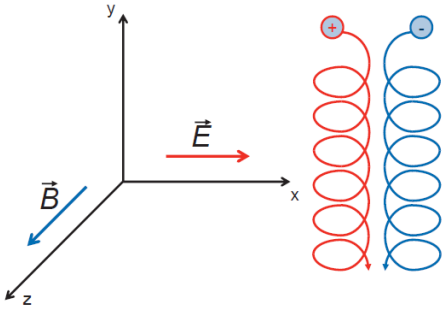

Figure 3.2: *ExB* Drift of Charged Particles in an Electromagnetic Field [6]

$$F = \frac{mv^2}{r} \tag{3.16}$$

$$F_{Lor} = Bqv \tag{3.17}$$

$$\frac{mv^2}{r} = Bqv \Rightarrow r = \frac{mv}{Bq} \tag{3.18}$$

Next, Equation (3.1) can be substituted in Equation (3.18) in order to describe the Lamor radius by Equation (3.19).

$$r_L = \frac{1}{B}\sqrt{\frac{2m_i \cdot U_B}{q_i}} \tag{3.19}$$

Hence, it can be seen that a stronger magnetic field B results in a smaller Lamor radius, whereas a larger particle velocity v results in a larger Lamor radius. As mentioned before, in many electric thrusters the propellant xenon is used. The mass of a xenon ion is with 131.293 u more than four orders of magnitude larger than the mass of an electron, which equals $5.457 \cdot 10^{-4}$ u. This causes the Lamor radius of a xenon ion to be way larger compared to that of an electron. This is an important aspect of the downscaling process of the HEMPT to the μHEMPT thrusters, since electron losses occur at the discharge chamber wall because of the fact that the maximum magnetic field strength is limited by the permanent magnets installed in the structure. The magnetic field strength cannot be increased infinitely because of mass and volume constraints. Next to that, due to this large difference in mass, the motion of the electrons can be changed easily whereas the force that is required to change the motion of the charged ions is larger.

In electric thrusters such as μHEMPT, the magnetic field properties change along the thrust direction in the discharge chamber. This is due to the fact that electrons need to be confined in required areas in order to increase the propellant ionisation. Since the magnetic field properties are not constant, it influences the Lorentz force on and the Lamor radii of the charged particles changes as well. As the magnetic field strength increases in the direction of the particle's direction of motion (i.e. drift), the magnetic field lines are compressed. This results in the fact that the Lorentz force is not perpendicular to the drift direction as before. Therefore, the charged particles will experience a force that has a component opposite that is not parallel to the drift velocity, which causes them to be decelerated. This is illustrated in Figure 3.3. Depending on the characteristics of the magnetic field, charged particles can be slowed down, reversed in direction or trapped in so called magnetic mirrors. With two of these mirrors in place, a magnetic bottle can be formed. This is shown in Figure 3.4 [15].

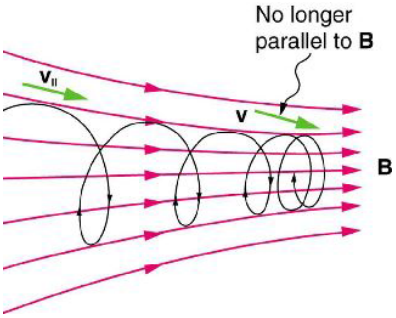

Figure 3.3: Compression of Magnetic Field Lines [14]

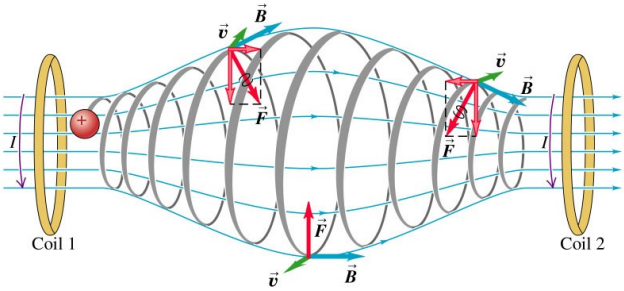

Figure 3.4: Magnetic Bottle Illustration [15]

In order to determine whether the charged particles are able to escape a magnetic mirror, the mirror ratio R_m can be used. It is defined by Equation (3.20). Here, the magnetic field at the starting point of the particle is used as B_0 as well as the magnetic field inside the magnetic mirror B_m. Next to that, $v_{\perp,0}$ is equal to the perpendicular velocity at the starting point and v_0 is equal to the absolute velocity. Finally, Θ_m is equal to the pitch angle inside the magnetic mirror of charged particle which is defined by the angle between the particle's velocity vector and the local magnetic field. The pitch angle can be used in order to determine whether a charged particle is trapped in a magnetic mirror or not.

$$R_m = \frac{B_m}{B_0} = \frac{v_0^2}{v_{\perp,0}^2} = \frac{1}{\sin^2(\Theta_m)} \tag{3.20}$$

$$v_{\parallel} < v_{\perp}\sqrt{R_m - 1} \tag{3.21}$$

Equation (3.20) is used in order to establish the reflection constraint in Equation (3.21). This constraint determines when charged particles are confined to a magnetic mirror. The interaction between charged particles is determined by Coulomb's law. In addition to that, there can only exist a finite amount of charged particles in a control volume. This is described by the Child-Langmuir law and will be treated in Section 3.3. In the next section, the electron emission from the emitter material will be discussed.

3.2. THERMIONIC EMISSION

In order to remove an electron from the lowest energy level and to emit it into vacuum, an energy of E_0 is required. Next to that, in order to emit an electron from the Fermi level E_f, it needs to be given an energy that is equal to $E_0 - E_f$, which is also called the work function W_0. This work function describes the *minimum* energy that is required in order to remove and electron from an uncharged specimen. This process is illustrated by Figure 3.5. It is shown how electrons are distributed amongst various energy levels within the material. Hence, the work function is an important parameter as materials with lower work functions require less energy (in the form of heat) in order to emit electrons. The work functions of common used emitter materials for cathodes are listed in Table 3.1 [16, 20, 52].

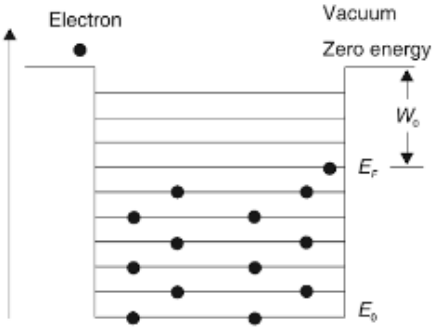

Figure 3.5: Electron Distribution among Energy Levels [16]

Table 3.1: Work Function Emitter Materials

Material	W_0 [eV]
Tungsten	4.87
LaB_6	2.69
CeB_6	2.5
Lithium	2.5
C12A7	2.4
BaO-W	2.1
Caesium	1.81
BaO	1.55

The cathode material needs to have a work function that is as low as possible. In this way, the minimum amount of energy is needed for an an electron in the highest occupied electron state of a material at 0 K to emit sufficiently far into vacuum in such a way that it is no longer affected by the electric fields from the material. The goal for the electron is to overcome the attractive forces of the surface atoms and the loss in kinetic energy due to the inter material collisions. If the material is heated until the electron has a sufficient amount of kinetic energy to escape its electron shell, then thermionic emission occurs. As thermionic emission is an important aspect for electron bombardment in electric propulsion systems, it will be explained below. It is described by Equations (3.22) and (3.23) [20, 30, 53].

$$J = AT^2 \exp\left(\frac{-e\phi}{kT}\right) \tag{3.22}$$

$$A = \frac{4\pi \cdot m_e \cdot k^2 \cdot e}{h^3} = \frac{4\pi \cdot 9.109 \cdot 10^{-31} \cdot \left(1.38 \cdot 10^{-23}\right)^2 \cdot 1.602 \cdot 10^{-19}}{\left(6.626 \cdot 10^{-34}\right)^3} = 1200641 \ \text{A m}^{-2}\,\text{K}^{-2} \tag{3.23}$$

In these equations, J is equal to the emitted thermionic current density, A is a constant (with a value of 120 $\text{A/cm}^2/\text{K}^2$, evaluated by Equation (3.23) [54]), T is the material temperature, k is the Boltzmann's constant, e is the charge of an electron, m_e is the mass of an electron, h is Planck's constant and ϕ is the work function.

From this equation it can be concluded that a material that has a low work function will emit a larger amount of current at a given temperature compared to a material that has a higher work function. Therefore, a cathode made from a material with a low work function does not need to be heated as strongly as another cathode made from another material with a higher work function in order to emit the same amount of electrons. The emitted electrons are used to bombard the propellant that is used in the propulsion system in order to create charged ions. These ions are then accelerated through the discharge chamber by means of an electrostatic field in order to generate the required thrust. The cathode can be constructed from different low work function materials. The main ones will be discussed in Section 4.3.1 to 4.3.6. Figure 3.6 gives an illustration of the possible emission current for these materials. Other materials that are used in order to assemble the emitter into the cathode structure are discussed shortly in Section 4.3.7 [55, 56].

Nevertheless, it has been discovered that the value for the Richardson constant A varies considerably from the theoretical value of 120 $A/cm^2/K^2$ as determined in Equation (3.23). This is due to different effects, such as variations in the crystal structure of the surface, variations in the surface coverage (for dispenser cathodes) and e.g. changes in the density of states at the surface of the emitter due to thermal expansion. It can be corrected for by applying a temperature correction to the work function by means of Equation (3.24). In this equation, ϕ_0 is equal to the classically reported work function at absolute zero temperature and α is an experimentally measured constant. Implying this into the Richard Dushman Equation (3.22) results in Equation (3.25) [57].

$$\phi = \phi_o + \alpha T \tag{3.24}$$

$$J = A\exp\left(\frac{-e\alpha}{k}\right)T^2\exp\left(\frac{-e\phi_0}{kT}\right) = DT^2\exp\left(\frac{-e\phi_0}{kT}\right) \tag{3.25}$$

In Equation (3.25) the constant D equals the temperature modified coefficient for the Richardson Dushman Equation (3.22). Because of the varying use in A and D, the variations in the surface stoichiometry and/or due to different crystal orientation in single crustal emitters, there exist several reported work functions for e.g. the emitter LaB_6. For hollow cathode and large area emitter applications such as electric propulsion the press sintered LaB_6 consists out of polycrystalline. Its work function is an average over different crystal orientations along the surface. The work functions and the literature values for A and D are summarised in Table 3.2. It is interesting to note that the actual emission current density of LaB_6 as determined by literature in Table 3.2 is close to the different values that are used for A, D and ϕ to within 25%. The focus lies on the LaB_6 emitter, however different cathode materials are given as well as a comparison. These emitter materials are discussed in more detail in Section 4.3 [58, 59].

Table 3.2: Work Function and A and D Values [1]

Emitter	A	D	ϕ
BaO-W 411 [60]	120		$1.67 + 2.82 \cdot 10^{-4}$ T
BaO-W 411 [57]		1.5	1.56
LaB_6 [61]		29	2.66
LaB_6 [62]		110	2.87
LaB_6 [58]	120		2.91
LaB_6 [28]	120		$2.66 + 1.23 \cdot 10^{-4}$ T
Molybdenum [28]		55	4.20
Tantalum [28]		37	4.10
Tungsten [28]		70	4.55

3.3. CHILD-LANGMUIR LAW

In the space applications where micro thruster systems play a role, there is a vacuum environment. Therefore the emitted electrons cannot be directly neutralised after emission as they would be in a conductive environment such as Earth's atmosphere. Hence, they form a volume of charge that is also called *space charge*. In conducted experiments and operating micro propulsion systems, these "clouds" of charged particles are attracted by the positive anode. Hence, a flow of electrons occurs between the closed electrical circuit from the cathode (emitter) to to the anode. However, the current flow that is possible between these stations is limited. This is described by the Child- Langmuir Law in Equation (3.26). It states that the space charge limited current I_A in a plane parallel vacuum diode varies by the three halves power of the anode voltage U_A and inversely as the square of the distance d that separates the cathode and the anode. Furthermore, ϵ_0 equals the vacuum permittivity, e the charge of a single electron, m_e the mass of an electron and A the cross sectional area over which the electrons are distributed [63, 64].

$$I_A = \frac{4\epsilon_0}{9}\sqrt{\frac{2e}{m_e}}\cdot\frac{A}{d^2}\cdot U_A^{\frac{3}{2}} \tag{3.26}$$

Thus, even if an unlimited amount of electrons would be able to be emitted from a cathode emitter, then the amount of electrons in a volume, or more specific, the current flow between the cathode and the anode, would be limited as described by the Child-Langmuir law in Equation (3.26). This is due to the fact that Coulomb repulsion of equally charged particles such as ions (and electrons) occurs in a volume which causes a saturation effect so that the amount of charged particles per volume is limited. Therefore, the current that can be realised between the cathode (emitter) and the anode depends on both the Child-Langmuir relation and the physical amount of possible electron emission of the emitter material as described by the Richardson law. With the current test setup that will be shown in Figure 6.9, the current flow that can be realised between the cathode and the anode is plotted in Figure 3.7. Results can be seen for cathode to anode distances d from 1 mm to 4 mm. The anode surface area equals $A = \pi R^2 = \pi \cdot 0.01^2$ m^2. It can be seen that for smaller distances between the cathode and the anode, a larger current flow can exist for an equal anode potential.

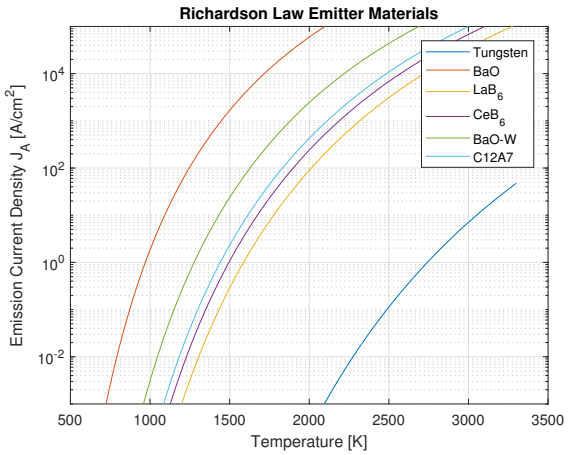

Figure 3.6: Richardson Law Emitter Materials

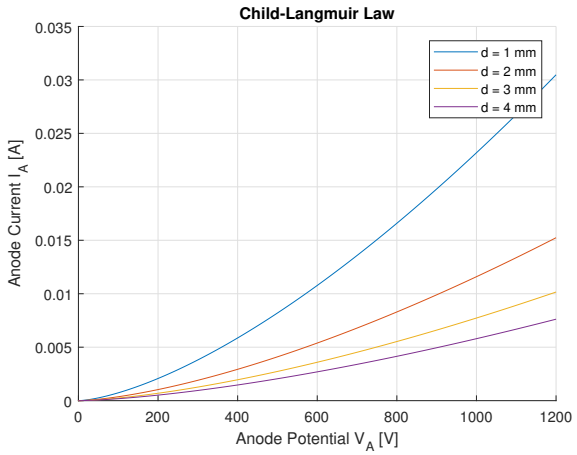

Figure 3.7: Child-Langmuir Law Current LaB_6 Cathode Setup

3.4. HIGH EFFICIENCY MULTISTAGE PLASMA THRUSTER CONCEPT

Currently, in order to study small satellite and CubeSat applications and to provide a feasibility demonstration, Airbus is developing a down scaled version of the High Efficiency Multistage Plasma Thruster (HEMPT) [65]. The HEMPT, which is also called a Cusped Field Thruster, is invented by Günter Kornfeld at Thales Electronic Systems GmbH in Ulm in Germany in 1998 [66]. It is capable of producing a thrust of 44 mN with a specific impulse of more than 2400 s [67]. This thruster system has some unique advantages which makes it potentially an attractive micro Newton thruster concept. These advantages include nearly erosion-free operation and simple system and interface design that requires only one high voltage supply and one mass flow controller. In order to illustrate a schematic of a cut through of the cylindrical HEMPT, Figure 3.8 is given [17].

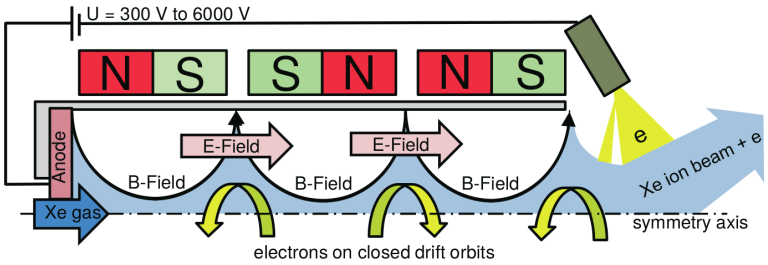

Figure 3.8: Schematic of the HEMPT Concept [17]

Figure 3.8 shows the location where the anode is mounted. The anode (Greek: $\alpha\nu o\delta o\zeta$, way up) is the electrode through which the conventional current flows into the polarised electrical circuit. Next to that, half of the discharge chamber is shown by the grey surrounding of the xenon gas inside. The discharge chamber is surrounded by a system of periodically poled permanent magnets. Using this magnet arrangement a special magnetic field topology is formed, as indicated by the black arrows. The radial magnetic field lines separate the discharge chamber into various magnetic cells. On the left hand side the xenon gas inlet is located.

Furthermore, on the right hand side, a neutraliser cathode (Greek: $\kappa\alpha\theta o\delta o\zeta$, way down) is placed. This is the electrode where the current leaves the electrical system. Its main purposes are to emit electrons that can be pulled into the discharge chamber in order to ionise the propellant and to neutralise the exiting flow. Therefore, it is also called a neutraliser in some occasions. By emitting electrons into the exiting beam the cathode prevents the spacecraft from becoming negatively charged because of the fact that positive charged propellant particles are exiting the thruster system. This is required because of the fact that a negatively charged spacecraft would affect the exiting plasma plume and eventually shut down the thrust.

Between the anode and the cathode the potential difference can vary between 300 V up to 1200 V (6000 V for the larger version). The emitted electrons from the neutraliser cathode are attracted by the anode, mirrored by the strong magnetic field gradients. This causes them to be trapped in the magnetic cells, which is necessary in order to enable a proper ionisation efficiency. Inside the discharge chamber the pulled electrons are bombarding the neutral xenon particles. This causes some of the xenon particles to lose their electrons and become ionised. In this manner, a plasma (i.e. a mix of charged particles) is formed. The magnetic field assures that the plasma is confined close to the rotation axis of the thruster system. Hence, the plasma has ideally almost zero interaction with the dielectric walls that surround the discharge chamber. The electrons inside the plasma are forced to follow the helical path's around the magnetic field lines as described in Section 3.1. They can collide several times with propellant particles before their kinetic energy and hence velocity is too low for them to become trapped inside the magnetic field. At this point, the electrons are thermalised and are dissipated by the anode in order to close the electric circuit.

On the other hand, the ions are not noticeable affected by the magnetic field due to their much larger mass compared to the electrons. Moreover, the xenon ions inside the discharge chamber generally have a Lamor radius that is larger than the dimensions of the HEMPT discharge chamber. They are accelerated towards the thruster exit plane, where trapped electrons act as an accelerating grid. Next to that, there exist a few ions that collide with non conductive ceramic discharge chamber walls. Because of this effect, these walls become charged positively. This causes other ions to be repelled from the walls and be focused towards the centre rotational axis of the discharge chamber. Hence, the interactions between the charged ions and the chamber walls are minimised which has beneficial effects in terms of erosion and thus lifetime of the thruster system.

Finally, in order to be able to use the thruster system in the targeted μN regime, there remain some challenges that need to be solved. This includes the manufacturing of the downscaled thruster geometry in a 1U[1] CubeSat volume. One of the major losses is caused by downscaling, since electron losses occur at the discharge chamber wall because of the fact that the maximum magnetic field strength is limited by available permanent magnets. Therefore, the Lamor radii of the electrons inside the discharge chamber are kept constant and this causes an increase of electron losses at the discharge chamber walls. [6, 17, 68].

[1] 1 CubeSat unit of 10 cm x 10 cm x 10 cm and max. 1.33 kg [19]

4

LITERATURE REVIEW

This chapter will provide the background information for the micro propulsion system (μHEMPT) and its cathode. The goal is to inform the reader with the technologies and methods that are used nowadays in order to establish high performance electric micro propulsion systems. First, an introduction to the topic is given in Section 4.1. Next different cathode types are discussed in Section 4.2. Afterwards, Section 4.3 elaborates on the different materials that are used in the cathode systems, both for the emitters and the general structure. Furthermore, the propellant compatibility is treated in Section 4.4. Finally, the current state of the μHEMPT is given in Section 4.5.

4.1. MICRO PROPULSION APPLICATIONS

The number of small satellites seeking launch continues to grow. The projected growth for the next years can be seen in Figure 4.1. Therefore, new opportunities are emerging to fly these satellites as secondary payloads on several launchers systems. As already briefly addressed in Chapter 1, satellites are becoming smaller and more powerful with high performance instruments and even propulsion systems for orbit keeping. Next to that, electric propulsion becomes important on formation flying missions, future interplanetary missions and orbit raising manoeuvres. This section discusses how the micro propulsion thruster technology coming from small satellites in Section 4.1.1 is interesting to be applied to nanosatellites in Section 4.1.2 [17, 18, 69–73].

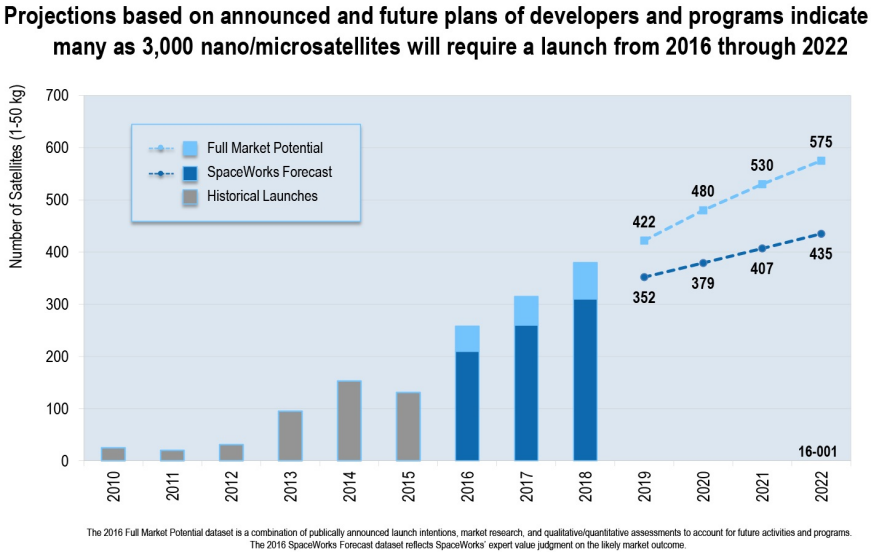

Figure 4.1: Projected Satellite Market [18]

4.1.1. SMALL SATELLITE APPLICATIONS

Airbus, Friedrichshafen, is investigating in electric propulsion systems that are used for highly precise attitude and position control systems for spacecrafts. Research in this field of propulsion engineering is being performed because of two reasons. First of all, there is a need for exploration of viable alternative micro Newton candidates that can be used on the European Space Agency (ESA) Laser Interferometer Space Antenna (LISA[1]) space mission. Next to that, there exist several planned science and Earth observation missions that will require suitable micro Newton thrusters that have a high technology readiness level. This is because of the fact that these missions have constraints both in terms of time and technical development risks. It is expected that electric propulsion is a key technology that can be used in order to meet these goals [17, 74, 75].

[1] `http://sci.esa.int/lisa/` | Visited on 06 September 2017

The Laser Interferometer Space Antenna mission serves as an all-sky monitor and is able to offer a wide view of a dynamic cosmos using the gravitational waves as new and unique messenger. In this manner the gravitational universe can be explored and unveiled even further. The mission consists out of a constellation of three satellites that are using laser interferometer technology in order to measure gravitational waves. In this manner it can probe the entire universe, from the smallest scale near the horizons of black holes up to the large cosmological scales. Next to the polarisation of the gravitational waves, the source parameters will be measured as well. In order to maintain the required orbit and constellation orientation, micro electric propulsion systems will be used [76, 77].

Using micro propulsion systems in space applications, drag-free propulsion systems can be realised. This allows for disturbance forces and torques applied on spacecraft to be counteracted. In this manner, the free-floating conditions can be maintained in e.g. ESA's LISA Pathfinder[2] mission, in order to acquire the proper scientific test conditions. Furthermore, the drag free propulsion system is capable of performing attitude and orbit control functions for the LISA Pathfinder satellite. The propulsion system on the LISA Pathfinder mission consists of micro Newton thrusters which are in the form of nitrogen cold gas thrusters. These are based on the ones that are originally developed for ESA's GAIA[3] mission [78, 79]. These thrusters have a controllability between 1 - 1000 μN and will also be operated on the Centre national d'études spatiales (CNES) Microsope missions [80]. Despite the fact that they are ideal for drag-free control of satellites, they have a low specific impulse of only 65 s and gas leakage occurs (which affects mission lifetime). Hence, the current development tends towards the micro propulsion systems. These systems have low mass and volume requirements and a long lifetime, but require a lot of power (in the order of 100 Watts for the larger ones) [81–83].

The impulse requirements for small satellites vary widely dependent on the mission according to Blandino [84]. With micro impulses as small as in the range of 50 - 100 μNs, deadband pointing, precision translation of the spacecraft or larger impulses in order to remove residual rotation during a spacecraft targeting slew can be realised. In addition to that, this precise control will allow future space missions that include interferometry spacecraft flying in tight formation. With impulsive thrust manoeuvres that have a deadband time between the firings of 20 - 100 s, the required impulse for a 1 kg mass can be as low as 29 μNs for 1 degree pointing requirements and 100 s deadband intervals. This impulse can decrease for more strict pointing requirements to as little as only 0.034 μNs. Considering slew requirements, thrust as low as 0.06 mN could be required to e.g. perform a 180^o rotation within one minute. Again, this strongly depends on the type of mission. As an example, a 10 kg inspector satellite that has been developed by JPL requires thrust up to 10 mN in order to meet its manoeuvrability requirements [85]. Since these low levels are interesting for various space missions that use a CubeSat as their platform as well, their applications will be discussed next.

4.1.2. CUBESAT APPLICATIONS

Because of the large scale miniaturisation of satellites and space systems, it is desired to realise micro electric thruster systems for the common used nanosatellites that are also called CubeSats. Currently, these CubeSats have a lifetime of 1 - 2 years and their in most cases their main purpose is to demonstrate new technologies in space. However, with a propulsion system, their mission life time can be increased to the range of 10 - 15 years and the mission objectives can be broadened. Examples range from large scale production constellation of nanosatellites that can provide global, timely and accurate weather forecasting data, (forest) fire recognition or cargo ship monitoring to orbit maintenance objectives, formation flying, orbit raising or even deorbiting. In addition to that other nanosatellite measurement arrays can be realised to e.g. measure deep space radio waves [86].

In formation flying missions the thrust requirements are strongly dependent on the required positioning control for the formation. For optical observations that are performed using interfereometry systems the positioning control needs to be very accurate and the thrust requirements are very strict. This means that the thrust requirements can range into the milli- and also micro-Newton range. Nonetheless, the possibilities for optics on CubeSats are often limited by the physical constraints. Therefore, distributed spacecraft architectures can be realised with less strict requirements in order to be able to perform a similar mission objective. With these architectures, the subsystems can be distributed over various spacecraft in order to allow for redundancies, large scale production and risk mitigation. Hence, the thrust requirements for CubeSat applications varies widely dependent on the mission objectives. This leads to the fact that thrust as well as in the milli- as in the micro-Newton range can be required at continuous or near-continuous thrusting [10].

[2] http://sci.esa.int/lisa-pathfinder/39981-engineering/?fbodylongid=1902 | Visited on 22 September 2017
[3] http://sci.esa.int/gaia/28820-summary/?dom=icopyright&src=syn | Visited on 22 September 2017

Currently, the power that can be generated on a CubeSat is one of the most important and also limiting factors when it comes to implementing micro electric thruster applications. Using triple junction gallium arsenide (GaAs) solar cells with en efficiency of 30%, the power delivered from a 1U, 2U and 3U solar panel is 2.3, 4.6 or 6.9 W respectively. These solar panels exists as commercial of the shelf (COTS) components and can be purchased at CubeSatShop[4]. The generated power on a CubeSat can be increased by installing additional deployable solar panels[5], which can also be easily obtained in the form of COTS components.

In order to verify whether a downscaled HEMPT thruster would be possible to implement on a CubeSat, a survey has been conducted by Frosch e.a. [2]. The goal is to establish possible thruster system constraints and operating scenarios. The survey shows that such a system would be possible on a 3U CubeSat. In this manner aspects such as orbit maintenance and orbit raising can be performed. The study analyses a typical sun synchronous, circular, Low Earth Orbit (LEO) with an orbital height of 550 km. This altitude is based on the fact that most CubeSats are deployed at this height. Furthermore, since power is a limiting factor, it is decided to implement the CubeSat in the survey with four deployable solar panels that have solar cells on both sides. In this way, $17 \cdot 7 = 84$ solar cells can be put. With the typical solar cell dimensions of 80 x 40 mm, this results in a total solar area of 0.25 m^2. Figure 4.2 gives an illustration of the 3U CubeSat with four deployed solar panels. Using the Systems Tool Kit from Analytical Graphics Inc., it has been determined that the average available bus power is equal to 20.6 W.

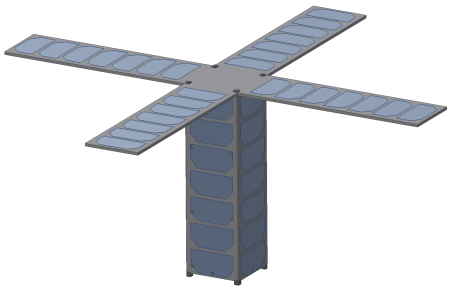

Figure 4.2: 3U CubeSat with deployed Solar Panels

Next, a power budget has been established. This contains the command and data handling (C&DS) subsystem, telemetry, tracking and command (TT&C), the electric power system (EPS), the attitude determination and control (AOCS) system and the thermal control system (TCS). In this manner a thruster budget for the micro electric thruster can be determined. Using an overall platform power consumption of 3 W and taking path losses into account, the available power for the propulsion system is equal to 6.3 W, in case the thruster is operated continuously. Non continuous thrusting in the form of cyclic thruster impulses during the sunlight period have been considered as well. This results in a higher thrust impulse because the thruster could be operated with a higher operational power of 11.2 W during the sunlight period only, but would cause the satellite to leave the sun synchronous orbit. The sunlight to eclipse ratio would decrease and would cause the average available power for the propulsion subsystem to decrease as well. Therefore, this option is disregarded [2, 3].

By assuming a specific impulse I_{sp} of 1000 s and a mass flow rate of 0.1 sccm, Tsiolkovski's Equation (4.1) can be used in order to determine a velocity increment (i.e. ΔV) of 791 m/s in one year. In this equation, v_e is equal to the exit velocity of the expelled mass relative to the spacecraft, M_{init} is equal to the initial mass prior to the thrusting phase and M_{end} is equal to the mass of the spacecraft after the thrusting phase. The exit velocity can be determined with Equation (4.2), by multiplying the specific impulse I_{sp} and the gravitational constant g_0. It follows that the required propellant mass is equal to 310 g.

$$\Delta V = v_e \cdot \ln\left(\frac{M_{init}}{M_{end}}\right) \tag{4.1}$$

$$v_e = I_{sp} \cdot g_0 \tag{4.2}$$

Using these parameters, Equation (4.3) is used in order to determine the altitude increase with the corresponding available ΔV. Here r is equal to the radius of the orbit, i.e. the radius of the Earth plus the orbital altitude. Next to that, μ_E is equal to the gravitational parameter of Earth, which equals $3.986004 \cdot 10^{14}$ m^3/s^2 [3] and v_c is the relative velocity of the circular orbit. With an available ΔV of 791 m/s, the orbit elevation that can be achieved is equal to 1705 km. If the cycling thrusting mode were to be used, the ΔV would be only 493 m/s. This parameter, and other ones used in the survey are listed in Table 4.1 in order to give a summary of the possibilities for a μHEMPT thruster on a 3U CubeSat.

[4] `https://www.cubesatshop.com/product/single-cubesat-solar-panels/` | Visited on 09 November 2017
[5] `https://www.cubesatshop.com/product/solar-panels/` | Visited on 09 November 2017

$$\Delta V = V_{c0} - V_c = \sqrt{\frac{\mu_E}{r_0}} - \sqrt{\frac{\mu_E}{r}} \tag{4.3}$$

Table 4.1: One Year Orbit raising for a 3U CubeSat [2]

Characteristic	Continuous	Cyclic
Initial satellite Mass [kg]	4	4
I_{sp} [s]	1000	1000
Mass flow [sccm]	0.1	0.1
Operation time [years]	1	1
Duty cycle [%]	100	63.2
Propulsion system power [W]	6.3	11.2
ΔV [m/s]	791	493
Orbit elevation [km]	1705	994
Propellant	Xenon	Xenon
Propellant mass [g]	310	196
Propellant volume (@ 300 bar) [ml]	351 (= 0.31 U)	222 (= 0.20 U)

In order to realise a miniaturised HEMPT for CubeSat applications with a propulsion system power range of 6 - 11 W, several challenges need to be overcome. These include maximising heating efficiency, thus minimising radiative and conductive heat losses, minimising cable losses and maximising emitter current emission. Next to that, the requirements for the ΔV vary widely and depend on the type of mission. Therefore, a closer look is taken into the parameters as they are defined by Wertz and Larson [3]. Orbit raising or plane changes require approximately 0.6 m/s per km of altitude change in a low Earth orbit at 250 km or 135 m/s per degree of orbital plane change respectively. These values strongly depend on the orbital altitude. Table 4.2 lists them for three different ones. Hence there exists various possibilities in terms of orbit manoeuvres that can be realised using a micro electric thruster on a CubeSat.

Table 4.2: ΔV Requirements for Orbit Raising and Orbital Plane Change Manoeuvres for Various Orbital Altitudes [3]

Earth orbital altitude [km]	Plane change ΔV [(m/s)/deg]	Altitude change ΔV [(m/s)/km]
250	135.35	0.58
500	132.86	0.55
750	130.97	0.52

CubeSats are launched from a Poly Picosatellite Orbital Deployer (P-POD), in order to provide safety to both the launcher and the satellite. These P-PODS come in different sizes so that they can house different size CubeSats. An example of a COTS Quadpack[6] can be seen in Figure 4.3. This deployer is capable of injecting four 3U CubeSats into orbit. These deployers allow for an extra cylindrical part to be put on the far end of the CubeSat. This part is, because of its shape, also called a tuna can. Because of this location, it is convenient to put an communication or propulsion system here and it is used as a baseline for thruster applications on CubeSats. The height of the cylinder is equal to 36 mm and the maximum diameter is equal to 64 mm. Figure 4.4 gives a schematic that shows the dimensions of a 3U CubeSat with the installed tuna can on the left hand side [19, 87].

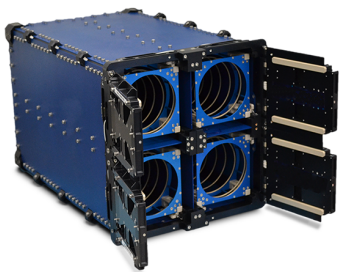

Figure 4.3: Quadpack CubeSat Deployer System

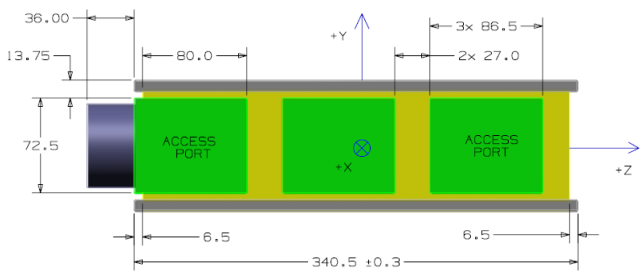

Figure 4.4: 3U CubeSat Dimensions with Tuna Can installed [19]

[6] https://www.isispace.nl/product/quadpack-cubesat-deployer/ | Visited on 09 November 2017

Because of the fact that important sectors of the commercial space market are going to require space missions with long orbit lifetimes, formation flying aspects or highly precise attitude and orbit control systems in the near future, high performance electric propulsion systems need to be ready to provide mass efficient orbit keeping support. In addition to that, these thruster systems will become advantageous candidates if the launcher market evolves to permit direct orbit injection strategies. Nevertheless, because of the long process of development and qualification of these electric propulsion systems, these activities require acceleration and support in order to aid the technology development and to cover the non-recurring costs. One of the promising electrostatic thrusters that can be used in a CubeSat structure is the μHEMPT, because of its low complexity, high efficiency and affordability. By creating a successful flight model of this system on a CubeSat structure, the technology readiness level (as discussed in Chapter 1) can be increased. A cathode is used in this system in order to emit electrons that are required in order to ionise the propellant. Different types of cathodes exist, which will be discussed next.

4.2. CATHODE TYPES

This section will describe what type of cathodes for micro propulsion systems are available. These include the thermionic cathodes that are discussed in Section 4.2.1, the hollow cathodes which are are dealt with in Section 4.2.2 and radio frequency cathodes that are described in Section 4.2.3 respectively. Finally, conclusions are given in Section 4.2.4.

4.2.1. THERMIONIC CATHODES

In low cost and low complexity electric thruster applications thermionic cathodes can be opted for. A thermionic cathode operates in vacuum and is heated in order to emit electrons by means of thermionic emission. In this manner, heat is supplied to the emitter material in order to increase the kinetic energy of the electrons so that it becomes sufficient to overcome its work function so that the electrons are able to leave the emitter material. This process is explained in more detail in Section 3.2 . The electrons are both used in order to create an electron discharge inside the thruster to ionise the propellant and create a plasma as well as to neutralise the exiting ion flow. Since these type of cathodes use a heater source they are also called hot cathodes [20].

The principle of thermionic emission is simple and effective, and therefore it is suitable to be used for down scaled micro thruster applications. This is due to the fact that no additional propellant tanks or plasma ignition and protection systems are required. There exist several materials that can be used as emitters for thermionic cathodes. They all have their own advantages and disadvantages and next to that, their own operating ranges and requirements. These emitter materials will be discussed in Section 4.3.

4.2.2. HOLLOW CATHODES

Typical and conventional hollow cathodes for space applications use a porous tungsten insert that is impregnated with an emissive mix of the materials barium, calcium oxides and alumina. In this configuration these hollow cathodes are also called dispenser cathodes because of the fact that the tungsten matrix acts as a reservoir for the e.g. barium which is dispensed from the pores in order to activate the emitter surface. An illustration of a hollow cathode that consists out of a hollow refractory tube with an orifice at one end can be seen in Figure 4.5. The chemical reactions that occur in the pores or at the surface of the emitter material at high temperatures create a barium-oxide dipole. This dipole is attached to an active site of the tungsten substrate, which causes the work function of the surface to be reduced to about 2.06 eV at temperatures over 1000 ^{o}C. The thermionic insert that is placed inside the structural cathode tube is usually wrapped by a heating element and heat shields [1, 20, 60, 88].

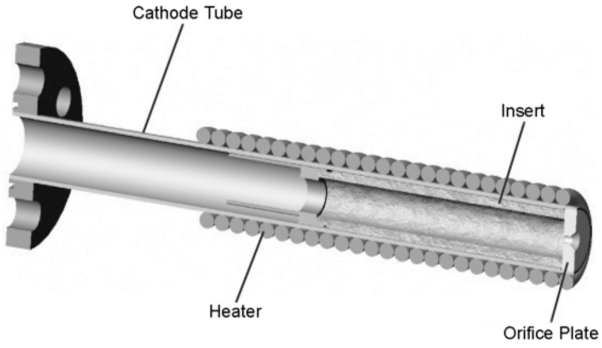

Figure 4.5: Graphical Illustration Hollow Cathode Setup [20]

Dispenser cathodes discharges are started by vacuum thermionic emission from the front of the cathode orifice plate due to e.g. barium that is diffused out of the orifice and activates the emitter surface. This process requires time in order for the diffusion and surface chemistry to establish and to activate the emitter surface before emission is initiated. Subsequently, at sufficient emission current, the ionisation of the propellant gas in the cathode to the keeper gap is able to provide a plasma that flows into the orifice. Next, this plasma couples to the insert region and the plasma discharge is initiated. This plasma is used in order to extract electrons through the orifice of the cathode into the thruster plasma [89].

On the other hand, LaB_6 operated hollow cathodes do not have a mechanism for the orifice plate to initiate current emission. Instead, a relatively large orifice diameter used in high current hollow cathodes allows a small amount of electric field to enter the insert region and extract electrons. This manner of ignition by discharge by coupling directly from the insert to the keeper and anode gas has been successfully tested with various cathodes. As the heater power increases until the discharge self heating can be conserved, the discharge current increases proportionally. In addition to that, as the current discharge has initiated, the heating of the cathode insert is established by the discharge current that flows through the potential drop in the hollow cathode. As the discharge currents increase, the potential drop in the cathode decreases. On the other side, if the discharge current decreases, the discharge voltage and the internal voltage drop inside the LaB_6 cathode increase. This causes the cathode performance to degrade [1].

Because of the fact that chemistry is involved in the formation of the low work function surface for the dispenser cathodes, they are subjected to possible poisoning. This can increase the work function of the emitter material, which causes the energy that is required to emit electrons to increase. Therefore, it is important to take care when handling the emitter materials in order to avoid poisoning by water vapor, atmospheric gases and impurities in the propellant that is used. The latter will be discussed in more detail in Section 4.4. Next to that, system complexity increases in realising a miniaturised version of a hollow cathode operated micro propulsion system because of the requirements for the cathode plasma and the cathode propellant feed system. Hence, the current aim is to first realise a successfully operating thermionic cathode for a micro propulsion system.

4.2.3. RADIO FREQUENCY CATHODES

Radio frequency (RF) cathodes employ electromagnetic fields that are induced by radio frequency currents. This type of cathode is investigated since the hollow cathodes are limited in lifetime by depletion and degradation of the emitter insert. Next to that, the hollow cathodes need to be heated for a certain period in order to start up the cathode and to initiate the electron emission. Therefore, ion engines that operate using hollow cathodes cannot be switched on quickly and next to that they often require careful handling in ground facilities because of poisoning issues.

A radio frequency cathode does not require a heater and can be ignited instantaneously. However, the ignition is not simple because of the fact that free electrons are required in the discharge chamber. These can be provided by the neutraliser, that is needed also in order to neutralise the ion beam at the exit of the thruster. In these type of cathodes, the plasma is generated by radio frequency electron bombardment. The acceleration of the charge carriers is realised by applying electromagnetic field topologies. Inside the electric field the electrons have a high probability of colliding with a neutral propellant particle, which causes the particle to be ionised. This process causes another electron to be created in the thruster chamber, which is accelerated again by the RF electric field and has another opportunity to ionise another neutral propellant particle. The frequency on which the RF voltage amplifier that drives the coil operates is dependent on the cathode geometry. In most cases, it is in the MHz range. In this manner, the RF cathodes has not only a high ionisation efficiency, but also a high propellant mass utilisation [90].

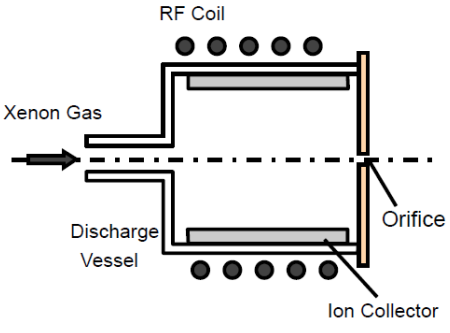

Figure 4.6: Radio Frequency Cathode Setup [21]

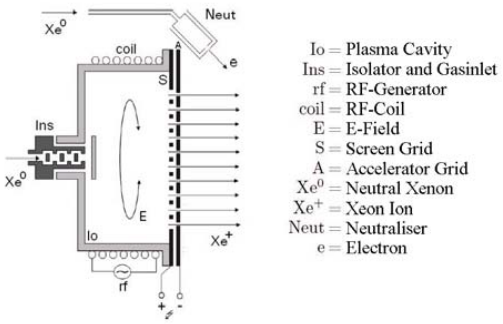

Figure 4.7: Illustration RIT System [22]

Figure 4.6 gives an illustration of a radio frequency cathode. Here it can be seen how the radio frequency coil is turned around the discharge vessel. This RF coil creates electric fields in its circumferential direction. Xenon is entered as the operation gas on the left hand side which is coupled by the electric field in order to produce the plasma. The ion collector is the electrode that is used to collect the ions [20, 21, 91].

Instead of an orifice plate, the ionised propellant can also be extracted via a system of grids at the open end of the plasma cavity. This is what is done in the Radio frequency Ion Thruster (RIT) by ArianeGroup. The principle is shown in Figure 4.7. More background information on the ArianeGroup research will be given in Section 5.1.2. As with the orifice plate in Figure 4.6, the purpose of the grid system in Figure 4.7 is to extract the ions from the plasma inside the thruster chamber. In a two grid system such as the one illustrated in Figure 4.7, the screen grid (indicated with S) is biased on a high potential compared to the spacecraft and the ground of the neutraliser. The screen grid is allowed to be in direct contact with the plasma, which causes it to also have a high potential. Typically the voltages are between 600 V and 1500 V. The purpose of the second grid, also called the accelerator grid, is to carry a negative potential. In this manner, electron back streaming in the thruster chamber is prevented. In addition to that, its potential needs to be sufficiently low in order enable an optimal ion trajectory for the emitted ions. The potential of the acceleration grid lies in the range of -70 V to -300 V. Finally, a neutraliser is used in order to neutralise the ion beam [22, 92].

An advantage of such a type of cathode is the long lifetime because of the usage of a RF coil in order to generate electrons instead of using an emitter material that eventually evaporates. In addition to that, the thrust noise is low. Nevertheless, it requires a high voltage power supply for both the RF coil and the grid system. In addition, a radio frequency generator and complex architectures are required. Therefore, in order to realise a low complexity, affordable *and* efficient cathode, either a thermionic or hollow cathode is preferred. These make use of various emitter and construction materials, which will be discussed next.

4.2.4. CONCLUSION

There exists several types of cathodes for electric propulsion systems. The ones that are discussed here that are interesting for micro propulsion applications in particular are a thermionic cathode, a hollow cathode and a radio frequency cathode. In order to perform a trade-off on above mentioned concepts, five trade criteria have been established. These are appropriate in order to define a well-argued trade-off.

1. Performance
2. Affordability
3. Compatibility
4. Lifetime
5. Complexity

Above mentioned trade criteria are now used in order to generate a Graphical Trade-off for the different cathode types described in Section 4.2. For the graphical trade off, the grading criteria are defined from best to worst as excellent (green), good (blue), correctable (yellow) and unacceptable (red). These are listed in Table 4.3.

Table 4.3: Ratings Graphical Trade-off

Graded	**Color**
Excellent	Green (G)
Good	Blue (B)
Correctable	Yellow (Y)
Unacceptable	Red (R)

These ratings will be used for the graphical trade-off, which can be seen in Table 4.4. In this table the trade criteria are listed in the first row and the design options are listed in the first column. A thermionic cathode can be realised using COTS components in a low complexity way. However, the performance in terms of electron emission and heater efficiencies might be lower compared to other systems. Nonetheless, this is a good step forward as an initial design option. Hollow cathodes could perform better in terms of efficiencies and current emission. However, they are more complex and use materials that are susceptible to poisoning. Radio frequency cathodes have a long life time, but are highly complex as they require a high voltage RF coil and a grid system. Therefore, in order to realise a low complexity, affordable and efficient cathode for the miniaturised HEMPT at Airbus, the thermionic cathode will be designed and tested first.

Table 4.4: Graphical Trade-off Cathode Types

Criteria ⇒ Cathode Type ⇓	**Performance**	**Affordability**	**Compatibility**	**Lifetime**	**Complexity**
Thermionic cathode	Acceptable (B)	COTS (G)	Good (G)	Acceptable (B)	Low (G)
Hollow cathode	Good (G)	COTS (G)	Suffer from poisoning (Y)	Acceptable (B)	Involved (Y)
Radio Frequency Cathode	Acceptable (B)	Reasonable (Y)	Good (G)	Long (G)	High (R)

4.3. CATHODE MATERIALS

This section describes what different kind of materials are being used for cathodes in micro propulsion systems. In addition to that, new materials that are in the focus of current research are described. Furthermore, poisoning will be addressed, which is a major problem for many of the cathode materials. The cathode emitter materials treated are tungsten, barium oxide, lanthanum hexaboride, cerium hexaboride, barium impregnated porous tungsten and calcium aluminate and will be discussed in Sections 4.3.1 to 4.3.6. Next to that, other materials that are used in order to establish a fully functioning cathode system are discussed in Section 4.3.7. Finally, conclusions on the discussed cathode materials are given in Section 4.3.8.

4.3.1. TUNGSTEN

Tungsten is a simple and affordable material to be used as a directly heated cathode. Despite the fact that tungsten has poor electron emission characteristics as will be shown in a moment, the material is widely available and not expensive. In the first prototypes at Airbus [8], thermionic cathodes with tungsten filaments of incandescent light bulbs are used. These are directly heated in order to realise a thermionic emitting cathode. Initially, the cathode system configuration consists out of six tungsten filaments in light bulb emplacements close to the exit plane of the thruster. This can be seen in Figure 4.8. The electrons that are emitted from the tungsten filament follow magnetic field lines in order to enter the thruster and interact with the neutral propellant particles.

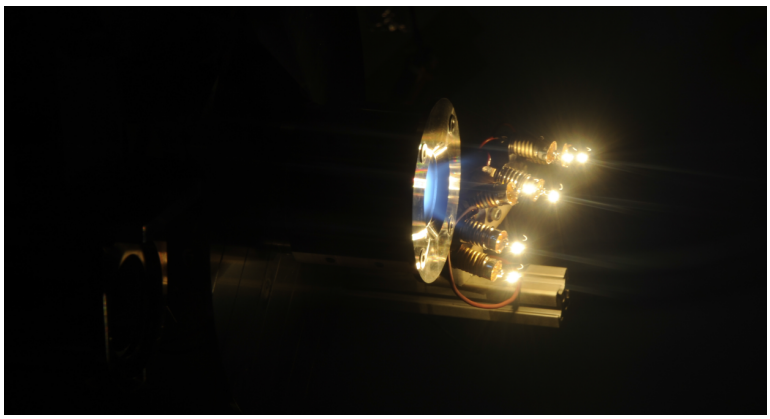

Figure 4.8: Tungsten Cathode Setup [8]

Tungsten is heated directly by the current passing through it. This cathode type does not only have a low complexity, but has high insensitivity against poisoning as well. Nevertheless, it has a high work function of 4.87 eV and therefore it needs to be heated to temperatures higher than 2600 K in order to emit a sufficient amount of electrons. In order to meet these temperatures, high heater power is required. This results in a very low efficiency with an electron emission of only 5 mA per Watt of heater power. Compared to BaO and boride cathodes efficiencies are ten to almost one hundred times smaller. Electron emission densities of around 1 A/cm^2 can be reached by operating the tungsten filaments at temperatures larger than 2600 K. In addition to that, the tungsten filaments are exposed to the ionised flow which erodes the material and limits the lifetime. The evaporation rate of the tungsten material is high and this is one of the greatest limiting factors to its lifetime. Its evaporation rate compared to other emitter materials will be shown in Figure 4.15. Exposure of the cathode to the ionised flow is a lifetime limiting factor for other refractory metal cathodes as well. Therefore, direct impingement of the ion beam on the cathode should be prevented [61, 93, 94].

4.3.2. BARIUM OXIDE

BaO dispenser cathodes are generally heated indirectly by means of a coiled tantalum sheated heather that uses a magnesium oxide powder insulation. A dispenser cathode consist out of refractory metal that contains a matrix of emitting material, e.g. BaO. The purpose of the metal matrix is to act as a reservoir from which the emitting material can diffuse electrons to the surface. Hence, an active layer with a low work function of around 1.55 eV can be maintained. BaO cathodes are able to provide sufficient amounts of electrons at temperatures lower than 1000 K. In addition to that, they are very efficient with electron emissions of 500 mA per Watt. Furthermore, due to excessive barium evaporation, the maximum achievable current density is close to 20 A/cm^2. The insulation material has a maximum operation temperature which is less than 1700 K. At this temperature, chemical reactions between the oxide insulation and the heater electrode or sheath material cause a reduction in the resistance and this ultimately can lead to failure of the heater [20, 60, 95, 96].

Nevertheless, BaO cathodes are very sensitive to poisoning. This is due to the fact that the cathodes operate by a low work function that depends on chemical reactions. This process can be easily affected by water vapour, impurities in the propellant used or handling the system in atmospheric conditions. Therefore, BaO dispenser cathodes in electric propulsion systems require an extremely high feed gas purity. This has resulted in a so called special propulsion-grade xenon that has a 99.9995% purity (five nines five). In addition to that, extensive spacecraft feed system cleaning techniques are required in order to minimise poisoning in the micro propulsion systems [1, 97].

4.3.3. LANTHANUM HEXABORIDE

LaB_6 has a bulk work function near 2.7 eV. This is higher than most impregnated cathodes which are around 2.0 eV. However, superior resistance to contamination from oxygen and water vapor is offered compared to other existing impregnated cathodes. Next to that, it does not require any special conditioning for electron emission. In order to emit electrons, this material needs to be heated to 1300 K. It is possible to operate a LaB_6 cathode at discharge currents as low as 3 A without any heater or keeper power required. In this manner, comparable flow rates and voltages to the impregnated cathodes can be achieved. The only limit to the lifetime of a LaB_6 cathode is its rate of evaporation. However, this is lower than the evaporation rates of other impregnates such as a porous tungsten emitter. The lifetime for LaB_6 emitters is an order of magnitude larger than for other dispenser cathode inserts. In addition to that, the work function of the LaB_6 emitter is not affected as the cathode materials evaporates. This is considered as a huge advantage, since it benefits to the lifetime of the cathode [1, 20, 24, 25, 98, 99].

LaB_6 hollow cathodes have a long flight heritage with applications in over 100 Russian Hall thrusters. Next to that, they are being researched in many universities as well as industry applications such as plasma sources, ion sources, arc melters, optical coaters, ion plates and scanning electron microscopes. The LaB_6 cathodes are generally used with all noble gases from helium to xenon, the reactive gases including hydrogen and oxygen and many various other materials such as the liquid metal bismuth. In addition to that, they have been successfully operated at emission current densities that exceed 20 A/cm^2 in pure oxygen as well as nitrogen plasma discharges. Furthermore, vented operating LaB_6 cathodes to water and air does not cause damage to the system [1, 100, 101].

Lanthanum hexaboride is a crystalline material that is established by press sintering LaB_6 powder into predefined rods or plates. Next, these are machined to the required shape. The polycrystalline LaB_6 cathodes have a work function of about 2.67 eV which is depended on the surface stoichiometry. In this configuration, they are able to emit over 10 A/cm^2 at a temperature of 1650 ^{o}C. Figure 4.9 gives an illustration of the LaB_6 crystalline structure. The smaller atoms (red) are boron and the larger (green) atoms are lanthanum. Since the cathode material is emitting as bulk, there is no chemistry involved in order to establish the low work function at the surface. In addition to that, the LaB_6 Cathodes are insensitive to impurities in the propellant used and the air to which the cathode is exposed during handling and operations. These poisoning contributors would be able to destroy BaO dispenser cathodes. Instead, the lifetime of LaB_6 cathodes is primarily determined by the evaporation rate of the emitter material at the used operating temperatures [23, 61, 102].

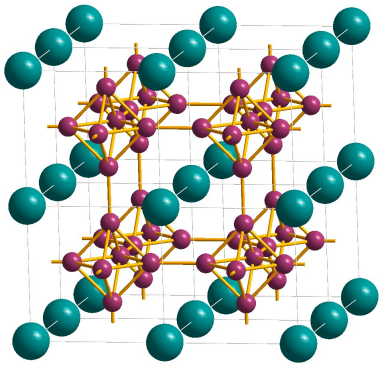

Figure 4.9: LaB_6 Crystalline Structure [23]

Lanthanum boride compounds that are heated above 1300 K in vacuum, start to evaporate their components in a rate that produces stable LaB_6. The thermionic emission of the material is described by the Richardson Dushman Equation (3.22). Nevertheless, the LaB_6 cathodes are susceptible to breakage from mechanical stress when they are clamped as well as to thermal shocks. Next to that, they need to be supported by materials that prevent diffusion of boron into the support material. This is due to the fact that boron diffusion would embrittle most of the contacting refractory metals at the higher temperatures at which LaB_6 operates. Because of these facts, they have to be supported by materials such as carbon, tantalum carbide, or rhenium in order to avoid this problem. Another solution is to create a support structure out of a material that has a lower operating temperature compared to the LaB_6 emitter. A graphite insert is also a good solution since it has a slightly larger coefficient of thermal expansion (CTE) compared to LaB_6. In addition to that, it provides good electrical contact and a low stress support and boron diffusion or boride formation is not an issue [61, 103–107].

Considering poisoning, it has already been mentioned that LaB_6 experiences very little poisoning effects. The natural substances that contribute the most to poisoning effects for dispenser cathodes are oxygen, water and other gases such as CO_2 and air. Figure 4.10 gives the the fraction of the possible thermionic emission as determined by Equation (3.25) for several partial pressures of oxygen and water. This is done for both the BaO-W (Section 4.3.5) and LaB_6 cathodes at different operating temperatures. It is important to note that the curve for water poisoning for LaB_6 cathodes is way off to the right and outside of the plotted area. From the figure it can be seen that BaO-W cathodes are strongly poisoned at partial pressures for oxygen at 10^{-6} Torr[7] and for water at pressures below 10^{-5} Torr. On the other hand, LaB_6 emitters are able to withstand larger partial pressures of oxygen up to to 10^{-2} Torr and 10^{-3} Torr, depending on the operating temperature.

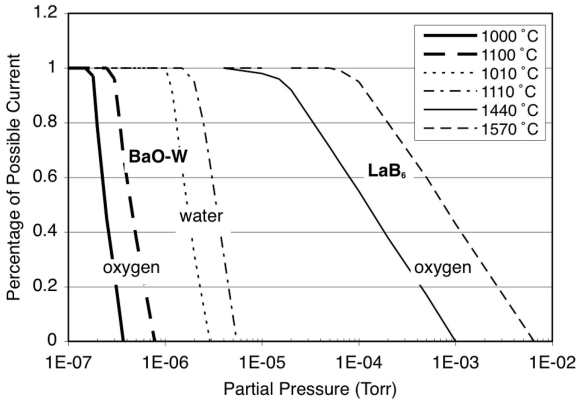

Figure 4.10: LaB_6 and BaO-W Poisoning due to Water and Oxygen [24]

This illustrates that LaB_6 cathodes are able to withstand two orders of magnitude higher impurity levels of the propellant used compared to the dispenser cathodes. It also means that they can tolerate the crudest grade of xenon that is commercially available, which is four nines pure, i.e. 99.99% xenon, without affecting the electron emission density or the lifetime of the system. Furthermore, LaB_6 cathodes do not require any conditioning, activation or purging procedures that would be required be dispenser cathodes. Hence, they are robust, have a long lifetime and are suitable for many applications [24, 60].

[7] 1 Torr = 1.33 mbar

4.3.4. CERIUM HEXABORIDE

CeB_6 has a bulk work function near 2.5 eV and could be a possible alternative to LaB_6, since it has an even lower evaporation rate. It is heated to 1900 K in order to emit electrons. With a similar cathode geometry as the a LaB_6 cathode, CeB_6 cathodes can be operated at discharge currents as low as 1.5 A without the need for a heater or keeper power. The CeB_6 cathodes show an equal resistance to poisoning compared to the LaB_6 ones and an even lower evaporation rate. Hence, their lifetime performance should be even better than the LaB_6 cathodes.

In order to investigate this D. J. Warner and R. D. Branam have tested CeB_6 cathodes with identical geometries but different insert materials, namely LaB_6 and CeB_6. The test for the CeB_6 cathode involves different operating conditions in terms of voltage, discharge current and propellant flow rates in order to investigate the mentioned lower work function by literature of 2.5 eV compared to the 2.67 eV of LaB_6. In order to start the CeB_6 cathode a potential of 500 V at 1.0 A of keeper current is required, while the heater power and the propellant flow rate are maintained at a constant level. After the ignition of the cathode, the heater can be turned off as long as the keeper current is maintained [108].

The performance of the CeB_6 cathode is similar to that of the LaB_6 cathode. This is noted by the similarity in plume mode operating conditions and the plasma densities, potentials and electron temperatures that have been measured during testing. The lower operating point of the CeB_6 cathode equals 1.5 A at a propellant flow rate of 1.5 sccm and with no heater and keeper power applied. In order to illustrate the cathode electron density of the tested LaB_6 and CeB_6 cathodes Figure 4.11 is given. The figure holds for an anode current of 4.0 A, a propellant flow rate of 4.5 sccm and with cathode heaters turned off. It can be seen that the performance of the two tested cathodes is strongly similar [25, 108].

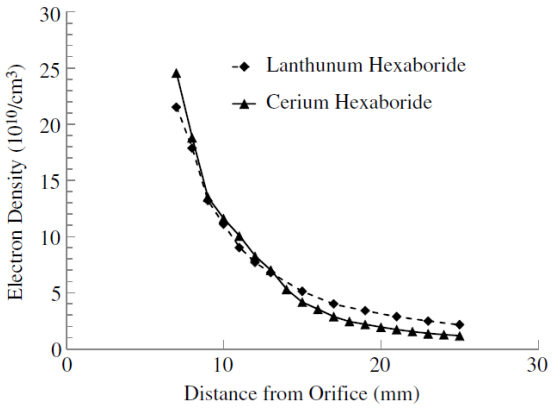

Figure 4.11: LaB_6 and CeB_6 Cathode Electron Density [25]

Nevertheless, during the test it has shown that the actual power delivered to the CeB_6 cathode by the heater is 9.0 W more than the LaB_6 cathode has received. Hence, it is possible that the CeB_6 cathode does not have a lower ignition voltage because of its lower work function but because of the larger amount of power that is received by the heater. Nonetheless, in the conducted test the CeB_6 performance deteriorates with time. For subsequent restarts of the cathode the ignition voltage needs to be increased to 650 V and the flow rates and heating times increase as well. This deteriorating performance is an indication of poisoning of the CeB_6 cathode due to trace amounts of oxygen and water vapor. This causes the work function of the emitter material to increase and next to that the cathode lower current limit increases. Hence, its performance degrades over time and can be surpassed by a LaB_6 cathode [109–111].

4.3.5. BARIUM IMPREGNATED POROUS TUNGSTEN

BaO-W has a work function of 2.1 eV. It uses a monolayer barium coating at the surface of the porous tungsten matrix in order to create a dipole with residual oxygen. In this manner, the potential barrier that the electrons need to overcome to be emitted is lowered. Since the work function is depending on a specific surface state, the BaO-W cathodes are susceptible to contamination by excess oxygen. Furthermore, the barium is able to evaporate quickly at the elevated temperatures at which the cathode operates. This limits the lifetime of these types of cathodes. The material needs to be heated to 1300 K in order to emit electrons. Due to the contamination risks, a high purity propellant gas such as e.g. 99.999% pure xenon is required [1, 25, 60, 108–110, 112].

4.3.6. CALCIUM ALUMINATE

C12A7 electride has a low reported work function, but recent research has increased the initial low reported value to a larger range of 0.6 eV - 2.4 eV [113–115]. Its work function is low in general due to its unique and charged lattice structure [116]. This low work function is comparable to those of cryptand and crown-ether-based electrides [117]. The lower work function indicates that equivalent electron emission can be obtained at lower operating temperatures. This improves the power efficiency since lower temperature cathodes lose less heat in the form of radiation heat losses that scale with T^4. C12A7 electride hollow cathodes are able to self heat from room temperature to their operating temperature as soon as they have been started by applying the proper keeper voltage and propellant flow rate. Next to that, a cathode that requires a low temperature to operate has the potential to not be only extremely efficient but also to be manufactured from low cost materials instead of refractory metals [118–121].

The C12A7 electride enables a cathode that can be started immediately from room temperature without the need for a heater. This is beneficial, since the heater is a common point of failure in various electric propulsion systems. C12A7 is a ceramic in which electrons are contained in sub-nanometer sized lattice cages (subcages) that act as conductive media. Because of the fact that C12A7 has a unique atomic structure and large size, its work function is lower than other cathode materials. The structure of the C12A7 electride is illustrated in Figure 4.12. The unit cell of C12A7 is positively charged and this is counteracted by two atomic oxygen ions O^{2-} that are floating amongst the subcages. In order to create the stable C12A7 electride, the two oxygen ions are replaced by four electrons. This can be done by various methods (3) that are described below [122–124].

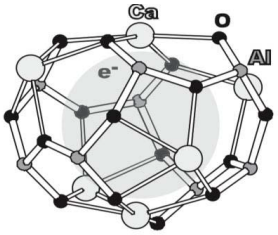

Figure 4.12: C12A7 Crystal Lattice Structure [26]

ELECTRIDE MANUFACTURING

1. **Calcium pellets -** In order to convert the C12A7:O^{2-} to the required electride form, calcium pellets are used. These are heated to a temperature of 1000 K in order to create a hot calcium vapor that is able to pull oxygen anions out of the crystalline cages. In this manner calcium oxide is formed. The conductivity (i.e. electron density) of the established electride is measured to increase in this way as it is exposed to the hot calcium. After 240 hours, the maximum conductivity and thus maximum achievable electron density of $2 \cdot 10^{21}$ is reached. Nevertheless, this method is not applicable on a large scale and the resulting calcium oxide layer that is formed on the electride's surface needs to be removed in order to complete the process [125, 126].

2. **Reduced melt -** In this synthetic method the precursors of the required electride, CaO and Al_2O_3 are heated to 1900 K in a semi-airtight carbon crucible. Next, as part of the solidification process, the reduced melt is slowly cooled to room temperature. This results in the non-conductive phase of calcium aluminate ($3CaOAl_2O_3$ + $CaOAl_2O_3$). Next, this compound is heated again to 1900 K in the carbon crucible and slowly cooled once again to room temperature. This results in the required crystalline electride [114, 122, 127, 128].

3. **Reduced melt (glass ceramic) -** This method is similar to the reduced melt method, but lets the reduced melt cool down to room temperature in a fast manner by using quenched air. This results in a clear, insulating and amorphous glass. Subsequently, the glass is heated above the crystallisation temperature of 1300 K in vacuum. Afterwards, it is slowly cooled in order to form the required electride [127].

WORK FUNCTION MEASUREMENT

Using the field assisted thermionic emission technique the work function of the obtained electride can be measured. This is done by Kim e.a. by using Equation (4.4), which is an elaborated form of the Richardson Dushman Equation (3.22). Electrons inside the crystalline energy are given kinetic energy trough a temperature increase. Using an external electric field the potential barrier at the material surface can be lowered. In this way, emitted current can be calculated as a function of the temperature T, work function ϕ and applied electric field E [60, 114].

$$J = AT^2 \exp\left(\frac{-e\phi}{kT}\right) \exp\left(\frac{e}{kT}\sqrt{\frac{eE}{4\pi\epsilon_0}}\right) \tag{4.4}$$

In this manner, a work function of 0.6 eV is measured by Kim e.a. [114]. However, Toda e.a. [115] measured a work function of 2.1 eV using the same measurement technique. It is concluded that the surface contaminants could play an important role in reducing the work function in the measurement made by Kim e.a. In different measurement techniques for establishing the work function for the crystalline electride the current emitted through photoemission is used. Photons interact with surface electrons in such a way that energy to the electrons is imparted for it to overcome the surface potential barrier and emit into vacuum (i.e. away from the crystalline structure). Photoelectron yield spectroscopy (PYS) as well as ultraviolet photoelectron spectroscopy (UPS) can be used. They will be discussed shortly below [55]. With both the PYS and the UPS measurement technique, a work function of 2.4 eV has been found by Toda e.a. [113].

1. **Photoelectron yield spectroscopy -** With PYS, the emitted current from the electride is measured as a function of the wavelength of an incident beam. Next, the square root of the emitted current is plotted versus the photon energy. Intercepting the linear trend line that fits to the data of these measurements results in the desired work function of the electride material [113, 129].

2. **Ultraviolet photoelectron spectroscopy -** With UPS, the kinetic energies of electrons that are photoemitted from an electride sample are measured. This is done when they are exposed to a fixed wavelength of ultraviolet light. Using this technique, only the electrons that are emitted through secondary electron emission are measured. This involves the electrons that are thermalised by inter-material collisions and are thus no longer dependent on binding energies within the crystalline structure. Therefore, the kinetic energies of these very electrons are only dependent on their thermal temperature distribution and the work function. By creating a electron intensity versus kinetic energy diagram and comparing that with known work functions, the work function of the electride is determined [113, 130].

In research conducted at the U.S. Naval Research Laboratory by Caruso and McDonald [131] on thermionic emission of a C12A7 electride in a close-spaced diode, the performance appears to strongly depend on operating temperature and material treatments. In testing the emission current for cathode temperatures of 700, 850, 980, 1096, and 1200 ^{o}C is measured. This is done using an anode potential that ranges from 0 V to 210 V. Surface emission increases for increasing temperatures as is expected by Equation (3.22), by about an order of magnitude per 100 ^{o}C for cathode temperatures that are higher than 850 ^{o}C at an anode potential of 210 V. First, the measurement at 1200 ^{o}C is conducted, after which C12A7 electride sample is annealed for 24 hours. Next, the measurements are taken for 700, 850 and 980 ^{o}C. Here it has been observed that at a cathode temperature of 700 ^{o}C, the emission current is fluctuating. Therefore, the C12A7 electride sample is annealed again at a temperature of 700 ^{o}C for another 20 hours. It is expected that electron emission improves after the annealing.

For the cathode operating at 700 ^{o}C, it has been discovered that the current emission density increases by more than 2 orders of magnitude after the annealing process for an anode potential of 210 V. However, for an operating temperature of 980 ^{o}C, the thermionic emission current is reduced by $1.0 \cdot 10^{-5}$ A/cm^2 for an anode potential of 10 V and by $1.6 \cdot 10^{-4}$ A/cm^2 at an anode potential of 210 V after the annealing process. As for the other cathode operating temperatures, a decreased thermionic emission after the annealing process is experienced as well. This decrease in performance may result from poisoning of the C12A7 electride cathode by oxygen or water vapor during the test campaign. Next to that, aspects such as phase transition, calcium depletion, increased sample resistance, or changes in the assembly of the diode are considered as contributors to the decrease of electron emission of the C12A7 electride after the annealing process. This again contributes to the promising, but uncertain performance of C12A7 as a cathode emitter.

In comparison with LaB_6 operation in a similar high temperature hollow cathode testbed the C12A7 electride can be operated at lower temperatures. In tests performed by Caruso and McDonald [27], LaB_6 ignition required 5.25 A of heater current and about 200 W of heating power. On the other hand, the C12A7 electride insert requires only just more than 30 W of heater power. Furthermore, steady state LaB_6 operation can be maintained with 5 A of discharge current and discharge powers in the range of 100 - 150 W. On the contrary, the C12A7 electride can be operated at discharge currents of only 150 mA and a power in the range of 21 - 27 W. If the heatsink cathode configuration is used, the C12A7 insert can be operated stable at an even lower power of 18 W. This includes the self heating mode, where no heater power is applied. Based on this performance and the area of the C12A7 insert, current densities of 20 - 40 mA/cm^2 are achievable. This places the estimated C12A7 electride performance in the region indicated in the plot in Figure 4.13 for cathode emitter performance by Goebel [132]. Hence, equal emission current densities can be achieved with the C12A7 electride as with LaB_6 at moderate temperatures. Lower temperatures are beneficial as less heater power is required and heat radiation losses can be dealt with more easily. The tests are performed in a large hollow cathode that is based on a Goebel design for use in Hall thruster. Hereby, identical cathodes are used for the LaB_6 and the C12A7 emitters [27].

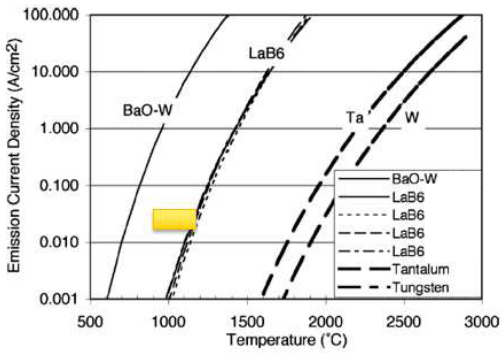

Figure 4.13: C12A7 Electride Emitter Performance (Indicated by Rectangle) [27]

In future tests with C12A7 electride cathodes it is recommended to be able to introduce oxygen and water vapor during the thermionic emission measurements. In this manner, the C12A7 can be subjected to poisoning conditions and its performance can be analysed compared to other cathodes. Furthermore, Langmuir probing is recommended in order to monitor the plasma conditions in the orifice of the cathode. Next to that, it gives information on the plasma characteristics and the performance of the cathode. Due to the durability and the low work function an instant initiation through an arc discharge method can be realised. Operating temperatures lower than 900 K have been observed in C12A7 electride hollow cathodes at low discharge currents of only 1.25 A. In order to keep the electride in its conductive form, a graphite sleeve can be integrated into the cathode. Next to that, it has been successfully operated with both xenon and iodine as propellants. Propellant compatibility will be discussed in more detail in Section 4.4 [118, 119].

4.3.7. CATHODE STRUCTURE MATERIALS

This section will elaborate on the various other materials that are used besides the emitter, in order to realise the complete cathode structure. They are listed below.

- **Aluminium -** In order to finalise the structure of the cathode or to realise an optical bench, an anode plate in diode mode testing or aluminised tape for optical properties, aluminium is used. Furthermore, it is used as general material for test equipment such as spacers, bolts and nuts. Aluminium has a high work function of about 4.1 eV and is therefore not suitable as an emitter material [33]. It is important to clean the aluminium parts from grease and volatiles using isopropyl alcohol before they are operated in the vacuum chamber. In this manner, outgassing is decreased and there are less imperfections that could affect the test setup.
- **Boron Nitride -** In order to electrically insulate the emitter from the heater and to make sure that the release electrons travel towards the anode, a boron nitride spacer is used. This material provides excellent electrical insulation, even at the high operation temperatures of 1900 K for the LaB_6 heater. Boron Nitride has a high decomposition temperature of 2800 ^{o}C in inert environments. By decreasing its thickness to only 0.5 mm, the thermal insulation is minimised so that heating can still be realised. The thermal conductivity of boron nitride equals $k = 34$ W/m·K and its thermal emissivity equals $\epsilon = 0.9$. It is important to only use pure grades of boron nitride that do not have binding agents such as oxides. This is because of the fact that these binding agents lower the melting temperature of the substance and that the oxides are able to react with refractory metals such as tungsten [45, 133].
- **Graphite -** The heater is made from graphite since it has good thermal properties. It has a high electrical resistance when compared to other metals. Therefore, its heat generation is high when a potential is applied to it. In atmospheric conditions, graphite starts to react with oxygen at temperatures of 750 K in order to initiate combustion. However, in vacuum, graphite is resistant up to 3800 K. Therefore, it is an ideal material to be used as heater. By creating a narrow and long segment in the heater, the heat generation increases. Hence, the repeating pattern shape is a characteristic of these type of heaters [134]. Next to that, material studies by Goebel e.a. [45, 132] have shown that graphite (and rhenium) have a high resistance to boron diffusion that could occur when operating LaB_6 or other boron compound emitters. This is due to the close packed hexagonal structure of the molecules.
- **Macor -** In order to thermally insulate the heated emitter from the rest of the cathode structure to prevent heat losses, macor is used. This ceramic has a low thermal conductivity[8] of only 1.46 W/m·K. Outgassing of the material is realised by performing a bake out, in which all the volatiles are released. However, the maximum use temperature is limited at 1300 K and this needs to be taken into account.

[8] http://accuratus.com/macorprps1.html | Visited on 06 November 2017

- **Molybdenum -** Molybdenum is a so called transition metal and has good electric conduction characteristics. Next to that, it is able to withstand extreme temperatures without expanding or softening. Its melting point is equal to 2896 K. Therefore, it is an useful material in applications where the heat is high such as thermionic cathodes. In one of the early concepts of the thermionic cathode at Airbus Defence and Space, it has been used in order to provide the potential application to the LaB_6 [8].
- **Silver -** In the current LaB_6 thermionic cathode at Airbus Defence and Space, silver wires are used in order to provide electrical contact from the power supply to the graphite heater. These have been used because of their availability. Compare to copper, silver has a slightly lower melting point of 1235 K with respect to 1357 K. Next to that, the electrical resistance of silver is with 1.59 mΩ slightly lower than copper, which equals 1.67 mΩ.
- **Tantalum -** Tantalum can be used both as heater as emitter material. Its properties are similar to tungsten, which means that the work function is high and that the electrical resistance is high. However, other emitter materials are more attractive due to their lower work functions.

4.3.8. CONCLUSION

Various materials that can be used in order to emit electrons have been discussed in Section 4.3. These are tungsten, barium oxide, lanthanum hexaboride, cerium hexaboride, barium impregnated tungsten and calcium aluminate. One of the main goals is to have a work function that is a low as possible. In this manner, the lowest amount of heater power is required in order to obtain a desired electron emission. Next to that, poisoning plays a very important role in the performance of the emitter. Furthermore, evaporation rate is an important aspect when one considers lifetime of the cathodes. Currently, *lanthanum hexaboride* (LaB_6) has the preference for a miniaturised low complexity, affordable and efficient cathode at Airbus. This is because of the fact that it has a decent work function, little sensitivity to poisoning and a low evaporation rate (i.e. a long lifetime).

In order to compare the performance of the LaB_6 current density emission versus the other emitters discussed in this section, it is interesting to plot the emission current density against the temperature. This has been done in Figure 4.14. Furthermore, it can be seen from Figure 4.14 that LaB_6 operates at higher temperatures than the BaO-W dispenser cathode in order to obtain the same emission current density. Next to that, the LaB_6 temperature is higher than other typical refractory metal emitters that are used for cathodes in micro propulsion systems. Using a LaB_6 cathode, emission current densities of 20 A/cm^2 for a total of 60 A of emission current at a operating temperature of 1700 ^{o}C can be achieved. Hence, this type of cathode can be operated at low discharge currents, which is favourable for miniaturisation [1, 25].

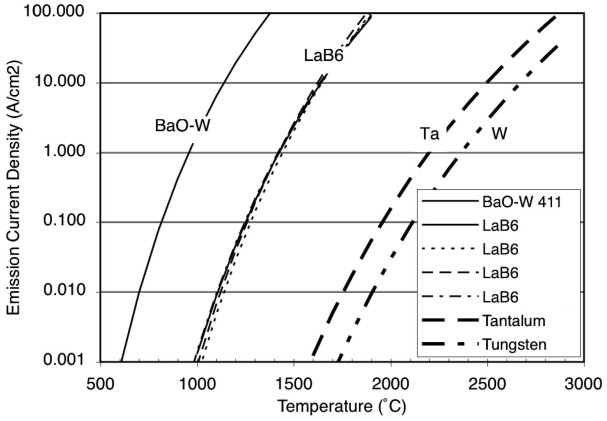

Figure 4.14: Emission Current Density vs. Temperature [1]

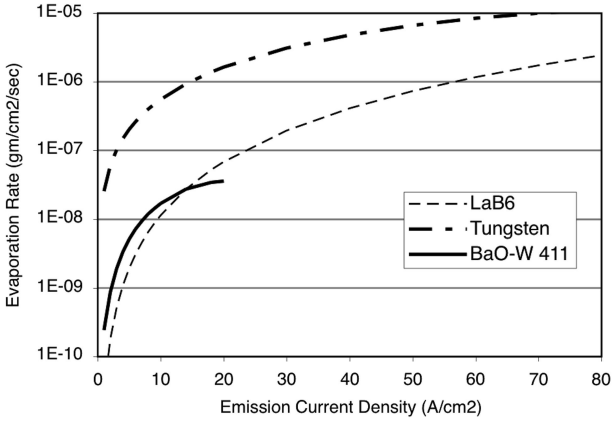

Figure 4.15: Evaporation Rate of LaB_6, Tungsten and BaO-W [28]

Furthermore, it is interesting to look at the evaporation rate of the mentioned emitter materials in Section 4.3. These are illustrated in Figure 4.15. Lanthanum hexaboride has a long lifetime because the evaporation rate is low. This can be seen in Figure 4.15. Its evaporation is even more than one order of magnitude lower than tungsten for the same current density. Until about 15 A/cm^2 emission current density, LaB_6 has a lower evaporation rate than the impregnate material that is used in dispenser cathodes. Hence, the LaB_6 cathodes do not only have a longer lifetime than dispenser cathodes because there is more material in the bulk LaB_6 than in the impregnated pores, but also because the evaporation rate is lower or at least comparable for emission current densities up to 20 A/cm^2. In addition to that, as the emitter material evaporates the inner diameter increases and so does the surface area. In turn, this causes the operating temperature and the required current density to decrease for a given discharge current. Subsequently, this causes the evaporation rate of the cathode insert to be reduced [28, 103].

4.4. PROPELLANT COMPATIBILITY

This section elaborates on the propellants that are being used in electric micro propulsion systems. Xenon is a good performing noble gas that is used in many applications and will be discussed in Section 4.4.1. Furthermore, krypton and bismuth have interesting characteristics that promise to be suitable as an electric thruster propellant. They are dealt with in Sections 4.4.2 and 4.4.3 respectively. Next to that, iodine proves to be very promising for CubeSat applications and will be treated in Section 4.4.4. Finally, Section 4.4.5 gives conclusions on the discussed propellants for electric thruster systems.

4.4.1. XENON

Many electric thrusters from nowadays operate on the noble gas xenon. It is inert, has a large atomic mass of 131 u and and a relatively low ionisation potential of 12.1 eV [33]. Hence, it does not degrade over time or corrode with any other systems of the spacecraft. In addition to that, xenon is not hazardous to handle and process. Next to that, with the possibility to be stored as a gas, there is no energy required in order to vaporise the propellant. However, xenon must be stored in either high pressure tanks or at cryogenic conditions, which adds weight to the system.

Furthermore, because of the low ionisation energy of around 12 eV, it requires little energy in order to ionise the neutral xenon particles in the discharge chamber. Being heavy, the impulse that can be acquired per unit volume of the propellant is high, which benefits to the thrust. This is explained in Section 3.1 in more detail. Therefore, xenon is a suitable candidate in many electric propulsion systems. Nevertheless, the high pressure storage does not allow for applications on CubeSats to be realised, as here high pressure propellant storage systems are not allowed by launcher requirements. In addition to that, xenon has a low concentration in the atmosphere, which causes worldwide xenon production to be limited to as much as 6000 m^3 per year. Because of this limitation and the increasing industrial demands for items that use xenon such as high efficiency lighting and windows, as well as plasma based micro fabrication systems, the xenon price varies a lot and can rise high [135].

4.4.2. KRYPTON

Krypton is another noble gas and has been examined to serve as an alternative to xenon. It has a lower atomic mass than xenon at 83.3 u (compared to 131 u), but the ionisation potential is slightly higher with 14.0 eV (compared to 12.1 eV for xenon) [33]. Being a noble gas, it can be easily implemented into various existing Hall effect thruster propellant feed systems, without the need for many modifications. However, the storage density of gaseous krypton is lower than xenon because of the higher critical temperature. Because of the lower storage density and the fact that krypton has a lower efficiency because of lower ionisation cross section and lower residence time, krypton is not commonly used in electrostatic thrusters.

Krypton has been tested by Nakles e.a. in the SPT-100 Hall thruster in comparison to xenon and it has been found that the thruster performance is lower than when it is operating on xenon. The SPT-100 operates nominally at a discharge voltage of 300 V and a discharge current of 4.5 A. In this manner, it produces 82 mN of thrust at an I_{sp} of 1600 s. The total efficiency is 50% averaged over the lifetime of the thruster [20]. Figure 4.16 gives an illustration of the flight model SPT-100 Hall thruster. Next to that, Figure 4.17 shows it in operation with xenon, whereas Figure 4.18 shows it in operation with krypton. In these figures, the distinctive propellant colours can be seen, as charged particles radiate as they accelerate.

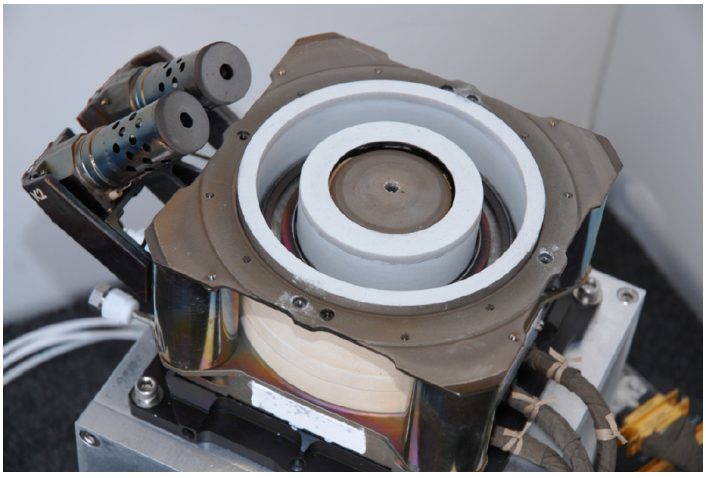

Figure 4.16: SPT-100 Hall Effect Thruster Flight Model [5]

Furthermore, in the performed tests it has been found that krypton does not provide a specific impulse that is substantially higher than that of xenon. Therefore, krypton would not be a propellant choice in order to realise mass savings. In addition to that, it has been found that the overall thruster efficiency when operating on krypton is 8% lower than when operating at xenon at the nominal operating condition. Thruster efficiency could be increased by increasing the power conditions, however this affects the life time of the system as a whole. Nevertheless, krypton is a very cost beneficial propellant as the price by mass is six times lower compared to xenon. Therefore, it remains a feasible alternative propellant to xenon (for the SPT-100), if the xenon propellant prices would dramatically increase in the future [5, 136, 137].

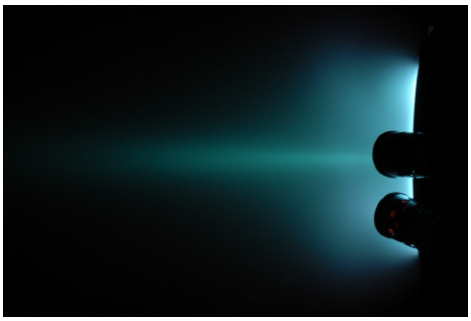

Figure 4.17: SPT-100 Operating on Xenon [5]

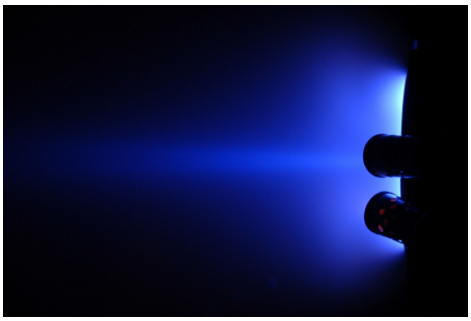

Figure 4.18: SPT-100 Operating on Krypton [5]

4.4.3. BISMUTH

Bismuth has a high atomic mass of 209 u and a low ionisation energy of 7.29 eV. In addition to that, it has a high density of 9780 kg/m^3 [33]. Because of these characteristics, it could be an interesting propellant for electric thruster applications. However, the boiling point is high at 1837 K. In order to realise vapor pressures of 100 Pa, a temperature of 1165 K is required. Because of these reasons, after extensive research, bismuth is generally not implied in electric thrusters. The high temperatures that are required in order to realise a functional propellant feed systems can only be realised using a lot of heater power. Moreover, a propulsion system that operates on bismuth has the risks of coating the spacecraft with a low vapor pressure metal that could have disastrous effects for the mission as a whole.

4.4.4. IODINE

High pressurised systems on secondary payloads such as CubeSats are not permitted because they are dangerous to the primary payload. All flight hardware pressure systems that have a operating pressure of more than 100 psi (6.89 bar) are classified as hazardous. Qualification for these systems on CubeSats would be time and cost consuming. Because of the fact that high pressure systems for secondary payloads such as CubeSats are typically not permitted by the primary launch customer, alternative propellants than xenon gas are investigated for the use in micro propulsion systems. The propulsion systems that are used on CubeSats make use of low pressure tanks, or have the propellants stored in their liquid or solid form. Hence, there is a need to find a suitable propellant that meets these requirements. The propellant iodine is considered suitable to be able replace xenon [4, 19, 138, 139].

Iodine is a propellant that can be stored as a solid granulate. In this manner, a high pressure system that is both hazardous and high weight is not required for a micro propulsion system. It has a similar atomic mass as xenon and next to that, the ionisation levels are similar to xenon as well. Iodine has an atomic mass of 126.9 u, but as halogen the natural state is diatomic (I_2). This means that the molecular mass is equal to 253.8 u. Atomic iodine has an ionisation energy that is equal to only 10.45 eV. Next to that, iodine has a relatively high vapor pressure at low temperatures. It is possible to achieve vapor pressures at a pressure of 100 Pa at temperatures of 39 ^{o}C. Thus, iodine has the characteristics that the atomic mass is comparable to xenon, while the ionisation potential is lower. This makes it an interesting solution for many spacecraft applications [135].

Furthermore, iodine can be obtained at a fraction of the price of xenon. It is more than 100 times less expensive compared to xenon and next to that it is also more abundant. In addition to that, iodine could offer the advantages of cryogenic propellant storage without the need for active cooling or insulation systems. The iodine propellant can be vaporised by heating the propellant. For this only a slight amount of heater power is required as 183 ^{o}C is able to generate an iodine pressure of 1 atm. By controlling the heater power the evaporation rate and thus the mass flow can be regulated. With this principle, the tank volume can be reduced by 50% compared to a xenon propellant tank and moreover, no pressurised tanks are required. Using iodine as a propellant, simple and compact micro propulsion systems for CubeSats can be realised. In addition to that, the ΔV that can be realised for e.g. a 1U iodine propulsion unit in a 12U CubeSat is more than 5 km/s. This is illustrated in Figures 4.19 and 4.20 [4, 29, 31, 140–142].

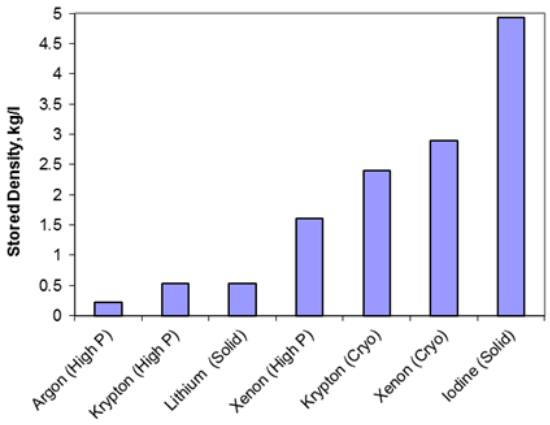

Figure 4.19: Iodine vs Alternatives [29]

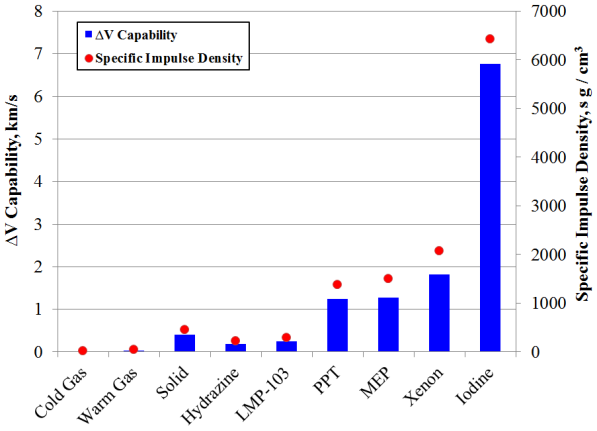

Figure 4.20: Cold Gas vs Noble Gas vs Halogen Propellants [29]

Researchers at Busek [31] have conducted iodine compatibility tests on electride hollow cathodes. This includes the development of an iodine propellant feed system. The feed system consists out of a heated iodine reservoir that is operated with a pressure transducer in order to be able to quantify the approximate flow rate. In this feed system all the feed lines between the propellant reservoir and the cathode are heated in order to prevent iodine condensation. Next to that, the reservoir is weighed at each day that test operations are conducted in order to be able to establish a flow rate calibration curve from the measured reservoir propellant weight and pressure. The C12A7 electride cathode has been successfully started using iodine propellant at room temperature without the use of a heater. Subsequently, it has been operated for close to 20 hours without any signs of electride degradation or contamination e.g. in the form of iodine deposition in the feed system. These 20 hours of testing included restarts of the cathode and exposure to atmosphere. Operations included constant iodine flow rates of 13 sccm and discharge currents ranged from 3 to 15 A. Figure 4.21 shows the C12A7 electride cathode in operation using iodine as propellant.

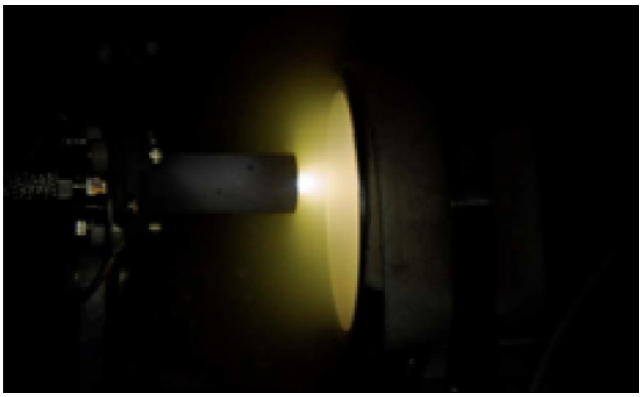

Figure 4.21: C12A7 Electride Cathode operating on Iodine [30]

Due to the halogen nature of iodine compared to xenon, the increased reactivity it brings along is initially concerning. This is especially the case when the use with Ba-W hollow cathodes is investigated. Nevertheless, the resistance to contamination for a electride hollow cathode is observed to be very high. In addition to that, there are no increasing difficulties in restarting the cathode in the tests that are conducted by Busek e.a. Nonetheless, it is in these tests that a black discoloration is observed on the outer surface of the tantalum cathode barrel and the exposed stainless steel nuts. Next to that, the tantalum radiation shielding is discoloured and damaged. This is due to the fact that iodine is reacting with the cathode structure in order to form iodine compounds. Figure 4.22 gives an overview of iodine vapor interaction with commonly used cathode materials. Iodine reacts with the tantalum cathode barrel in order to form tantalum pentaiodide (TaI_5). In addition to that, iodine is well known to be react with stainless steel at temperatures starting from room temperature. This explains the discoloration on the stainless steel nuts on the cathode structure [143, 144].

Iodine Vapor Literature Search

A literature search for iodine vapor interaction found two sources that qualitatively and in some cases quantitatively documented the resistance of various materials to iodine.

Systems	Metal or Alloy	Base Elements	Dry Iodine Vapor @ 25 °C	Dry Iodine Vapor @ 100 ° C	Dry Iodine Vapor @ 300 °C, 0.53 atm (Corrosion Rate mm/year)	Dry Iodine Vapor @ 450 °C, 0.53 atm (Corrosion Rate mm/year)
Nickel Alloys	Pure Nickel	Ni	Resistant	Resistant	0.27	1.2
	Inconel 600	Ni-Cr-Fe	Resistant	Resistant	0.107	0.54
	Inconel 625	Ni-Cr-Mo	Resistant	Resistant	0.057	No Data
Noble Metals	Pure Platinum	Pt	Resistant	Resistant	0	0.006
	Pure Gold	Au	Resistant	Resistant	0	0.024
Refractory Metals	Pure Tungsten	W	Resistant	Resistant	0	0.008
	Pure Molybdenum	Mo	Resistant	Resistant	0.003	0.033
	Pure Tantalum	Ta	Resistant	Resistant	0.005	0.88
Aluminum	Pure Aluminum	Al	Unusable	Unusable	Unusable	Unusable
Copper Alloys	Pure Copper	Cu	Resistant	Unusable	Unusable	Unusable
	Brass	Cu-Zn	Resistant	Unusable	Unusable	Unusable
Iron Allloys	Iron, Cast Iron, Steel	Fe	Resistant	Unusable	Unusable	Unusable
	Enamelled Cast Iron	Fe + Duran or Pyrex	Resistant	Resistant to 200 °C	Unusable	Unusable
	316 Stainless Steel	Fe-Cr-Ni	Resistant	Resistant	0.4 Est.*	2.1
	304 Stainless Steel	Fe-Cr-Ni	Resistant	Resistant	0.6 Est.*	3.2

* Estimated corrosion rate at 300 °C based on extrapolation from 450 °C data

Figure 4.22: Iodine Vapour Reactivity [29]

J. Szabo e.a. [31] have conducted iodine exposure tests on cathode materials. On most of them, as illustrated in Figure 4.22, the iodine deposition on the tested samples is minor or non-existent. However, on magnet iron the reaction is highly visible. This is illustrated in Figures 4.23 and 4.24, which show the magnet iron exposed to xenon and iodine respectively. One way to mitigate these reactions on the iron is to coat them with nickel in order to protect the iron. Nickel samples have shown to not form a lot of corrosion except for some minor discoloration. This is illustrated in Figures 4.25 and 4.26 for xenon and iodine exposure respectively.

With these conducted tests there remain two important aspects to keep in mind. The first one **1)** is to take the reaction time into account. Whereas material samples have been tested for several tens of hours and no reactions have been observed, space missions generally last longer than this with a couple of years and reactions after long periods thus remain important. The second aspect **2)** is that the sample tests are conducted in a vacuum chamber. This gives iodine particles the chance to reflect from the chamber walls and to interact with the samples, whereas in space they would only travel away from the spacecraft system. Hence, it is expected that reaction rates are lower in space than in the test environment.

Furthermore, iodine deposition on spacecraft surfaces is not expected because of the high vapor pressure of I_2 at the expected spacecraft temperatures. Hence, a C12A7 electride cathode with the use of iodine as propellant appears to be a promising solution for micro electric propulsion systems. In addition to that, LaB_6 has been successfully operated with iodine propellant as well. The only downside of LaB_6 compared to C12A7 is that more heater power is required in order to initiate a discharge [138, 145, 146].

Figure 4.23: Magnet Iron exposed to Xenon [31]

Figure 4.24: Magnet Iron exposed to Iodine [31]

Figure 4.25: Nickel exposed to Xenon [31]

Figure 4.26: Nickel exposed to Iodine [31]

In order to minimise the reflection of iodine particles from the vacuum chamber walls and to be able to better understand the weak points regarding iodine corrosion and crystal growth in the test facility, iodine compatibility research for the High Efficiency Multistage Plasma Thruster is performed at Airbus by Papendorf e.a. [4]. After iodine is heated in its propellant tank and extracted by means of sublimation, the possible problem of deposition occurs in which crystals can grow on components in the test facility that can affect their performance. As an example, an iodine crystal that exists within the bearing of the turbopump can cause a faster wear out. Another example is the reflectivity of a mirror that can be affected by iodine crystal formation on its surface. There exist several mitigation techniques that can be applied in order to minimise forms of iodine corrosion. They are shorty described below.

- **Material selection -** First of all, it is recommended to not use different refractory metals such as tungsten or molybdenum for the cathode barrel and radiation shielding parts as they would still react with iodine at the higher operating temperatures. Instead, one could opt to use a graphite barrel with grafoil or platinum radiation shielding. In this manner, the graphite part will be able to adsorb and desorb iodine with certain temperature fluctuations but reactions or corroding is prevented.

  This can be realised by manufacturing a graphite cathode barrel and orifice plate and by covering the orifice plate at the downstream location with a platinum plate. The purpose of the platinum plate is to prevent discharge arcs occurring between the graphite part and the keeper in cathode starting processes. A downside of this solution however is the fact that graphite erodes and deforms. Therefore, the platinum plate can be used in order to mitigate this problem. Platinum will corrode due to the iodine vapor at some point in time, but this process occurs at a rate of more than 150 times slower compared to tantalum.

- **Boxing -** If shielding with iodine resistant materials is not possible, e.g. on mirror surfaces, then boxing can be used. In this technique iodine contact between materials is avoided by using physical barriers. One can think of boxes that have small vents or holes. Nevertheless, for gaseous iodine this remains difficult.

- **Barrier gas -** Furthermore, a barrier gas can be used in order to realise a permanent gas flow alongside iodine sensitive components. This is helpful for e.g. bearings in turbopumps that are located in high pressurised areas. On the other hand, this method could induce artificial gas leakages that could increase the pressure in areas where it is not desired.

- **Designing for deposition -** Deposition of iodine vapour can be lowered if the pressure in the control volume is kept below the iodine gas pressure curve. In this manner, the iodine remains gaseous. The iodine vapour pressure versus temperature can be seen in Figure 4.27. It also illustrates the melting point at 1 bar pressure at T_{solid} = 113.7 ^{o}C and the boiling point at T_{liquid} = 184.4 ^{o}C. On the other hand, one can also opt to let deposition occur, but in a controlled way. Deposition can be realised by letting the pressure and temperature lie above the curve given in Figure 4.27. This has been realised in a design by Papendorf e.a. [4] by means of a liquid nitrogen (LN2) cooled cold plate, which can be put after the exit of the electric thruster.

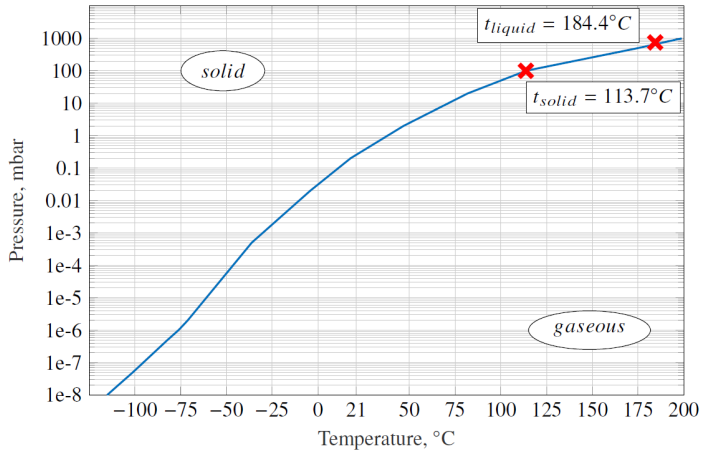

Figure 4.27: Iodine Vapour Pressure vs. Temperature [32, 33]

- **Chemical reaction -** Another way of preventing iodine deposition is to let the iodine vapour particles react with a protector element. In order for this to be realised, a material needs to be used that has a good reactivity with iodine. Next to that, this material needs to remain intact after the reaction has taken place in order to minimise outgassing and fragmentation. Only in this way, it can be assured that the iodine particles do not affect the test facility.

In the test facility at Airbus, this has been realised by installing a cold trap in the vacuum line between the turbopumps and the forestage pump. It consists out of a spiral stainless steel tube, which is surrounded by LN2. In this manner, the iodine vapour will condense on the inner walls of the spiral. Next, it is filtered from the gas flow towards the forestage pump. Despite the fact that stainless steel has a bad compatibility with iodine, as given by Figure 4.22, it can be easily realised and also replaced. However, it does require cleaning with isopropyl alcohol in order to dissolve the condensed iodine. This cleaning method is recommended, since iodine has a good solubility in alcohol [33].

In addition to that, copper wool is installed in the tube that enters the rotary vane pump. This part acts as a reactive filter in order to let the iodine vapour chemically bound to the copper. Copper proves to be a suitable candidate in this application because of the fact that copper iodine (CuI) crystals keep on forming at pressures as low as 0.3 mbar [147]. The method has been validated by both visual inspection and weighing the copper wool part prior and after iodine thrusting operations. Figure 4.29 gives an illustration of the copper wool with residual iodine (white CuI crystals) after an iodine thruster test.

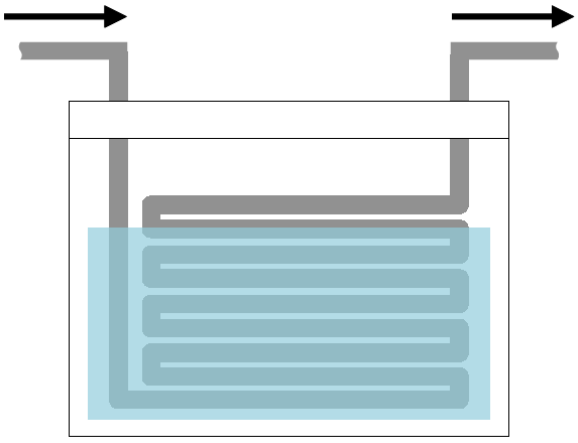

Figure 4.28: LN2 Cooled Cold Trap [4]

Figure 4.29: Copper Wool with Residual Iodine [4]

With the necessary measures taken in order to protect the test facility at Airbus from iodine corrosion, it has been found that traces inside the vacuum chamber are negligible. This is due to the fact that the temperature and pressure conditions are far away from any of those that could allow for iodine deposition. This has been verified by performing wiping tests with isopropyl alcohol paper tissues that showed no traces of iodine. On the cryopump however, iodine deposition does occur. This is due to the low temperatures (- 230 ^{o}C) on which the pump operates. Figure 4.30 clearly shows the distinct purple colour of iodine crystal formation on the first stage shield of the cryopump. Next to that, the removed first stage shield can be seen in Figure 4.31 and at this point the iodine has reacted with the metal. The reactants can be wiped easily, but pitting corrosion on the stainless steel parts remains [4].

Figure 4.30: Iodine Crystals on Shield of First Stage Cryopump [4]

Figure 4.31: First Stage Shield Iodine Reactants Cleaning [4]

In a similar way, iodine deposition has been found at the cold trap and, as has been shown, in the copper wool as well. In the case of long tests where a lot of iodine is used, the deposited iodine crystals could block the vacuum line and affect the test facility performance. In the worst case, the pressure in the vacuum lines increases by that much to the point where the turbopumps shut down due to overload. In order to prevent this from happening in the future, the forestage pump is replaced by a pump that is able to handle corrosive gases. In this manner, the cold traps and the copper wool trap are no longer required. This reduces system complexity and effort by means of no longer having to refill the cold trap with LN2 during testing and replacing the copper wool after testing.

As for the other parts of and in the test facility that have been exposed to iodine, the research performed by Papendorf e.a. [4] elaborates on compatibility from a material point of view. Whereas Dankanich e.a. [29] mention that aluminium and iodine are unusable together because of oxidation effects, reality proves otherwise. Instead, it strongly depends on the operating conditions. The outcome of the tests with aluminium iodine propellant tanks has been thoroughly positive. Aluminium has been exposed to iodine for 40 hours, from which eight are in heated conditions. After this period, no major corrosion is observed. The only aspect that needs to mentioned is that there occurs a discolouration of the aluminium on its surface. However, this can be wiped away easily by using isopropyl alcohol. Therefore, one needs to take care when using aluminium and iodine together, but mentioning them unusable would be an exaggerated term. If the iodine deposited aluminium parts are exposed to atmospheric conditions, moisture is attracted and this speeds up the oxidation process. The same thing happens with carbon steel and stainless steel parts. Therefore, care needs to be taken when handling them (together with iodine) outside of vacuum conditions. A summary of the investigated compatibility of various materials with iodine is given in Table 4.5 [4].

Table 4.5: Iodine Material Compatibility [4]

Metals	Assessment	Reference	Polymers	Assessment	Reference
Aluminium	Not recommended	[148–150]	ABS	Not recommended	[148]
Brass	Not recommended	[138, 147]	Epoxy	Excellent	[148, 149]
Copper	Not recommended	[138, 147]	Kapton	Excellent	[151]
Gold	Excellent	[138]	PEEK	Fair	[152]
Hastelloy C	Good/Excellent	[138, 148–150]	Polyamides/Nylon	Not recommended	[147–150]
Inconel	Good/Excellent	[138, 147]	Polyacetal/POM	Not recommended	[148–150]
Nickel	Good	[138, 147]	PPE/Noryl	Excellent	[148, 149]
Platinum	Excellent	[138, 153]	PTFE	Excellent	[148–150]
Stainless steel	Fair	[148–150]	PVC	Not recommended	[148, 149]
Carbon steel	Excellent	[138, 148, 150]	-	-	-
Titanium	Excellent	[148, 149, 154]	-	-	-

From Table 4.5 it can be seen that the nickel-base alloys such as Hastelloy C and Inconel have a good compatibility with iodine. These materials are often used in corrosive and high temperature environments such as turbines. The compatibility of steel, dependent on the type, is not good with iodine. This corresponds with the reference given in Figure 4.22. In the research performed by Papendorf e.a. [4] it has also been shown that iodine easily reacts with steel components. Carbon steel provides a better compatibility however, as its carbon percentage is higher. Titanium is an even better compatible metal with iodine.

As for the polymers, compatibility widely varies. Acrylonitrile Butadiene Styrene (ABS) is a 3D printed material that is used in order to mount the iodine propellant tank in the research performed by Papendorf e.a. [4]. It has been found that the use with iodine is not recommended. Polymers such as Polyether ether ketone (PEEK), a good thermal resistor, Polyphenylene ether (PPE) and Polytetrafluoroethylene (PTFE, teflon) have good compatibility, whereas other polymers such as Nylon, Polyoxymethylene (POM, an easy machinable polymer) and Polyvinylchloride (PVC, plastic tubing) are not recommended to be used with iodine.

Considering the parts that are used for the cathode system, it is in general recommended to store them in nitrogen purged bags or other nitrogen rich environments. Here, oxygen levels and low and in this manner, oxidation and contamination risks are minimised and the quality and performance of the cathode can be ensured. Furthermore, it is important to use organic cleansing solvents such as isopropyl alcohol on components that are in direct proximity to the emitter material in order to prevent contamination by outgassing. In this manner degradation in performance of the emitter material is reduced.

4.4.5. CONCLUSION

There exist various propellants that can be used for electric thruster systems. The main ones that are discussed and their properties are listed in Table 4.6. According to the thrust Equation (3.4) it is desired to have a propellant with a large ion mass. Therefore, heavier propellants are able to generate more thrust in electric thrusters for an equal amount of power. In addition to that, it is desired to have a low ionisation potential, so that neutral particles can be ionised with as little energy as possible. Xenon is generally the most used propellant since it has a large atomic mass and a relative low ionisation potential. Next to that, because of its inertness the contamination and handling aspects do not create problems. For CubeSat and other (future) applications, iodine proves to be a promising propellant since it can be stored as a solid granulate and it does not require any pressurised propellant tanks. However, its contamination to other satellite components needs to be taken into account.

Table 4.6: Characteristics Discussed Propellants for Electrostatic Thrusters [5]

Parameter	Xenon	Krypton	Bismuth	Iodine
Atomic mass [u]	131.3	83.8	209	126.9
1st Ion. pot. [eV]	12.1	14.0	7.3	10.5
2nd Ion pot. [eV]	21	24	16.7	19.1
Stable Isotopes	9	1	1	1
Odd Isotopes	2	1	1	1
Density (@ 207 bar)	1.11	0.91	9.78	4.93
100 Pa Temperature [K]	103	177	1165	312

Furthermore, the noble gas radon could be an excellent propellant. It has a large atomic mass of 222 u and a first ionisation potential[9] of 10.75 eV. However, it is typically not used because of its intrinsic radioactivity. Next to that, it decays quickly (it has a half life of only 4 days, which does not make it very practical as a propellant) and moreover, it is even more scarce than xenon. Finally, the resource costs are very high. Therefore, it is not a suitable propellant for electric thruster applications and it is not discussed further here [155, 156].

[9] `https://chemglobe.org/ptoe/_/86.php` | Visited on 14 November 2017

4.5. CURRENT STATE μHEMPT THRUSTER AND CATHODE

This section elaborates on the current state of the μHEMPT thruster and its cathode. The down scaled version of the μHEMPT is designed to be implemented on a 3U CubeSat structure and to provide a thrust of 20 - 100 μN. The total efficiency of the thruster system is currently low with 3 - 7 % and leaves room for improvement. It can be e.g. increased by focusing the emitted ions along the main thrust axis and thereby increasing the divergence efficiency. The μHEMPT is currently under development and being improved throughout. The current characteristics and the targeted onces of the μHEMPT are summarised in Table 4.7 [7].

Table 4.7: Current μHEMPT General Characteristics [6] [7]

Parameter	Symbol	Operating Range	Targeted Range
Mass flow [sccm]	$\dot{m}$	0.2 - 0.4	< 0.2
Anode potential [V]	U_{anode}	155 - 1200	> 500
Anode current [mA]	I_{anode}	1 - 10.8	1 - 15
Thrust [μN]	T	55 - 75	20 - 100
Specific Impulse [s]	I_{sp}	155 - 326	> 1000
Power To Thrust Ratio [W/mN]	$PTTR$	24 - 67	< 65
Divergence efficiency [%]	η_{div}	57 - 64	> 80
Total efficiency [%]	η_{tot}	1 - 3	> 10

Considering the thermionic LaB_6 cathode, the key parameters of the operation point of the latest functioning cathode test are listed in Table 4.8 [8]. In order to realise the targeted values in Table 4.7, the goal is to obtain an emission current of 10 mA. The next design iteration will consist out of a round LaB_6 insert that has a diameter of 3 mm and a height of 2 mm. It can be seen in more detail in the technical drawing in Appendix A.5. It is heated by a graphite heater that provides heat through conduction to the emitter material. The dimensions of the graphite heater can be seen in Appendix A.1. In order to electrically insulate the heater from the emitter, a boron nitride spacer is used. This part has a thickness of only 0.5 mm in order to allow machining and to provide as little thermal resistance between the heater and the emitter as possible. The spacer is shaped as such so that it fits exactly within the heater and is able to house the cylindrical LaB_6 emitter. It can be seen in more detail in Appendix A.2. Furthermore, macor discs are used in order to house the heater legs and to thermally insulate the heated part from the rest of the structure. The technical drawing of the macor top and bottom discs can be seen in Appendices A.3 and A.4 respectively. In this manner, the cathode can be assembled. This can be seen in Figure 4.32.

Table 4.8: Current μHEMPT Cathode Characteristics [8]

Parameter	Symbol	Value
Input Current	I	17.76 A
Total input power	$P_{in,tot}$	87.6 W
Cathode power	$P_{in,cat}$	62.7 W
Cathode resistance	$R_{cathode}$	198.8 mΩ
Cabling resistance	$R_{cabling}$	87.9 mΩ
Emitter temperature	T_{emit}	1269 K
Anode potential range	U_A	0 - 3000 V
Minimum saturating anode potential	$U_{A,sat}$	2000 V
Saturated emission current	$I_{A,sat}$	163 μA
Saturated emission current density	$J_{A,sat}$	679 μA/cm^2

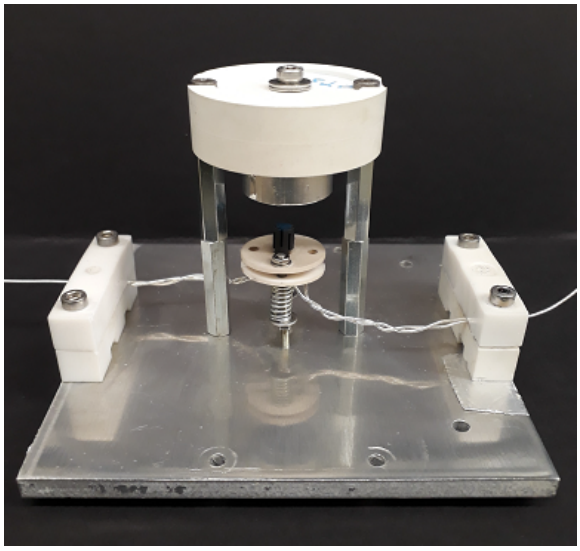

Figure 4.32: Illustration Test Setup

Previous cathode tests at Airbus have shown that current only flows between the emitting cathode and the anode if the LaB_6 emitter is electrically insulated from the graphite heater. Otherwise, it would be possible for the emitted electrons to flow into the heater circuit and travel towards the heater ground. Hence, the boron nitride spacer has been realised. This material provides good electrical insulation throughout the entire temperature range at which the cathode is operated. As shown in Table 4.8, there exist some losses in the connecting wires to the heater in the form of cable resistance. This can be solved for by using low loss large cross sectional area electric wires.

It is important to mention that as graphite belongs to the group of thermistors, its electrical conductivity increases as the temperature increases. In other words, this means that its resistances decreases as the temperature increases. Hence, the current that is required to heat the graphite increases as the temperature requirements go up. This is valid until a temperature around 700 ^{o}C, after which the electrical resistivity for graphite starts to increase again. This is illustrated in Figure 4.33, that plots the electrical resistivity versus temperature of POCO graphite [34]. These values fall into the range of most conventional graphites. In the performed cathode tests, the LaB_6 emitter starts to glow at a cathode power of 9 W. The glowing indicates that the sufficient temperatures of the emitter are met in order to establish electron emission [8, 157].

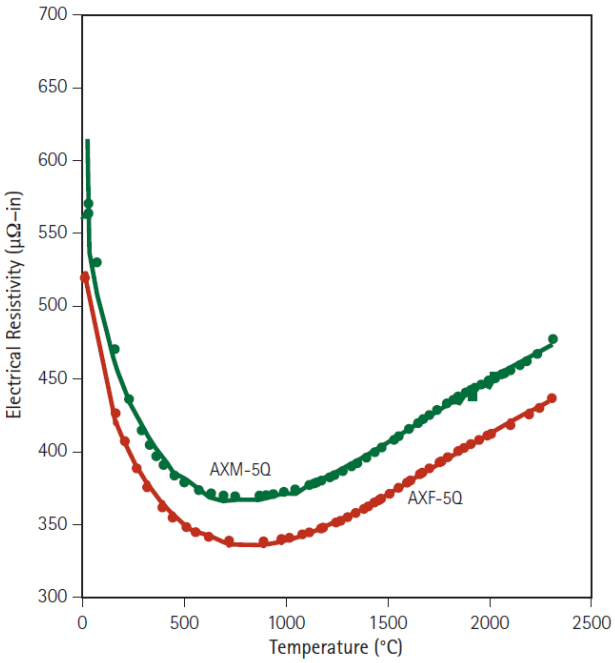

Figure 4.33: Electrical Resistivity vs. Temperature for POCO Graphites [34]

Currently, the current flow between the cathode and the anode is limited by Richardson law, as described by Equation (3.22) in Section 4.3. This indicates that the emitted current from the LaB_6 approaches the threshold value of a maximum amount of electrons that it is able to emit. With an applied anode potential of 2000 V, the emitter current equals 163 μA. Taking the LaB_6 surface area into account, this relates to an emission current density of 679 $\mu A/cm^2$. This is several orders lower than the ideal emission current density of 2.677 mA/cm^2 as determined with Equation (3.22). This is due to outgassing of surrounding materials in the vacuum that affect (deposit) the emitter material. Next to that, previous sputtering attempts on the emitter surface affect it as well. These values are summarised in Table 4.8.

In the next iteration, the goal is to reuse the graphite heater, but in a modified fashion. By decreasing the thickness of the heater, the heat output can be increased for equal input currents. Next to that, the thickness of the boron nitride spacer will be reduced to 0.5 mm. In addition to that, its total surface area will be reduced in order to minimise heat radiation losses. This is realised by letting the boron nitride spacer having the same length as the heating part of graphite heater, i.e. 6 mm. These updated components can be seen in Appendix A and will be used in order to perform the next LaB_6 thermionic cathode tests. These test will indicate whether a thermionic cathode will be a feasible solution to realise an efficient, low complexity and affordable micro electric thruster. Next to that, tests will be conducted in which iodine acts as the propellant. In addition to that, the possibility for a (hollow) LaB_6 thermionic cathode with a tungsten / rhenium filament heater will be investigate. Furthermore, a look will be taken into the possibility of realising a C12A7 hollow cathode.

5

MARKET SURVEY

The goal of this chapter is to conduct a market analysis in order to find results on what different companies are developing electric micro propulsion systems. Their functionality and performance will be evaluated. Different micro propulsion systems coming from various companies are discussed in Section 5.1. Next to that, a look is taken to the different cathodes that are on the market for micro propulsion systems in Section 5.2. Subsequently, other manufacturers of electric propulsion systems are discussed in Section 5.3. Finally, Section 5.4 gives the conclusions on the conducted market analysis.

5.1. MICRO PROPULSION SYSTEMS

In this part various micro propulsion systems are discussed that are being developed by different companies. These are the Pulsed Plasma Thruster (PPT) in Section 5.1.1, the Radio Frequency Ion Thruster (RIT) in Section 5.1.2 by ArianeGroup e.a., the colloid and electrospray thrusters by NASA e.a in Section 5.1.3 and in Section 5.1.4 the Field Emission Electric Propulsion (FEEP) system by the European Space Agency (ESA) e.a.. Next to that, the μHEMPT by Airbus is discussed in Section 5.1.5. Finally, conclusions are given in Section 5.1.6.

5.1.1. PULSED PLASMA THRUSTERS - NASA E.A.

A long existing type of low power electric thrusters are the pulsed plasma thrusters. They are able to achieve a high specific impulse and are therefore ideal for applications in small satellites that require accurate attitude control, precision spacecraft control or low thrust manoeuvres. A pulsed plasma thruster (PPT) consists out of a power source, a power processing unit and the thruster system. The power source is typically realised by electrical power that comes from solar panels. This is due to the fact that PPTs operate at low power levels. An arc of electricity is passed through the propellant, which can be solid teflon. This causes ablation and sublimation of the fuel, and with the heat generated by the arc the resultant gas turns into plasma. PPTs are are able to accelerate plasma that is formed in the accelerating electrodes in short and discrete bundles of thrust. The pulsed nature of the thruster therefore means that between the pulses, the energy can be stored in capacitors, ready for the next discharge. This makes the thruster versatile, since it can be used for velocity corrections as well as attitude control. Next to that, PPTs are simple, robust and use COTS components to decrease mass, size and costs [158].

The PPT has been first developed in the 1950s by groups in the United States of America, Europe and the Soviet Union. The first PPT that has flown in space was aboard the Zond-2 spacecraft in 1964. Since then, they have been developed throughout. In 1966, the first USA PPT has flown in space onboard the LES 6 spacecraft. It has been developed by the MIT Lincoln Laboratories from then onwards and this has resulted in the LES 8/9. This PPT is able to provide a thrust of 600 μN with a specific impulse of 1075 sec [159]. Between 1981 and 1988, three US Navy NOVA satellites have been launched that use two PPT systems per spacecraft in order to realise drag correction propulsion for seven years in a low Earth orbit . They are capable of realising a thrust of 378 muN with a specific impulse of 300 seconds [160]. Later, the Earth Observing 1 (EO-1) satellite is launched in 2000 and is developed by NASA and Primex Aerospace. It uses one dual axis PPT. The PPT is illustrated in Figure 5.1. It is capable of producing a thrust of 1400 μN at an exhaust velocity of more than 13,700 m/s. Doing so, it requires 127.4 Watts of power to operate. This results in a power to thrust ratio of 91 [35]. In addition to that, Busek is developing micro pulsed plasma thrusters since 2002. The goal here is to create a simple and non toxic thruster, that can be eventually implemented in CubeSats. Their latest version, the BmP-220, uses less than 7.5 Watts to generate a thrust of 20 μN-s (impulse bit). Furthermore, the PTTR is in the range of 50 W/mN. The weight is 0.5 kg and with a volume of 10 x 10 x 7 cm it will fit in a CubeSat [161]. These pulsed plasma thrusters are summarised in Table 5.1 [9].

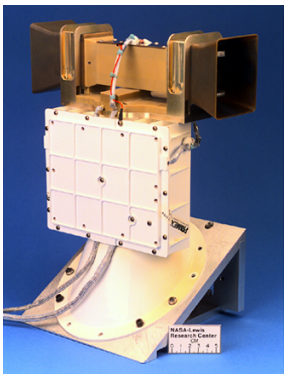

Figure 5.1: EO-1 Earth Orbiter Flight Pulsed Plasma Thruster [35]

Table 5.1: PPT Performance Characteristics [9]

Characteristic	LES 8/9	NOVA	EO-1	BmP-220
Thrust [mN]	0.600	0.378	1.400	0.15
I_{sp} [s]	1075	300	1150	536
Power [W]	31.8	18.9	127.4	7.5
Mass [kg]	7.33	6.35	5	0.5
PTTR [W/mN]	53	50	91	50
TRL [-]	9	9	9	5

PPTs are interesting for precision pointing, constellation maintenance applications and orbit changing manoeuvres. They are simple, solid-state devices that have a high reliability. However, the thruster efficiency is generally low and the thrust cost is high. This is due to the fact that energy losses occur by delayed ablation of the propellant and fast conductive heat transfer from the propellant towards the rest of the spacecraft.

5.1.2. RADIO FREQUENCY ION THRUSTERS - ARIANEGROUP E.A.

The radio frequency ion thruster (RIT) is invented at the University of Giessen in Germany by Horst Löb in the 1960s. Ever since then, many RIT systems have been developed. This has lead to the first in-flight experience of a RIT system on the Artemis mission in 2001. Nowadays, different RIT systems are being developed for a wide range of applications. In these systems, plasma is generated in a discharge chamber and ions are extracted from the plasma by an electrostatic grid system. The propellant that is used is normally xenon, because again of its high atomic mass and low ionisation energy. Next to that, it is inert and this has several advantages in terms of handling and contamination.

In ion engines, either a cathode can be used in order to generate a plasma from which electrons are extracted and injected into the discharge chamber to ionise the propellant as described in Sections 3.4, 4.2.1 and 4.2.2, or a magnetic coil is used to realise a radio frequency ion thruster. This coil is wrapped around around the discharge chamber and generates an oscillating and predominantly axial magnetic field. This is used in order to realise the oscillating electric field that follows the curvature of the cylindrical discharge chamber. Hence, electrons that are present to small degrees within any propellant gas are accelerated in order to cause ionisation. In this manner the plasma is formed. This plasma contains free (relative) light weight electrons and heavier positive ions. The heavy positive ions are accelerated by an electrostatic field in order to create the required thrust. This is explained in more detail in Section 4.2.3. Advantages are in terms of lifetime since no emitter material is required in the cathode, but on the other hand, the electron energy cost per thrust producing ion that is generated by a radio frequency ion is higher than for emitter electron bombardment [10].

Various miniature ion engines are being developed, although not yet specifically for CubeSat Applications, but for formation flying techniques on future space telescope space systems [162, 163]. Ion engines are attractive in these applications because of the use of the inert propellant xenon. This does not contaminate the sensitive optical surfaces and next to that, it allows for smooth thrust modulation. Furthermore, with ion engines there is no need for reaction wheels, that could induce jitter in the sensitive high accuracy pointing mechanisms. Therefore, amongst others, ArianeGroup is performing research in this area. They are developing their RIT2X series. The thrust range varies between 50 μN up to 165 mN. Because of the low thrust possible, highly precise AOCS[1] requirements can be met using these systems. The RIT 2X series electrostatic thruster[2] is the largest one of its kind that is currently being developed by Ariane Group and has a thrust level from 80 mN up to 205 mN. It can be seen in Figure 5.2 [11, 164, 165].

[1] Attitude Orbit and Control Systems

[2] `http://www.space-propulsion.com/spacecraft-propulsion/propulsion-systems/electric-propulsion/index.html` | Visited on 19 September 2017

Figure 5.2: Radio Frequency Ion Thruster RIT 2X Series [11]

Another example of a RIT system is the RITμX by ArianeGroup that is in development since the year 2000. Next to that, micro ion engines are being developed by Janson at Aerospace Corporation [166] and by Brophy e.a. at JPL in the form of an ion thruster on a chip concept [167]. The latter one promises to be feasible for future applications and has led to the Miniature Xenon Ion Thruster (MiXI) that is designed for the Terrestrial Planet Finder (TPF) [168] and other exoplanet missions [36, 162, 163, 169, 170]. With a thruster mass of 200 g it is capable to produce a thrust up to 1.5 mN at a specific impulse of 3200 s using xenon as propellant. It is illustrated in Figures 5.3 and 5.4 respectively.

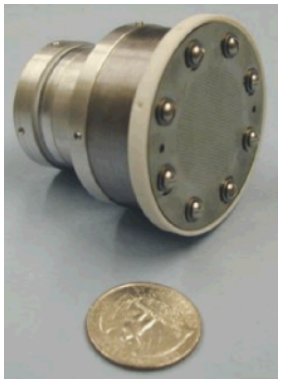

Figure 5.3: JPL Miniature Xenon Ion Thruster (MiXI) [36]

Figure 5.4: MiXI in Operation [36]

Radio frequency thrusters are interesting for miniaturisation since they do not require an internal cathode. This leads to development both in the Unites States of America and Europe. In the USA, The Pennsylvania State University is developing on the Miniature Radio Frequency Thruster (MRIT) [38]. Operating on argon as propellant, it is capable of achieving a thrust of 59 μN a power of 15 W and a specific impulse of 5480 s. Next to that, in Europe the University of Giessen is developing on the μNRIT-2.5 thruster [37]. This thruster has a weight of 210 grams and is able to produce a thrust of 0.5 mN using a power of 30 W. It operates on xenon. The μNRIT-2.5 thruster is shown in Figure 5.5 and the MRIT thruster can be seen in Figure 5.6. Table 5.2 summarises the characteristics of the discussed thruster systems. RIT thrusters are well known for their high performance at relative low complexity, narrow beam divergence and excellent thrust stability and fast thrust response [171, 172].

Table 5.2: RIT Performance Characteristics [10] [11]

Characteristic	**MiXI**	**μNRIT-2.5**	**MRIT**	**RIT μX**	**RIT 2X**
Thrust [mN]	0.01 - 1.5	0.05 - 0.60	0.001 - 0.060	0.050 - 0.500	80 - 205
I_{sp} [s]	2500 - 3200	2861	5480	300 - 3000	2700 - 3800
Power [W]	13 - 50	13 - 34	n/a	> 50	2300 - 5000
Electrical efficiency η_e [%]	> 40	4 - 47	15	8000 - 12000	2.7
Mass utilisation η_m [%]	> 70	15 - 52	n/a	n/a	n/a
Diameter [cm]	3	2.5	2	7.8	33
Mass [g]	200	210	n/a	440	10000
Propellant	Xenon	Xenon	Argon	Xenon	Xenon
PTTR [W/mN]	33	57	n/a	100	24
TRL [-]	3	5	4	5	5

Figure 5.5: μNRIT-2.5 Miniature Ion Thruster [37]

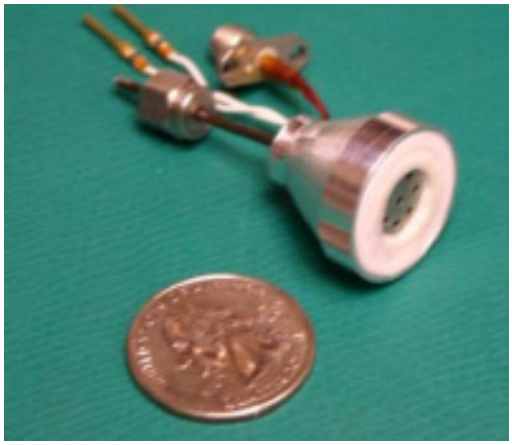

Figure 5.6: MRIT Micro Ion Thruster [38]

Although the miniature ion engine technology such as the RIT thrusters is primarily developed for formation flying missions, it can be adapted in order to be used on CubeSats or similar nanosatellites in order to provide large ΔV capabilities. In this manner, these spacecraft can perform orbit raising manoeuvres, orbital plane changes and realise an extended mission lifetime by means of thrusting to counteract drag. Micro ion engines such as the ones discussed here could be realised in a 3U CubeSat architecture where the engine itself takes up 1U, the PPU could be integrated in the electronics unit (1U) and the third 1U would be available for the remaining satellite subsystems (AOCS, C&DH, etc.) and the payload. In order to achieve the required power levels that range into several 10s of Watts, deployable solar panels would be required to host the micro ion engine structure.

5.1.3. COLLOID AND ELECTROSPRAY THRUSTERS - NASA E.A.

The miniaturisation of ion and Hall thrusters comes with certain challenges and efficiency losses since the plasma chamber needs to be miniaturised. Therefore, there is also research being performed in electrostatic thrusters that do not require a plasma discharge and emit ions or charged droplets directly from a propellant column using an applied electrostatic field. In electrospray thrusters, the propellant is fed through up along an emitter by means of capillary forces. The emitter can either be a sharp needle or a narrow slit. The emitter experiences an electric field that is established between the emitter and the opposing electrode. Using the surface tension of the emitter material and the applied electrostatic forces, the electric field can be intensified near the emitter tip in order to distort the electrically conductive propellant into a sharp so called Taylor cone. The shape of the Taylor cone enhances the electric field strength.

Ions can be extracted from the propellant if field emission is used. Usually, liquid metal propellants are used for this such as caesium. These systems are generally known as Field Emission Electric Propulsion thrusters, and will be discussed next in Section 5.1.4. The thrusters that mainly use droplet emissions are known as colloid thrusters and will be discussed here. It is important to note that with recent propellants for these systems, that are also called ionic liquids, both ion and droplet emission can be realised. This is solely dependent on the operating conditions that include flow rate, temperature and applied voltage. Main advantage of these systems is that without the need for a generation of a plasma discharge, they can be miniaturised extremely well. As an example, the emitter tips can be in the sub-millimetre regime [12, 173].

Colloid thrusters have been analysed initially in the United States of America by Perel and Mahoney [174–176] and at Northrop Grumman [177, 178]. Using glycerol propellants doped with either sodium iodine or sulphuric acid thruster performances ranging from 1 - 334 μN per emitter at specific impulses ranging from 450 - 1450 s are realised. The power to thrust ratios range from 4 - 10 W/mN. The sizes of the emitter range from 100 μm to 2 mm. Now that satellites are being miniaturised more and more (as described in Section 4.1), these technologies are becoming even more interesting in order to realise e.g. formation flying missions and nanosatellite missions. Hence, colloid thruster systems have been realised by Perel e.a. [179] that operate using a 1 μN emitter and next to that, by Pranajaya e.a. [180] that use a 50 μN capillary device that can be implemented with up to 100 emitters on a nanosatellite mission. The latter is able to produce a thrust of 1 μN per emitter with a specific impulse of 500 s at a power to thrust ratio of 10 W/mN. The system as a whole, which includes a feed system and a power processing unit (PPU), is being designed to have a mass lower than 500 g and a size of 10 x 10 x 20 cm so that it can fit into a 3U CubeSat nanosatellite structure. In this manner, the remaining 1U can be left for the satellite payload and other subsystems.

In addition to that, colloid thruster development is being performed at NASA in collaboration with Busek and JPL for the Laser Interferometry Space Antenna mission [39, 40, 181, 182]. As explained in Section 4.1.1, the goal of this mission is to detect gravity waves by moving the spacecraft of the constellation with respect to each other and detecting these movements by using laser interferometry. Micro propulsion with thrust levels that have a precision of up to 0.1 μN is required in order to be able to distinguish these movements by gravity waves from other orbital disturbances such as atmospheric drag, magnetic perturbations, third body effects and solar pressure. Therefore, the New Millennium ST-7 colloid thruster has been realised. It consists out of multiple clusters that future thruster heads which are oriented by 90 degrees with respect to each other in order to provide precise control. This can be seen in Figure 5.7. Next to that, a single thruster head can be seen in Figure 5.8. The whole module contains the propellant storage, the feed system and the PPU. A single thruster head as the one depicted in Figure 5.8 is able to produce a thrust in the range of 5 - 38.5 μN with a precision of less than 0.01 μN [182]. Hence the thrust precision requirement of 0.1 μN that is mentioned before can be realised. The specific impulse is in the range of 190 - 240 s and depends on the temperature of the propellant. The propellant is heated and requires 24 W for initial warm up and 16 W afterwards during normal operations.

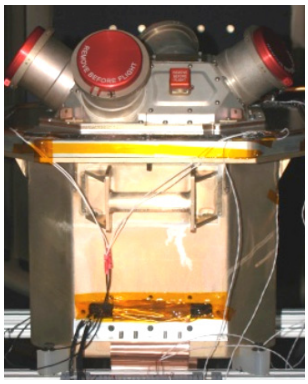

Figure 5.7: ST-7 Colloid Thruster Module [39]

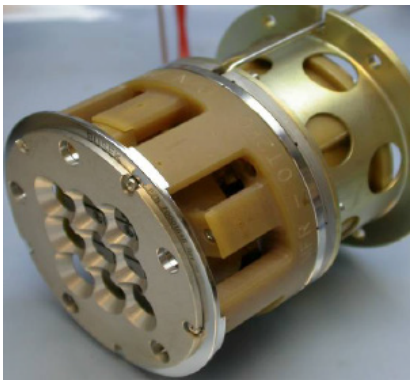

Figure 5.8: ST-7 Cluster Head [40]

In the current configuration, such a system would be too large for CubeSat applications. Nonetheless, a single thruster head could be used in order to realise a individual thruster for a CubeSat. A single thruster head as shown in Figure 5.8 consists out of nine emitters. Such a single emitter can be seen in Figure 5.9. Using ionic liquids as propellant, colloid thrusters (both in the form of charged droplet as well as ionic emission) can be implemented in CubeSat missions in order to extend their capabilities. With the wide range of specific impulses ranging from couple of hundreds up to a few thousand seconds, either low power to thrust modes using low I_{sp} can be used in order to perform rapid manoeuvres, or high power to thrust modes using high I_{sp} can be realised in order to perform large ΔV manoeuvres. In order to summarise the performance of the mentioned thrusters, Table 5.3 is given. The Northrop Grumman colloid thruster and the ST-7 require miniaturisation in order to be implemented on CubeSats, but prove to be promising. The colloid thruster that is in development by Pranayaja e.a. is designed to fit in a 3U CubeSat.

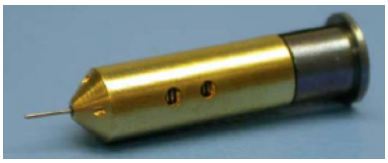

Figure 5.9: Single ST-7 Colloid Thruster Emitter [40]

Table 5.3: Colloid Thrusters Performance Characteristics [12]

Characteristic	TRW (Northrop Grumman)	Pranayaja (Stanford Uni.)	ST-7 (NASA)
Thrust [μN]	1 - 334	50	5 - 35.8
I_{sp} [s]	450 - 1450	500	190 - 240
Mass [kg]	2.98	0.5	15
Power (max) [W]	-	-	24.6
Power (nominal) [W]	-	-	16
PTTR [W/mN]	4 - 10	10	447
TRL [-]	5	4	7

5.1.4. FIELD EMISSION ELECTRIC PROPULSION - ESA E.A.

A field emission electric propulsion (FEEP) system has a short lifetime and a low dynamic range. In addition to that, the system complexity is medium and the thrust noise is low. The thrust of a single FEEP thruster is generally in the order of tens of micro Newtons. This thrust range makes FEEP thrusters interesting for AOCS applications. FEEP thrusters can be categorised according to the propellants that they use. The typical ones are liquid metals such as caesium, indium or gallium. These are being used because of their high atomic mass, low ionisation potential and good wetting properties. This makes them ideal for electric propulsion characteristics in terms of FEEP applications. FEEP thrusters are not pressure fed, instead propellant is supplied to the emitter tip by capillary forces. This allows for very compact feed systems that do not require valves nor pressurised propellant tanks.

Development of FEEP thrusters that make use of caesium as propellant initiated more than 30 years ago. The propellant flows between a pair of metal surfaces that end in a sharp slit. This slit has a gap that measures only one micron across. The caesium is kept into place by surface tension at the entrance of the slit, until an electric field is generated. In this manner tiny Taylor cones are formed in the liquid metal that have positive ions that shoot from the tip of the cones in order to create thrust. The propellant is ionised and accelerated by the strong electrical field that exists on the tip of the needle. This principle is illustrated in Figure 5.10. The ESA FEEP engine has a thrust range of 0.1 - 150 micro Newtons and is illustrated in Figure 5.11 [41, 42].

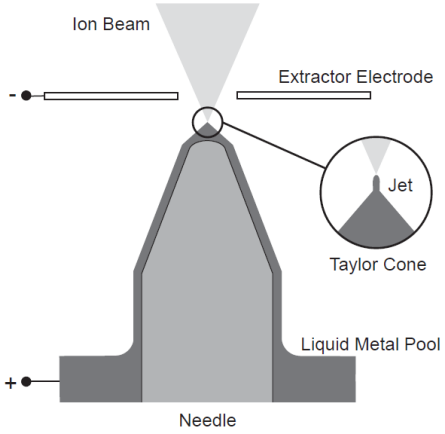

Figure 5.10: FEEP Schematic [41]

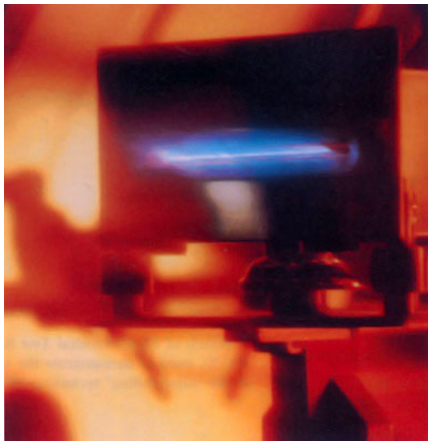

Figure 5.11: Intense Ion Beams generated by FEEP Thruster [42]

In order to initiate the evaporation and the ionisation, a strong electrical field is needed between the needle and the extractor electrode. The potential difference that is applied between the two is in range of 5 kV to 12 kV. Using a beam current between 1 μA and 100 μA, specific impulses of 8000 s can be realised. FEEP systems have the advantage that no mass flow controller, pressure regulator, propellant tank or pipework are required. Instead, the propellant feeding is realised via a capillary force. Nevertheless, a high voltage supply is required in order to realise the high potentials and the propellant heating. Next to that, the lifetime of the thruster can be affected by contamination on the extractor electrode by evaporated propellant. In the case of caesium FEEP thrusters, complications exist in the form of propellant handling as caesium is very corrosive and reacts with already small amounts of water, oxygen or CO_2. In this way caesium hydroxides, oxides and carbonates are formed that have high melting temperatures. These formed substances are able to clog the emitter slits and degrade the performance of the thruster. Also, the propellant needs to be stored in a specific propellant tank in order for the capillary forces to be applicable.

In other research institutes, FEEP thrusters for highly precise AOCS that operate using Indium are being investigated in Austria (Austrian Research Centres Seibersdorf (ARCS)) since 1995 [183]. Next to that, the development of FEEP thrusters that are miniaturised has been started at the University of Pisa and Centrospazio and later also in Alta in Italy under funding from ESA [12]. Here the focus is on a FEEP that uses caesium as propellant. By varying the slit widths of the emitter from 2 to 70 mm, the produced thrust ranges from 40 μN to 1.4 mN. The power to thrust ratio is equal to 66 W/mN. The power is relatively high compared to other thrusters, because of the high I_{sp} of around 9000 s. Furthermore, Dresden University of Technology started research on FEEP systems in 2012 [41, 184–186]. Figure 5.12 gives an illustration of the FEEP-5 thruster that has been developed by Centrospazio and Alta. Next to that, Table 5.4 lists various FEEP slit emitter designs.

Figure 5.12: FEEP-5 Thruster by Centrospazio & Alta [10]

Table 5.4: FEEP Performance Characteristics [10]

Characteristic	**ARCS**	**ARCS**	**ARCS**	**Centrospazio**	**Centrospazio**
Designation	IN-FEEP 100	GOCE MTA	IN-FEEP 1000	FEEP-5	FEEP-50
Thrust [mN]	0.001 - 0.1	0.002 - 0.65	0.001 - 0.1	0.04	1.4
Mass [kg]	0.3	3.5	1.5	0.6	1.2
I_{sp} [s]	8000 - 12000	8000 - 12000	8000 - 12000	8000 - 12000	9000
Power [W]	0.5 - 10	6 - 52	2 - 80	2.7	93
PTTR [W/mN]	100	80	80	67.5	66
TRL [-]	5	7	6	5	5

In order to integrate FEEP thrusters into CubeSats, a power processing unit (PPU) would be required, as well as additional deployable solar arrays in order to generate the required power. This is because of the fact that the power to thrust ratios are rather high. The feed system can be integrated relatively easily, as it consists out of a simple system. The propellant reservoir and the capillary feed system can be manufactured as part of the thruster head. FEEP thrusters can achieve very high specific impulses as has been shown in Table 5.4. However, this leads again to high power to thrust ratios that required either long transfer times or high power levels.

5.1.5. ELECTROSTATIC THRUSTERS - AIRBUS E.A.

The high efficiency multistage plasma thruster is invented at Thales Electron Device (TED) by Günter Kornfeld in 1998 [187]. He has derived the basic features of the thruster system from travelling wave tubes and their electron collectors. In these devices the electron beam is used in order to amplify a microwave signal that is confined in a magnetic field with a predetermined cusp field configuration. In this manner, the idea is to develop a thruster where the plasma has little contract with the walls and as such to strongly increase the system life time. This is realised by minimising the wall erosion effects that occur by the plasma and electrons that impinge the walls of the thruster discharge chamber. In order to use the HEMPT in the micro Newton thrust range, a study is initiated by Airbus in 2009. The HEMPT is well known for its long life time and low system complexity. In addition to that, the dynamic range of the thruster is high. Nevertheless, the thrust noise of the thruster is not as good as the other types of thrusters that are discussed in this chapter. This is because of the fact that the μHEMPT design is simple. Figure 5.13 gives an illustration of the μHEMPT model. The current characteristics of the thruster are summarised in Table 5.5 [65, 188–190].

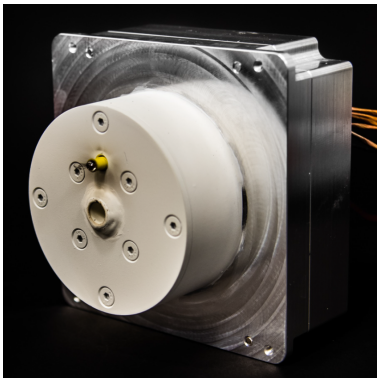

Figure 5.13: μHEMPT Model [7]

Table 5.5: μHEMPT Characteristics [7]

Characteristic	**μHEMPT**
Thrust [μN]	55 - 75
Mass [kg]	0.425
I_{sp} [s]	155 - 326
Power [W]	2.2
PTTR [W/mN]	24 - 67
TRL [-]	4

5.1.6. CONCLUSION

Because of the fact that important sectors of the commercial space market are going to require space missions with long orbit lifetimes in the near future, high power ion engines for electric propulsion systems need to be ready to provide mass efficient orbit keeping support. In addition to that, these thruster systems will become advantageous candidates if the launcher market evolves to permit direct orbit injection strategies. Nevertheless, because of the long process of development and qualification of these electric propulsion systems, these activities require acceleration and support in order to aid the technology development and to cover the non-recurring costs.

All the electric micro propulsion systems discussed in this chapter are able to provide a high dynamic thrust range, good thrust noise properties and high efficiencies when compared to cold gas thruster systems. The characteristics of the discussed micro propulsion systems are summarised in a qualitative manner in Table 5.6 [6].

Table 5.6: Micro Propulsion System Characteristics

Characteristic	PPT	RIT	FEEP (and colloid)	μHEMPT
Complexity	Low	High	Medium	Low
Dynamic thrust range	Low	Medium	Low	High
Thrust noise	Medium	Low	Low	Medium
Lifetime	Middle	Long	Short - Middle	Very long
PTTR	High	Medium	High (low for colloid)	Low
Thrust / Mass ratio	Low	High	Medium	Medium
TRL	High	Medium	Medium	Low

There exist various companies that are manufacturing micro propulsion systems. In Europe, ArianeGroup, ESA and Airbus are developing on different types. The goal is to create a high performance micro propulsion system that has little losses and can be applied on various type of satellites, with the focus on CubeSats in particular. This is realised by creating simple and long life systems. High efficient micro propulsion systems need little propellant mass and can be operated without the need for large power supplies. Pulsed plasma thrusters have a low efficiency and a high thrust cost. Radio frequency ion thrusters have a high complexity and a medium dynamic range. In addition to that, they have low thrust noise and a long life time. FEEP Thrusters have a medium complexity and a low thrust noise, but a rather short lifetime. The μHEMPT system has a low complexity and a long life time.

5.2. CATHODES FOR MICRO PROPULSION SYSTEMS

This section discusses several cathodes that exist on the market. These include the NJK1120A cathode by New Japan Radio Co. in Section 5.2.1. Next to that, the LaB_6 thermionic cathode by Kimball Physics is described in Section 5.2.2. Furthermore, a recent hollow cathode that is heated by a filament heater is described in Section 5.2.3. Finally, conclusions are given in Section 5.2.4.

5.2.1. NEW JAPAN RADIO CO. - NJK1120A BAO CATHODE

New Japan Radio Co. produces the NJK1120A barium oxide cathode that is indirectly heated by means of radiation. This is realised using a radiative rhenium tungsten filament heater. This cathode is capable of emitting currents of 10 A/cm^2 at temperatures of 1300 K. In order to realise this operating temperature, a heater power of 2.4 W is required. Furthermore, according to the manufacturer, the poisoning by exposure to air is little and has no influence on the performance of the cathode. Figure 5.14 gives an illustration of the NJK1120A cathode [43].

Figure 5.14: NJK1120A Cathode [43]

In order to test the performance of this cathode and the capability of the micro Newton thruster test facility to support performance testing, it is operated in the vacuum chamber at Airbus. The cathode is tested in direct diode mode, which is explained in more detail in Section 6.2.1. In this mode a large metal plate is installed directly in front of the cathode, to which a high potential can be applied. In this manner, this plate acts as an anode that attracts the emitted electrons. The applied potential is in the range of 1000 - 2000 V. By using a heater potential of 7.5 V the aforementioned heater power of 2.4 W is realised by the power supply. Next to that, the discharge current over the metal plate is measured in order to obtain information on the electron emission of the cathode.

Test results have shown that only little discharge current can be realised using this cathode as an electron emitter. With a anode potential of 2000 V and a heater power of 7.5 V, only 20 mA of discharge current has been measured. This results in an average required power per emitted current of 0.25 W/mA. This is as high (i.e. as low) as current emission by previous tested tungsten filament cathodes. This poor performance could yet be due to poisoning effects by handling in atmosphere. As described in Section 4.3.2, BaO cathodes are very sensitive to poisoning. Next to that, the heater mechanism might not be the most efficient solution. Because of these facts and other important aspects such as complexity and mission lifetime, subsequent iteration cathodes make use of LaB_6 in order to realise a thermionic cathode for electron emission.

5.2.2. KIMBALL PHYSICS - THERMIONIC LaB_6 CATHODE

Kimball Physics is a company from the United States of America that produces LaB_6 thermionic cathodes. With an experience of more than 40 years in ultra high vacuum electron and ion optics, the available technology is promising. A large single crystal cylinder is realised in order to create a large planar emitting surface. This can be seen in Figure 5.15. The goal of this technology is to increase the beam currents. It can be ordered either as a stand alone cathode or on a mounted ceramic base as is illustrated in Figure 5.15. The ceramic base is able to thermally insulate the emitting part of the cathode. The cathode is capable of emitting 500 mA at an operating temperature of 1900 K and a heater current of 11 A. This results in a power to current emission ratio of 0.20 W/mA [44].

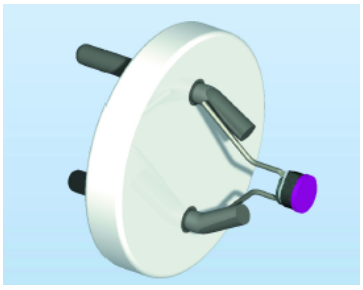

Figure 5.15: Kimball ES-440 LaB_6 Single Crystal Cathode [44]

5.2.3. FILAMENT HEATED HOLLOW CATHODE

Another type of cathode that is interesting to discuss is a boron nitride (BN) ceramic encapsulated hollow cathode by McDonald e.a. [45]. It has serpentine grooves in order to house a filament heating element. This can be seen in Figure 5.16. The heater wire can be either of tungsten or rhenium. However, as described in Section 4.3.7, it is recommended to use high purity boron nitride, which does not contain oxygen atoms. This is because of the fact that tungsten is able to react with the oxide binders, which could lead to failure of the heater filament. This heater type is particularly interesting because the heater application can be implemented in a next generation thermionic LaB_6 cathode. In this manner, the heater electrical circuit remains isolated from the emitter electrical circuit by means of the BN spacer. In addition to that, heat can be contained by encapsulating the heater filament with a BN surrounding outer sleeve [45].

Figure 5.16: Helical Winded Heater around Boron Nitride Encapsulated Hollow Cathode [45]

In order to obtain a lit LaB_6 emitter inside the hollow cathode for electron emission, a heater power of 200 W is used [45]. The cathode tube itself is made from graphite, because it has a high resistance to boron diffusion. Furthermore, in order to accommodate the thermal expansion of the graphite tube within the BN sleeve, while yet maintaining a good thermal conductive interface, a thin flexible graphite sheet is inserted. This provides good thermal conduction and allows for tolerances in machining the hollow cathode components.

5.2.4. CONCLUSION

There exist several types of cathodes on the market for electric propulsion systems. For micro electric propulsion systems, one can purchase off the shelf directly heated thermionic cathodes from Kimball Physics. Other options are radiative heated barium oxide hollow cathodes from New Japan Radio Co. or more recent and in development rhenium wire heated hollow cathodes. The last option yet requires miniaturisation. Nevertheless, the concept is promising. They are summarised in Table 5.7. Here, the operating temperature is listed, the heater power that is required to get them at that operating temperature, and the power that is required to obtain the discharge current.

Table 5.7: Market Cathodes Characteristics

Characteristic	**NJK 1120** [43]	**KP ES-440** [44]	**McDonald e.a.** [27]
Operating temperature [K]	1300	1700	1700
Heater power [W]	2.4	10	200
Power to current ratio [W/mA]	0.25	0.20	0.47

5.3. OTHER ELECTRIC PROPULSION MANUFACTURERS

Currently, the main electric propulsion system manufacturers come from Europe, Russia and the United States of America. In Europe, there exist the SNECMA PPS5000[3] [191–193] by Safran, the QINETIQ system[4] [194, 195] by QinetiQ, the ArianeGroup RIT-22[5] [11, 164, 165] and the high power HEMPT systems [65, 188]. These are mostly high power electric thrusters that are designed for various small satellite missions that involve orbit-raising [196].

Outside Europe, the main candidates are the Fakel SPT-140[6] [197–201] and the Aerojet BPT4000[7] [74, 202–206]. Fakel is a Russian electric propulsion development company. They have realised the first flight of a Russian stationary plasma thruster (SPT) Hall thruster in 1971 [101]. Many subsequent flights have made use of lanthanum hexaboride cathodes. The SPT-100 thruster that is designed and built by Fakel, is extensively tested by NASA in the 1990s [207, 208]. In 1991, the American launcher company Space Systems Loral has partnered with Fakel in order to qualify the flight model SPT-100 thruster for American flight standards. Subsequently, seven spacecraft that use a SPT-100 propulsion system are launched and eleven more (in 2011) are being manufactured. Currently, the SPT thruster system has more than nineteen years of cumulative on-orbit experience with a single thruster system. This makes Fakel one of the most dominant players on the market considering Hall effect thrusters [5].

5.4. CONCLUSIONS AND RECOMMENDATIONS

Different type of electric thruster systems exist on the market that can be applied for various purposes. At Airbus, the goal is to develop a low complexity, affordable and efficient electric thruster system. Therefore, a downscaling of a High Efficiency Multistage Plasma Thruster is being performed. This results in a high dynamic thrust range, a low thrust noise and a long life time.

Fakel from Russia is one of the main players when it comes to electric thruster systems since they have a long flight heritage. Next to that, they have flown many of their thrusters on various satellite programs. Nevertheless, miniaturisation is not being researched extensively and because of the fact that important sectors of the space market will require these systems for many different applications, development in the micro Newton range (several μN up to 10 mN) is being performed at Airbus. It is recommended to investigate the possibilities with thermionic cathodes, since they lead to low complexity and cost effective designs. Should this not be feasible, the realisation of hollow cathodes needs to be considered. These have a higher complexity, but have more flight heritage.

[3] https://www.safran-aircraft-engines.com/space-engines/satellites/pps-5000 | Visited on 19 September 2017
[4] https://www.qinetiq.com/en-gb/what-we-do/space/electric-propulsion | Visited on 19 September 2017
[5] http://www.space-propulsion.com/spacecraft-propulsion/propulsion-systems/electric-propulsion/index.html | Visited on 19 September 2017
[6] http://www.fakel-russia.com/index.php?option=com_content&view=article&id=131:spt140du&catid=56&lang=en&Itemid=117 | Visited on 19 September 2017
[7] http://www.rocket.com/propulsion-systems/electric-propulsion | Visited on 19 September 2017

6

EXPERIMENTAL SET-UP

This chapter will discuss the laboratory setup that is used in order to test the performance of the cathodes for the micro propulsion system. These tests are performed in a vacuum chamber on site at Airbus in Friedrichshafen. First, the micro Newton thruster test facility is discussed in Section 6.1. Next to that, the executed test modes are described in Section 6.2. Finally conclusions on the test setup are given in Section 6.3.

6.1. MICRO NEWTON THRUSTER TEST FACILITY

This section will elaborate on the test facility that is used in order to measure the performance of the micro electric thruster system as well as its subsystems such as e.g. the cathode. The micro newton test facility is established in order to perform independent micro-Newton thruster developments for space applications. It characteristics are as such that they comply with the requirements of the Euclid[1], NGGM[2], and the LISA missions. This includes highly precise direct thrust measurements in order to characterise thrust noise as well as absolute thrust measurements of the investigated micro propulsion systems. First, Section 6.1.1 discusses the vacuum chamber that is used. Next, the thrust measurement system is treated in Section 6.1.2. Afterwards, the plasma diagnostics system is described in Section 6.1.3 [48].

6.1.1. VACUUM CHAMBER

The vacuum chamber consists out of a 1500 l vacuum tank, that can be evacuated to $2 \cdot 10^{-7}$ mbar without any gas ballast (by e.g. an operating electric thruster inside). This is realised using a 5.5 l/s forepump, two 700 l/s turbopumps and a helium operated cryopump that has a pumping speed of 10,000 l/s. Combined, the whole vacuum chamber has a pumping capability of 11400 l/s. Figure 6.1 gives an overview of the vacuum chamber by means of a schematic. The tested leaking rate of the vacuum chamber is less than 10^{-9} mbar l/s. In this configuration, a minimum pressure of $1.2 \cdot 10^{-7}$ mbar can be reached. If a thruster with a mass flow of 0.5 sccm (e.g. μHEMPT) is in operation inside the chamber, then a minimum pressure of $3.5 \cdot 10^{-6}$ mbar can be reached, since propellant particles need to be pumped out in this case. Most micro electric thrusters operate with a propellant flow of less than 0.5 sccm [65, 189, 210]. Therefore, using the ideal gas law, the required pumping speed of in the 10^4 l/s range has been realised.

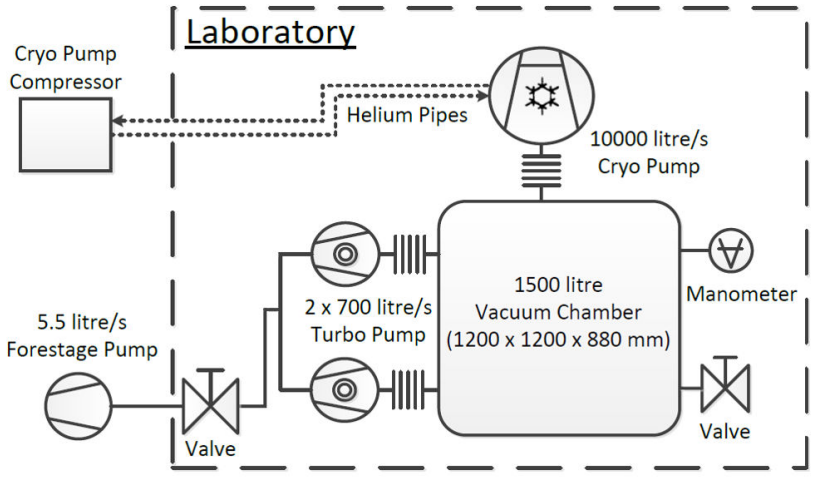

Figure 6.1: Schematic Vacuum Chamber [6]

[1] http://sci.esa.int/euclid/ | Visited on 12 October 2017
[2] Next Generation Gravity Mission [209]

All these characteristics follow from recommendations of the American Institute of Aeronautics and Astronautics (AIAA), the National Aeronautics and Space Administration (NASA) and the European Space Agency (ESA). With these pressure ranges it is possible to test a various range of electric thrusters, such as Hall Effect thrusters that are usually tested in the 10^{-5} mbar regime [211], or gyroscopic inertial thrusters that are tested in the 10^{-6} mbar range [212]. At a pressure of 10^{-5} mbar, space components can be qualified officially [213]. In order to measure the pressure inside the vacuum chamber a Pirani/Bayard-Alpert manometer system is used. This system combines two measurement principles in one device. For initial low pressures, the Pirani element is used to measure pressures down to 10^{-3} mbar. Afterwards, for lower pressures, the hot cathode gauge (i.e. Bayard Alpert manometer) takes over in order to provide accurate pressure measurements down to 10^{-10} mbar with an accuracy in the range of 3 - 6 % [6, 214].

Next to that, it is important that the vacuum chamber is large enough in order to avoid negative influences from the chamber walls to the thruster. In addition to that, it needs to be capable to house all the required test and measurement equipment. Nevertheless, large vacuum tanks are expensive in terms of purchasing, operating costs (as a larger volume need to be evacuated) and maintenance. Taking these aspects into account, a 1500 l vacuum tanks has been established. Figure 6.2 shows the vacuum chamber at Airbus and next to that, Figure 6.3 shows the inside of the chamber. The vacuum chamber can be accessed by two doors; on the front and the rear side. This has been realised in order to gain easy access to any instrument and test equipment inside the chamber. Furthermore, the noise background is an important aspect to the noise sensitive thrust measurements. In order to obtain high accurate measurements in micro Newton propulsion systems in a vacuum chamber, the chamber needs to decoupled from the ground to minimise background noise. Therefore, it is put on four vibration damping systems in a rectangular formation. In addition to that, the fore stage rotary vane pump is placed outside of the facility in a separate container since it creates a large amount of vibrations and noise. Finally, the vacuum chamber is constructed as such, that it can be easily modified and adjusted to user requirements [215–218].

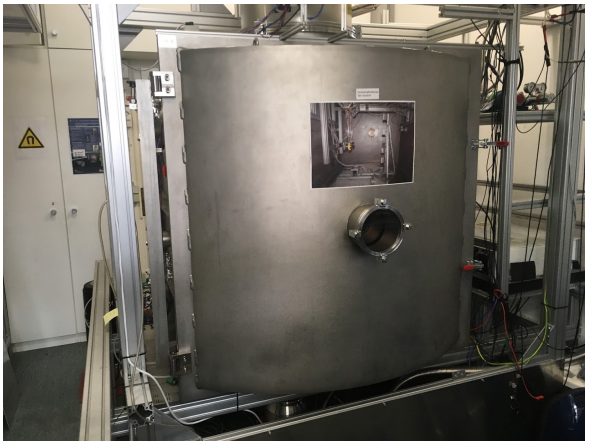

Figure 6.2: Vacuum Chamber at Airbus

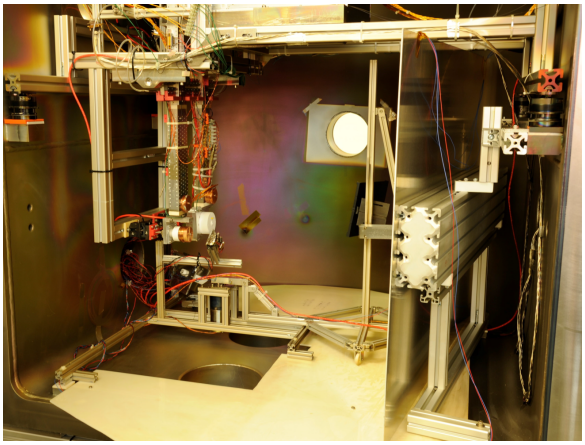

Figure 6.3: Vacuum Chamber Interior

6.1.2. THRUST BALANCE

The thrust of the micro propulsion systems inside the vacuum chamber is measured by means of a direct thrust measurement that is realised using a double pendulum thrust balance that has a sub-μN resolution of 0.1 μN. Next to that, it is able to perform thrust noise measurement with high precision. These high resolution requirements are established so that highly precise attitude and orbit control system (AOCS) thrusters can be tested. These include candidates for ESA's Laser Interferometer Space Antenna (LISA) mission, down scaled micro propulsion systems for CubeSat applications and future space missions. The measurable thrust range is from 0 - 2500 μN [219, 220].

The thrust balance consists out of two identical hanging pendulums. One acts as a measurement pendulum, whereas the other acts as a reference pendulum. This is illustrated in Figure 6.4. The thrust measurement is realised by using a heterodyne laser interferometer on the pendulums as the measurement pendulum is deflected by the thrust of the micro propulsion system and the reference pendulum is not. Using the translation difference x between the two and the predetermined spring constant k, the thrust can be obtained by using Hooke's law in Equation (6.1). With the assumption that both (identical) pendulums are equally influenced by external noise and using the relative difference in translation, external noise contributors can be excluded. This noise can come from various contributors that have been discussed earlier such as e.g. seismic noise. Since both pendulums are equally affected by this, the noise will not be measured. In this manner, high resolutions in the pico-metre regime would be possible theoretically. Nevertheless, because of background that is unpreventable, translations in the nanometre regime are

measurable. These correlate to a thrust accuracy of 0.1 μN. Furthermore, eigenfrequencies and other highly frequent noise contributors are damped by using an eddy current break in the upper part of the pendulum system [6].

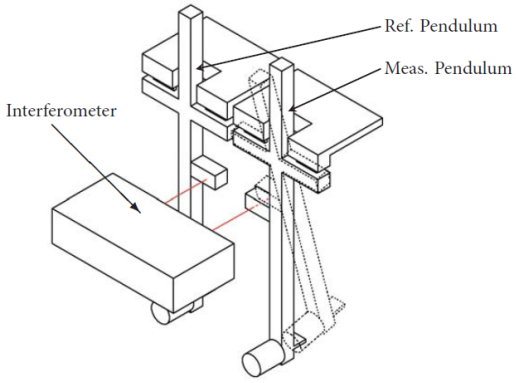

Figure 6.4: Thrust Balance Schematic [6]

$$F = -kx \tag{6.1}$$

The spring system consists out of 20 leaf springs, that besides spring damping provide a support of the pendulum to the thruster balance structure. Using a symmetric spring setup for the both the measurement and the reference pendulum, the deviation of both spring constants due to thermal expansion is minimised. Nonetheless, a calibration is required in order to be able to precisely determine the spring constant so that highly accurate thrust measurements can be performed. The calibration is performed by applying a highly accurate electrostatic force on the pendulums. This is realised by applying a predefined voltage on the electrostatic comb on the backside of the pendulum. In this manner the spring constant is evaluated by applying different voltages and thus electrostatic forces. The worst case maximum uncertainty that includes the calibration process and the overall relative error in the measurement chain is 3.78 % [6].

6.1.3. PLASMA DIAGNOSTICS SYSTEM

In order to measure the electric parameters of the propulsion system under test including basic ion plume properties, a plasma diagnostics system is used. It consists out of a patented gridless retarding potential analyser system and several Faraday cups. The instruments on the plasma diagnostics system are mounted on rotatable jib arm in order to allow for 180^o plasma plume measurements. The rotation is controlled by a stepper motor (Phytron VSS 52 [221]) that has a resolution of 200 steps and a step accuracy of 5% for 1.8^o. The stepper motor is operated by a digital controller that can provide a step resolution of 1/256. In addition to that, the stepper motor is connected to the jib arm by means of a transmission that has a gear ration of 1 : 256. Hence, the resolution that can be realised by the jib arm as a whole is $2.7 \cdot 10^{-5}$ ^{o}. Furthermore, the measurement system can be easily adjusted in order to measure different thruster systems that each have their own specific characteristics. The system is shown in Figure 6.5. The probes are based on a design of the University of Giessen by H. P. Harmann [222], W. Gaertner [223] and P. Koehler [190, 224].

Figure 6.5: Plasma Diagnostics System

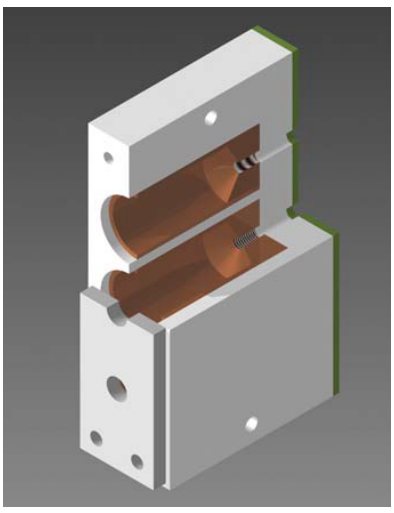

Figure 6.6: Faraday Cups Unit [6]

The Faraday cups that are placed on several locations on the plasma diagnostics system as can be seen in Figure 6.5 are used in order to measure the ion current. The cups are assembled in a POM[3] housing in groups of three in a single unit. Each unit is able to independently perform Faraday cup diagnostics. The POM is both used as an insulator material for the cups from each other and from the ground. Next to that, it services as a mechanical housing for the cups. A electron shield (shown in front of Figure 6.6) made out of aluminium is used to prevent electron influx. In this manner, only the ion current from the ion plume will be detected by the cups. The Faraday cups are able to measure a current between 0 and 0.2 μA with a resolution of 15.3 pA and an accuracy of 0.5%. However, this resolution is affected by various noise sources such as electrical noise and ion beam divergence. Because of these effects, the resolution is limited to 600 pA. A three cup unit is displayed in Figure 6.6 [6].

The rear side of a Faraday cup unit houses an electronic circuit board. It is made sure that each of the three cups in a single unit has its own transimpedance amplifier, filter and gain amplifier. In this manner, the cups have their own independent electronic circuit for measurements. Next to that, the resistance on the circuit for each probe can be easily replaced in order to allow for various thrust range measurements. Hence, both the micro Newton as well as the mini Newton thrust ranges can be measured so that different ion thrusters can be tested inside the vacuum chamber at Airbus.

Furthermore, a retarding potential analyser (RPA) is used in the setup in order to obtain information about the ion energy. This is the square box placed in the centre of the plasma diagnostics system that can be seen in Figure 6.5. It is shown in more detail in Figures 6.7 and 6.8 respectively. The purpose of this device is to use a series of grids in order to selectively filter ions and determine the ion energy distribution. The first and outer grid of the system is exposed to the ion plume and its purpose is to protect the RPA from electron influx. The second grid acts as a retarding grid and slows down the incoming ions with respect to their energy. Furthermore, a secondary electron repelling grid is used in order to suppress secondary emission electrons that emanate from the first two grids and the collector. It is possible to adjust the voltage of a retarding grid in order to determine its retarding characteristics. Next, a copper plate acts as the ion collector. This can be seen in Figure 6.8. The design of the RPA that includes the size of the grids, the intermediate spacing and transparencies is based on published data by Gärtner, Böhm and Perrin [223, 225–227].

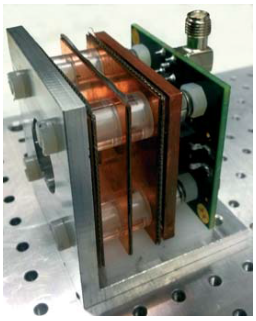

Figure 6.7: Retarding Potential Analyser

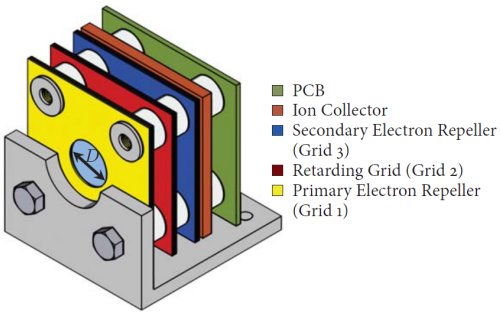

Figure 6.8: Retarding Potential Analyser Schematic [6]

[3] Polyoxymethylene

6.2. CATHODE TEST MODES

This section will discuss the modes in which the cathode can be tested in order to evaluate its performance. These are the diode mode and the thruster mode, which will be treated in Sections 6.2.1 and 6.2.2 respectively.

6.2.1. DIODE MODE

Diode mode testing is used in order to verify the functionality of the thermionic LaB_6 cathode. With this method, an aluminium plate is installed in front of the cathode. Next, a high voltage is applied to this plate in order to increase its potential. Hence, this plate acts as an anode and is able to attract the emitted electrons by the emitter (cathode) in order to close the electrical circuit. In Figure 6.9 this is shown where the anode consists out of a cylindrical part of aluminium that is placed using spacers and insulating boron nitride (white) above the emitting cathode. The LaB_6 emitter is placed inside the graphite heater on the insulating macor discs. Furthermore, clamping of the electrical wires is realised in order to obtain a strain relieved test setup.

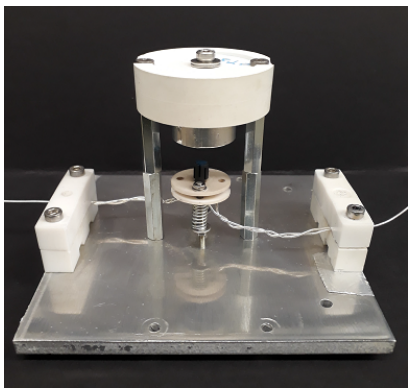

Figure 6.9: Diode Mode Testing [8]

The spacing between the emitter material and the anode is set to 4 mm initially. This has been done by taking the Child-Langmuir Equation (3.26) into account, as explained in Section 3.3. The anode should not be placed too close to the emitter by 1 or 2 mm, because then radiative heat losses and sputtering will affect the performance. Both the graphite heater, the boron nitride spacer and the LaB_6 material have very high temperatures and as radiation heat losses scale with T^4 and $1/r^2$, the radiative heating of the anode material plays an important role in relation to the conductive heating of the emitter material. Next to that, sputtering and deposition of graphite particles on the surrounding parts will affect the performance if the distance d between the emitter and the anode is small [228].

6.2.2. THRUSTER MODE

In thruster mode testing the aluminium plate is removed and the thruster is installed in order to act as an anode. Hereby, the functionality of the micro thruster system as a whole can be tested, where the emitted electrons guided into the discharge chamber of the thruster by means of the applied magnetic field. This test mode is illustrated in Figure 6.10, in which tungsten bulbs are used as a cathode.

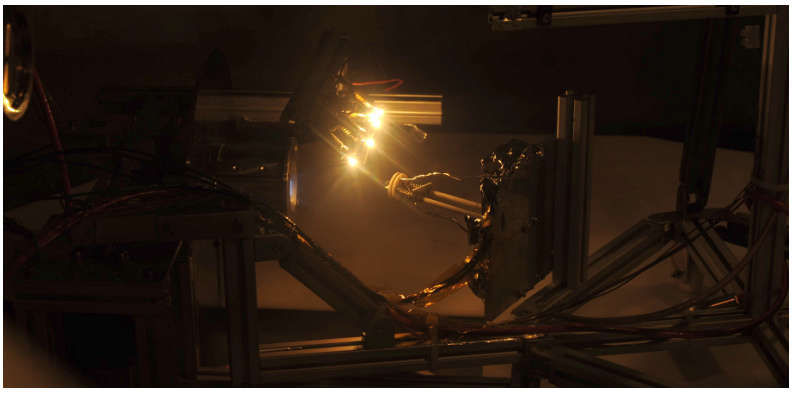

Figure 6.10: Thruster Mode Testing [8]

6.3. CONCLUSION

The test setup has been realised in order to be able to characterise the performance of various micro electric thrusters. In order to do so, high accuracy measurements of both the thrust and the ion plume are required. Table 6.1 gives a summary of the range, resolution and accuracy of the equipment that is used in order to realise the measurements. It can be seen that for each measurement the resolution is small enough for the errors to have little effect on any measurement uncertainties that could occur.

Table 6.1: Test Setup Characteristics

Measurement System	**Range**	**Resolution**	**Accuracy**
Vacuum Chamber	P_{amb} - $1.2 \cdot 10^{-7}$ mbar	10^{-10} mbar	3 - 6 %
Vacuum Chamber (thruster operating)	P_{amb} - $3.5 \cdot 10^{-6}$ mbar	10^{-10} mbar	3 - 6 %
Thrust range	0 - 2500 μN	0.1 μN	3.78 %
Rotatable jib	0 -180^o	$2.7 \cdot 10^{-5}$ ^{o}	5 % for 1.8^o
Faraday cup	0 - 0.2 μA	600 pA	0.5 %

Furthermore, it is possible to perform cathode tests in direct diode mode and in thruster mode. In the latter, the operating thruster is used as anode whereas for the direct diode mode, an aluminium part with a high potential is used as anode.

7

CONCLUSION AND RECOMMENDATIONS

This chapter discusses the literature study report by giving conclusions and recommendations. These are given in Sections 7.1 and 7.2 respectively. Furthermore, a preliminary thesis proposal is given in Section 7.3. Here, the thesis outline will be given.

7.1. CONCLUSION

In order to reflect on the research questions that are posed in Chapter 2, they are discussed in this part. Afterwards, conclusions on the current status are given.

1. What research has been performed in the field of micro propulsion engineering for low thrust (up to 10 mN) satellite missions?

   (a) What kind of cathodes have been used for electric propulsion in space up to know?

   - Various type of cathodes can be used for electric thruster applications. One option are thermionic cathodes, where an emitter material is directly (conductive) or indirectly (radiative) heated in order to emit electrons. This is a simple solution but the performance in terms of electron emission and heater efficiency is limited. Next to that, hollow cathodes can be used. These make use of low work function emitters such as barium oxide (1.55 eV) that are dispensed in the cathode tube. In this manner, the performance is high but so is the complexity. Finally, radio frequency cathodes can be selected. These have a long lifetime since they do not require an emitter insert. On the other hand, the system is complex and a high voltage power supply is required for both the radio frequency coil and the accelerator grid system.

   (b) Which materials have been used for these neutralisers and what are their properties?

   - Several materials can be used as electron emitters. The selection mainly depends on the value of the work function, i.e. the energy (heat) that is required to realise electron emission. Next to that, poisoning is an important aspect and life time (i.e. evaporation rate) needs to be taken into account as well. The most common emitter materials are listed in Table 7.1

Table 7.1: Work Function Emitter Materials

Material	W_0 [eV]
Tungsten	4.87
LaB_6	2.69
CeB_6	2.5
C12A7	2.4
BaO-W	2.1
BaO	1.55

   (c) Are there any new materials in the focus of the current research?

   - Current research focuses on LaB_6 and C12A7. These emitter materials are interesting because they show little sensitivity to poisoning, have a low evaporation rate and thus a long life time. Next to that, they have a reasonable work function and moreover, they are interesting emitter materials that could be used together with iodine as an operating propellant. This is important in particular because of the fact that micro electric thruster applications for CubeSats and other nanosatellites in the future will require an alternative propellant than xenon. This comes from the fact that secondary payloads (i.e. CubeSats) are not allowed to contain high pressurised propellant systems. Moreover, with iodine as a propellant, weight savings up to 50% can be reached.

(d) How are the different neutraliser materials being handled with respect to poisoning?

- There exist sensitive and insensitive emitter materials that can be used for cathode applications. The sensitive ones should be handled with care and in clean room conditions. These are the barium compound emitters. On the other hand, tungsten, C12A7 and the boron compounds such as LaB_6 and CeB_6 show less sensitivity to poisoning. Nonetheless, poisoning remains an important factor and it is recommended to have them stored in inert conditions such as e.g. a nitrogen purged volume. In this manner, poisoning is minimised [24, 60].

(e) Are the neutraliser materials compatible with different type of propellants?

- The barium compound neutraliser materials have a high sensitivity to poisoning. Hence, even if they are operated with noble gasses such as xenon or krypton as a propellant, the purity needs to be high. This results in the requirement for a special space grade xenon that has the highest purity available of 99.9995%. In this manner, the amount of oxygen and water vapour is minimised as much as possible, so that contamination risks are minimised [1, 97].

  The other emitter materials are compatible with various types of propellants such as e.g. xenon and krypton. Next to that, recent tests have shown that LaB_6 and C12A7 are compatible with iodine as well. In these tests no signs of degradation in performance or contamination of the emitter has been observed [31, 118, 119].

(f) Is the neutraliser compatible with iodine as a propellant?

- Both LaB_6 and C12A7 cathodes have been successfully tested with iodine as the operating propellant of the electric thruster system [31]. Nevertheless, it remains important to consider possible iodine deposition and to thermally design the cathode system for this. In this way, it can be reassured to minimise iodine deposition. Next to that, future cathode testing with iodine in thruster mode is required in order to analyse iodine compatibility.

2. What technology in the field of micro propulsion engineering for space systems is available on the market?

- Various electric thruster applications exist. These are pulsed plasma thrusters (PPT), radio frequency ion thrusters (RIT), colloid and electrospray thrusters, field emission electric propulsion (FEEP) systems and finally, the high efficiency multistage plasma thruster (HEMPT). They differ in complexity, thrust range, thrust noise and lifetime. Next to that, power to thrust ratio is an important aspect. The HEMPT has the lowest complexity and the longest lifetime. Furthermore, commercial off the shelf components can be used to realise an affordable micro electric thruster system. Therefore, this type of thruster is currently being developed at Airbus.

3. What is the position of Airbus on the market with respect to micro propulsion applications for space systems?

- Currently, Airbus is developing the μHEMPT in order to realise a nearly erosion-free operating micro electric thruster. The goal is to create a low complexity, affordable and long lifetime electric thruster system. In this manner, it can be implemented in the future on nanosatellites and CubeSats. With a propulsion system available on CubeSats, their mission objectives can be increased widely. The μHEMPT system needs only little propellant and can be operated without the need for large power supplies. The thruster system can fit into a tuna can shape cylinder extension that is installed at the far end of a 3U CubeSat with a diameter of 64 mm and a height of 36 mm.

4. What type of cathode should be used to realise the electric thruster system as a whole?

- In order to keep the complexity low and the performance high, a LaB_6 thermionic cathode will be designed for the micro electric thruster system. Vacuum chamber tests will show whether the performance is as predicted and whether design improvements are required. A hollow cathode can also be an option if the performance of the thermionic cathode turns out to be low. However, this slightly interferes with the low complexity design objective.

The goal with the μHEMPT is to achieve a thrust in the range of 20 - 100 μN, so that orbit raising manoeuvres in the range of 1500 - 1750 km can be realised within one year. In this manner, CubeSat mission lifetimes can be extended from the current 1 - 2 years up to 10 - 15 years. In addition to that, with thruster systems available on CubeSats, their mission objectives can be increased. One can think of formation flying missions, space telescope architectures, frequency array constellations, global timely and accurate weather forecasting platforms, global (forest) fire detection systems or cargo ship monitoring systems. In addition to that, deorbiting applications can be realised, which is an important topic nowadays.

The cathode emits electrons which are led into the discharge chamber of the thruster. The emitter material is heated to temperatures above 1300 K in order to provide sufficient thermal energy to the electrons to be emitted by means of an enclosed graphite heater. A boron nitride spacer is placed in between the graphite heater and the emitter material so that electrical insulation between the two can be realised. This material can cope with the high operating temperatures of the lanthanum hexaboride (LaB_6) emitter material and is able to thermally conduct the heat from the graphite heater. With an anode voltage in the range of 155 - 1200 V a current emission of 163 μA is currently achieved. In future iterations of the cathode, it is aimed to increase the emitted current by improving the cathode design, lowering the cable losses and lowering heat radiation losses.

Currently, the μHEMPT thruster is operated with the noble gas xenon. Because of its large atomic mass, the low ionisation energy and inert properties this propellant is used for many electric thrusters. However, it needs to be stored in pressurised vessels at pressures around 300 bar. These propellant tanks will require many qualification tests in the form of safe life demonstration, stress analysis, vibration testing and fatigue properties which would all cost a lot in terms of time and money. In addition to that, pressurised systems are typically not allowed on CubeSats by the primary launch customer if the CubeSats are launched piggy back as a secondary payload. Therefore, the alternative propellant iodine is being investigated. It has similar propulsive performances as xenon, but can be stored as a solid granulate. Therefore, it eliminates the need for any pressurised vessels and thus CubeSat applicability is ensured. In addition to that, weight can be reduced by using a simple propellant (feed) system. This contributes to one of the main goals of the system as a whole which is low complexity.

7.2. RECOMMENDATIONS

When the vacuum chamber tests are performed, it is important to take radiation losses into account. These are especially important for emitter materials that are operated at high temperatures such as lanthanum hexaboride (T > 1300 K), as radiation heat losses scale with T^4. Radiation heat losses inside the vacuum chamber are possible due to the temperature differences between the test setup and the walls of the chamber. In order to take these into account, one can make an assessment of them using initial estimations from the heat radiation equation or by making a model in a thermal modelling suite such as ESATAN. Furthermore, radiation losses can be minimised by covering the test setup with a aluminium foil house or a multi-layer insulation blanket. Nevertheless, it is important to keep in mind that emitted electrons should not be able to travel to such an equipment if it is used in the test setup.

Considering the storage of the cathode parts, it is recommended to use nitrogen purged bags or environments. Here, oxygen levels and low and in this manner, oxidation and contamination risks are minimised and the quality and performance of the cathode can be ensured. Furthermore, it is important to use organic cleansing solvents such as isopropyl alcohol on components that are in direct proximity to the emitter material in order to prevent contamination by outgassing. In this manner degradation in performance of the emitter material is reduced.

Finally, it is recommended to perform qualification and acceptance tests on the cathode system in the near future. In this manner, the current technology readiness level (TRL) can be increased from 4 to 6. The current TRL is 4. This means that the cathode has been tested on a component level in a laboratory environment (i.e. vacuum chamber). After the commercialisation and qualification the TRL can be increased to 6. At that level, the cathode prototype can be demonstrated in a relevant environment (i.e. either ground or space).

7.3. PRELIMINARY THESIS PROPOSAL

Now that the literature study is conducted, the main thesis period commences and therefore a preliminary thesis proposal will be given. In order to do so, a reflection will be made first to the thesis research questions as they are posed in Section 2.1.2. They are shortly discussed below.

1. What criteria are relevant for assessing the performance of various types of cathodes for micro propulsion systems?
    - The main parameters that will be analysed in the cathode tests are the required heater power (input) to realise the desired discharge current (output) of 10 mA. If the cathode is operational, it will be tested in thruster mode as well so that a general characterisation of the thruster as a whole can be given next to that of the cathode. This results in values such as power to thrust ratio (PTTR) and thrust to mass ratio.
2. What is the value and quality of the different types of cathodes in view of the assessment criteria?
    - This research question concerns the comparison of the different types of cathodes that are tested. In order to give a clear and concise comparison between them, various parameters such as heater power and discharge current will be compared. Next to that, qualitative aspects such as contamination and ease of assembly, integration and verification will be addressed.
3. What do we learn from comparing results from the analyses and results of the different types of cathodes in order to establish recommendations on how to develop an efficient cathode for micro propulsion systems?
    - This question serves as the final research question that needs to be reflected on in order to give proper conclusions on the cathode design for a micro electric thruster.

The research objective of the thesis will be to realise a low complexity, affordable and efficient operating cathode for the high efficiency multistage plasma thruster at Airbus by comparing the thermal, mechanical and electrical performance of different cathodes that make use of various emitter materials. In order to give a brief overview of the main thesis period of six months, or 26 weeks, a timeline is given in Figure 7.1. This timeline lists the main activities.

First, a next iteration design of a thermionic LaB_6 cathode will be made and tested. This is done in the first four weeks, i.e. December 2017. Afterwards, either a more detailed design or a different cathode design will be realised. This involves improving on the thermal aspects of the cathode design in order to minimise heat losses. In addition to that, the setup will be optimised from an electrical point of view so that all the electrical connections are optimised and reliable. Furthermore, the first cathode tests in the vacuum chamber will indicate whether it is required to add magnets in order to introduce a magnetic field. This field can be used to assist the electrons in following the desired path from emitter (cathode) to the high voltage anode. This iteration, including the testing phase and the evaluation will take place from week 5 - week 13.

Next, the objective is to perform a short analysis to establish the current state and performance of the cathode. This also includes the compatibility analysis with the micro electric thruster in order to give a complete system status overview. If the cathode is operational in diode mode, it will be tested in thruster mode as well. Thruster mode testing will result in the desired results considering iodine propellant compatibility. Next to that, thruster mode testing involves important design decisions in order to allow future application and utilisation on CubeSats and other nanosatellites. Afterwards, the goal is to optimise the design and validate the overall performance. This period until week 23 will include items such as a sensitivity analysis, risk mitigation and compliance checks. Finally, in week 24 - 26, the thesis work will be evaluated and presented.

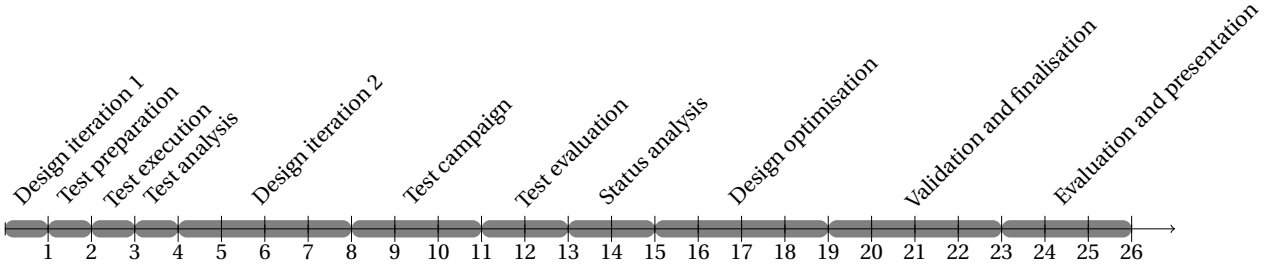

Figure 7.1: Timeline Thesis Period (in Weeks)

REFERENCES

[1] D. M. Goebel, R. M. Watkins, and K. K. Jameson, *LaB_6 Hollow Cathodes for Ion and Hall Thrusters*, Vol. 23 (Journal of Propulsion and Power, 2007).

[2] S. Frosch, *Electric Propulsion CubeSat Parameter Survey* (Duale Hochschule Baden-Württemberg Ravensburg, 2016).

[3] J. R. Wertz and W. J. Larson, *Space Mission Analysis and Design*, 3rd ed. (Microcosm, 1999).

[4] D. Papendorf, *Development and Test of an Iodine Feeding System for Electric Propulsion* (University of Stuttgart, 2017).

[5] M. R. Nakles, W. A. Hargus, J. J. Delgado, and R. L. Corey, *A performance comparison of xenon and krypton propellant on an SPT-100 Hall thruster*, 32nd ed. (International Electric Propulsion Conference, 2011).

[6] F. G. Hey, *Development and Test of a Micro-Newton Thruster Test Facility and Micro-Newton HEMP Thruster* (Technische Universität Dresden, 2016).

[7] M. Schramm, *Development and Test of a μHEMPT Engineering Model for CubeSat Application* (University of Stuttgart, 2017).

[8] S. Frosch, *Development of a LaB6 Cathode for Micro Electric Thrusters* (Duale Hochschule Baden-Württemberg Ravensburg, 2017).

[9] R. J. Cassady and W. A. Hoskins, *A Micro Pulsed Plasma Thruster (PPT) for the "Dawgstar" Spacecraft* (Primex Aerospace Company, 2000).

[10] J. Mueller, R. Hofer, and J. Ziemer, *Survey of Propulsion Technologies Applicable to Cubesats* (Jet Propulsion Laboratory, 2010).

[11] S. C. Borgmeyer, *Electric Propulsion Systems and Components* (Ariane Group, 2015).

[12] J. Mueller, *Thruster Options for Microspacecraft: A review and Evaluation of State-of-the-Art and Emerging Technologies*, Vol. 187 (Micropropulsion for Small Spacecraft, Progress in Astronautics and Aeronautics, 2000).

[13] L. Guerra and P. Graf, *Cost Estimating Module* (National Aeronautics and Space Administration, 2008).

[14] P. P. Uroine and R. Hinrichs, *Magnetic Field Strenght: Force on a Moving Charge in a Magnetic Field* (Technische Universität Dresden, 2012).

[15] P. Lam, *Magnetic Field and Magnetic Forces* (Pearson Addison Wesley, 2008).

[16] M. Advadhanulu and P. Kshirsagar, *A Textbook of Engineering Physics* (S. Chand, 2014).

[17] F. G. Hey, T. Brandt, and G. Kornfeld, *Downscaling a HEMPT to micro-Newton Thrust levels: current status and latest results*, 30th ed. (International Symposium on Space Technology and Science, Japan, 2015).

[18] E. Buchen and D. DePasquale, *Nano / Microsatellite Market Assessment* (SpaceWorks Enterprises, 2014).

[19] R. Munakata, W. Lan, and S. Lee, *Cubesat Design Specification* (California Polytechnic State University, 2014).

[20] D. Goebel and I. Katz, *Fundamentals of Electric Propulsion: Ion and Hall Thrusters* (Wiley, 2008).

[21] H. Watanabe, T. Hatakeyama, I. Masatoshi, and A. Okutsu, *Study on Radio Frequency Cathode for Ion Engines*, Vol. 7 (The Japan Sociey for Aeronautical and Space Sciences, 2009).

[22] H. J. Leiter, *Entwicklung, Bau und Test eines RIT15 "Breadboard Engineering Models"* (University of Giessen, 2010).

[23] J. Etourneau, J. Mercurio, R. Naslain, and P. Hagenmuller, *Structure Electronique de Quelques Hexaborures de Type CaB6*, Vol. 2 (Journal of Solid State Chemistry, 1970).

[24] H. E. Gallagher, *Poisoning of LaB_6 Cathodes*, Vol. 40 (Journal of Applied Physics, 1969).

[25] D. J. Warner and R. D. Branam, *Ignition and Plume Characteristics of Low-Current Cerium and Lanthanum Hexaboride Hollow Cathodes*, Vol. 26 (Journal of Propulsion and Power, 2010).

[26] Y. Toda, H. Yanagi, E. Ikenaga, J. J. Kim, M. Kobata, S. Ueda, and T. Kamiya, *Work Function of a Room-Temperature, Stable Electride [Ca24Al28O64]4+(e-)4*, Vol. 19 (Advanced Materials, 2007).

[27] M. S. McDonald and N. R. S. Caruso, *Ignition and Early Operating Characteristics of a Low- Current C12A7 Hollow Cathode*, 35th ed. (International Electric Propulsion Conference, 2017).

[28] W. H. Kohl, *Handbook of Materials and Techniques for Vacuum devices* (Reinhold, 1967).

[29] J. Dankanich, D. Calvert, H. Kamhawi, T. Hickman, J. Szabo, and L. Byrne, *The Iodine Satellite (iSat) Project Development towards Critical Design Review*, 34th ed. (International Electric Propulsion Conference, 2015).

[30] L. P. Rand, *A Calcium Aluminate Electricde Hollow Cathode* (Colorado State University, 2014).

[31] J. Szabo, M. Robin, S. Paintal, B. Pote, V. Hruby, and C. Freeman, *Iodine Propellant Space Propulsion*, 33rd ed. (International Electric Propulsion Conference, 2013).

[32] R. E. Honig, *Vapor pressure curve for the more common elements* (RCA Laboratories, 1957).

[33] J. R. Rumble, *Handbook of Chemistry and Physics*, 98th ed. (CRCPress, 2017).

[34] E. Ambrosetto and D. Pedersen, *Properties and Characteristics of Graphite* (POCO Graphite an Entegris Company, 2015).

[35] E. J. Pencil, *Pulsed Plasma Thrusters* (National Aeronautics and Space Administration, 2004).

[36] R. Wirz, R. Sullivan, J. Przybylowski, and M. Silva, *Discharge Hollow Cathode and Extraction Grid Analysis for the MiXI Ion Thruster*, Vol. 2008 (International Journal of Plasma Science and Engineering, 2008).

[37] D. Feili, B. Lotz, S. Bonnet, H. Loeb, and H. Puetman, *µRIT-2.5 – A New Optimized Microthruster of Giessen University*, 31st ed. (International Electric Propulsion Conference, 2009).

[38] T. Trudel, S. Bilen, and M. Mici, *Design and Performance testing of a 1-cm Miniature Radio Freqeuncy Ion Thruster*, 31st ed. (International Electric Propulsion Conference, 2009).

[39] J. Ziemer, *Delivery of Colloid Micro-Newton Thrusters for the Space Technology 7 Mission*, 44th ed. (AIAA/ASME/SAE/ASEE Joint Propulsion Conference, 2008).

[40] N. Demmons, *ST7-DRS Mission Colloid Thruster Development*, 44th ed. (AIAA/ASME/SAE/ASEE Joint Propulsion Conference, 2008).

[41] M. Tajmar, A. genovese, and W. Steiger, *Indium Field Emission Electric Propulsion Microthruster Experimental Characterization*, Vol. 30 (Journal of Propulsion and Power, 2004).

[42] D. Nicoline and P. E. Frigot, *ESA Designs its smallest ever space engine to push back against sunshine* (European Space Agency, 2009).

[43] R. Ogura, *NJK1120A Cathode* (New Japan Radio Co., 2008).

[44] G. Sutto, *Extended Life LaB_6 Cathode User Information* (Kimball Physics Inc., 1991).

[45] M. S. McDonald, A. D. Gallimore, and D. M. Goebel, *Note: Improved heater design for high-temperature hollow cathodes*, Vol. 88 (Review of Scientific Instruments, 2017).

[46] P. Verschuren and H. Doorewaard, *Designing a Research Project*, 2nd ed. (Eleven International Publishing, 2010).

[47] N. E. Jensen and J. A. Gonzalez del Amo, *Present and Future of Space Electric Propulsion in Europe* (European Space Agency, 2015).

[48] F. G. Hey, M. Vaupel, I. G. Moneva, D. Papendorf, C. Braxmaier, and M. Tajmar, *The Next Generation milli-Newton µHEMPT as Potential Main Thruster for Small Satellites*, 35th ed. (International Electric Propulsion Conference, 2017).

[49] G. P. Sutton and O. Biblarz, *Rocket Propulsion Elements*, 9th ed. (Wiley, 2016).

[50] T. Uhlig, F. Sellmaier, and M. Schmidhuber, *Spacecraft Operations* (Springer, 2015).

[51] H. P. Harmann, N. Koch, and G. Kornfeld, *Physics and Evolution of HEMP-Thrusters*, 30th ed. (International Electric Propulsion Conference, 2007).

[52] C. Kittel, *Introduction to Solid State Physics*, 8th ed. (John Wiley and Sons Ltd., 2004).

[53] R. Eisberg and R. Resnick, *Quantum Physics of Atoms, Molecules, Solids, Nuclei and Particles*, 2nd ed. (John Wiley & Sons Inc., 1985).

[54] S. Dushman, *Electron Emission from Metals as a Function of Temperature*, Vol. 21 (Physical Review Journals Archive, 1923).

[55] K. L. Jensen, *Advances in Imaging and Electron Physics*, Vol. 149 (Electron Emission Physics, 2007).

[56] O. W. Richardson, *The Emission of Electricity from Hot Bodies* (Longmans, Green and Company, 1921).

[57] A. T. Forrester, *Large Ion Beams* (Wiley-Interscience, 1988).

[58] E. Storms and B. Mueller, *A Study of Surface Stoichiometry and Thermionic Emission Using LaB_6*, Vol. 50 (Journal of Applied Physics, 1979).

[59] J. Pelletier and C. Pomot, *Work Function of Sintered Lanthanum Hexaboride*, Vol. 34 (Applied Physics Letters, 1979).

[60] J. L. Cronin, *Modern Dispenser Cathodes*, Vol. 128 (IEE Proceedings (Solid-State and Electron Devices), 1981).

[61] J. M. Lafferty, *Boride Cathodes*, Vol. 22 (Journal of Applied Physics, 1951).

[62] D. Jacobson and E. K. Storms, *Work Function Measurement of Lanthanum-Boron Compounds*, Vol. 6 (IEEE Transactions on Plasma Science, 1978).

[63] C. D. Child, *Discharge from Hot CaO*, Vol. 32 (Physical Review Journals Archive, 1911).

[64] I. Langmuir, *The Effect of Space Charge and Residual Gases on Thermionic Currents in High Vacuum*, Vol. 2 (Physical Review Journals Archive, 1913).

[65] A. Keller, *Feasibility of a down-scaled HEMP Thruster* (University of Giessen, 2013).

[66] N. Koch, G. Kornfeld, and G. Coustou, *The HEMP Thruster - An Alternative to Conventional Ion Sources?* (Thales, 2003).

[67] J. Haderspeck, S. Weis, B. van Reijen, A. Genovese, A. Lazurenko, R. Heidemann, P. Holtmann, K. Ruf, and N. Püttmann, *HEMP Thruster Assembly Performance with increased Gas Tubing Lengths of Flowing Control Unit*, 34th ed. (International Electric Propulsion Conference, 2015).

[68] F. G. Hey, M. Vaupel, and C. Braxmaier, *HEMPT Downscaling, Way Forward to the First EM for CubeSat Applications*, 35th ed. (International Electric Propulsion Conference, 2017).

[69] K. Lemmer, *Propulsion for CubeSats*, Vol. 134 (ACTA Astronautica, 2017).

[70] R. Zeledon and M. Peck, *Electrolysis Propulsion for CubeSat-Scale Spacecraft* (AIAA Space Conference & Exposition, 2011).

[71] D. Schmuland, R. Masse, and C. Sota, *Hydrazine Propulsion Module for CubeSats* (Small Satellite Conference, 2011).

[72] K. Woellert, P. Ehrenfreund, A. J. Ricco, and H. Hertzfeld, *CubeSats: Cost-effective science and technology platforms for emerging and developing nations*, Vol. 47 (Advances in Space Research, 2011).

[73] H. Heidth, J. Puig-Suari, A. S. Moore, S. Nakasuka, and R. J. Twiggs, *CubeSat: A new Generation of Picosatellite for Education and Industry Low-Cost Space Experimentation*, 14th ed. (AIAA/USU Conference on Small Satellites, 2000).

[74] J. A. Gonzalez del Amo, *Activities on Electric Propulsion at ESA* (Space Propulsion Conference, Rome, 2016).

[75] A. Bulit, J. P. Luna, and J. A. Gonzalez del Amo, *Experimental Investigations on the Influence of the Facility Background Pressure on the Plume of the RIT-4 Ion Engine*, 32nd ed. (International Electric Propulsion Conference, Wiesbaden, 2011).

[76] K. Danzmann, H. Audley, and S. Babak, *Laser Interferometer Space Antenna* (Albert Einstein Institute Hannover, 2017).

[77] A. L. Verlaan, H. Hogenhuis, and J. Pijnenburg, *LISA Telescope Assembly Optical Stability Characterization for ESA* (Netherlands Organisation for Applied Scientific Research, 2012).

[78] G. Noci, G. Matticari, P. Siciliano, L. Fallerini, L. Boschini, and V. Vettorello, *Cold Gas Micro Propulsion System for Scientific Satellites fine pointing: Review of Development and Qualification activities at Thales Alenia Space Italia*, 45th ed. (AIAA/ASME/SAE/ASEE Joint Propulsion Conference and Exhibit, 2009).

[79] J. Jarrige, P. Thobois, C. Blanchard, P. Elias, D. Packan, L. Fallerini, and G. Noci, *Thrust Measurements of the GAIA Mission Flight-Model cold gas thruster*, Vol. 30 (Journal of Propulsion and Power, 2014).

[80] J. Berg, P. Touboul, and M. Rodrigues, *Status of MICROSCOPE, A Mission to Test the Equivalence Principle in Space*, Vol. 610 (Journal of Physics: Conference Series, 2015).

[81] B. S. Rock, J. J. Blandino, and M. A. Demetriou, *Propulsion Requirements for Drag-Free Operation of Spacecraft in Low Earth Orbit*, Vol. 43 (Journal of Spacecraft and Rockets, 2006).

[82] P. Marchetti, J. J. Blandino, and M. A. Demetriou, *Electric Propulsion and Controller Design for Drag-Free Spacecraft Operation*, Vol. 45 (Journal of Spacecraft and Rockets, 2008).

[83] S. Singh, S. D'Amico, and M. Pavone, *High-Fidelity Modeling and Control System Synthesis for a Drag-free Microsatellite* (Department of Aeronautics and Astronautics, Stanford University, 2015).

[84] J. J. Blandino, J. M. Parker, D. P. Thunnissen, and G. B. Ganapathi, *The Preliminary Design and Status of a Hydrazine Millinewton Thruster Development*, 35th ed. (AIAA/ASME/SAE/ASEE Joint Propulsion Conference and Exhibit, 1999).

[85] J. Mueller, H. Goldberg, and L. Alkalai, *Micro-Inspector Spacecraft Testbed: Breadboard Subsystem Demonstrations*, 5th ed. (Conference on Human/Robotic Technology and Vision for Space Exploration, 2007).

[86] D. Lev and J. Herscovitz, *Carbon Dioxide Based Heated Gas Propulsion System for Nano-Satellites*, 31st ed. (AIAA/USU Conference on Small Satellites, 2017).

[87] R. J. Twiggs, J. Puig-Suari, and C. Turner, *The Development and Launch Support Infrastructure for Eighteen Different Satellite Customers on One Launch*, 15th ed. (AIAA/USU Conference on Small Satellites, 2001).

[88] R. Levi, *Improved Impregnated Cathode*, Vol. 26 (Journal of Applied Physics, 1955).

[89] W. G. Tighe, D. M. Goebel, R. Longo, and K. R. Chien, *Hollow Cathode Ignition and Life Model*, Vol. 43 (American Institute of Aeronautics and Astronautics, 2005).

[90] D. Rafalskyi and A. Aanesland, *A Neutralizer-Free Gridded Ion Thruster Embedded Into A 1U Cubesat Module*, 35th ed. (International Electric Propulsion Conference, 2017).

[91] L. Bardos, *Radio frequency hollow cathodes for the plasma processing technology*, Vol. 87 (Surface and Coatings Technology, 1996).

[92] H. J. L. R. Killinger, *Development of the Radio Frequency Ion Thruster RIT XT - A Status Report*, 27th ed. (International Electric Propulsion Conference, 2001).

[93] H. Kaufman, *Technology of Electron-Bombardment Ion Thrusters*, Vol. 36 (Advances in Electronics and Electron Physics, 1975).

[94] L. Turner, *Electronics Engineer's Reference Book*, 6th ed. (Newnes-Butterworth, 1976).

[95] G. C. Soulas, *Status of Hollow Cathode Heater Development for the Space Station Plasma Contactor*, Vol. 32 (American Institute of Aeronautics and Astronautics, 1994).

[96] W. G. Tighe, K. Freick, and K. R. Chien, *Performance Evaluations and Life Test of the XIPS Hollow Cathode Heater*, Vol. 43 (American Institute of Aeronautics and Astronautics, 2005).

[97] D. M. Goebel and E. Chu, *High Current Lanthanum Hexaboride Hollow Cathodes for High Power Hall Thrusters*, 32nd ed. (International Electric Propulsion Conference, 2011).

[98] D. M. Goebel, I. Katz, Y. Mikellides, and K. Polk, *Extending Hollow Cathode life for Deep Space Missions*, Vol. 40 (The American Institute of Aeronautics and Astronautics, 2004).

[99] D. J. Warner, R. D. Branam, W. A. Hargus, and D. M. Goebel, *Low Current Cerium Hexaboride and Lanthanum Hexaboride Hollow Cathodes*, Vol. 46 (American Institute of Aeronautics and Astronautics, 2008).

[100] B. A. Arkhopov and K. N. Kozubsky, *The Development of the Cathode Compensators for Stationary Plasma Thrusters in the USSR*, 22nd ed. (International Electric Propulsion Conference, 1991).

[101] V. Kim, *Electric Propulsion Activity in Russia*, 23rd ed. (International Electric Propulsion Conference, 2001).

[102] E. Storms and B. Mueller, *Phase Reliationship, Vaporization and Thermodynamic Properties of the Lanthanum-Born System*, Vol. 82 (Journal of Chemical Physics, 1978).

[103] K. N. Leung, P. A. Pincosy, and K. W. Ehlers, *Directly Heated Lanthanum Hexaboride Filaments*, Vol. 55 (Review of Scientific Instruments, 1984).

[104] D. M. Goebel, Y. Hirooka, and T. Sketchley, *Large Area Lanthanum Hexaboride Electron Emitter*, Vol. 56 (Review of Scientific Instruments, 1985).

[105] D. M. Goebel, J. T. Crow, and A. T. Forrester, *Lanthanum Hexaboride Hollow Cathode for Dense Plasma Production*, Vol. 49 (Review of Scientific Instruments, 1978).

[106] L. J. Favreau, *Cataphoretic Coating Lanthanum Boride on Rhenium Filaments*, Vol. 36 (Review of Scientific Instruments, 1965).

[107] A. N. Boers, *Electron Gun Using Long-Life Lanthanum Hexaboride Cathode*, Vol. 38 (Journal of Applied Physics, 1992).

[108] L. A. Christman, G. A. Schwind, and L. W. Swanson, *A Comparison of CeB_6 and LaB_6 Thermionic Cathodes*, 49th ed. (Annual Meeting of the Electron Microscopy Society of America, 1991).

[109] L. W. Swanson and D. R. McNeely, *Work Functions of the (001) Face of the Heaborides of Ba, La, Ce and Sm*, Vol. 83 (Journal of Surface Science and Technology, 1997).

[110] P. R. Davis, M. A. Gesley, G. A. Schwind, L. W. Swanson, and J. J. Hutta, *Comparison of Thermionic Cathode Parameters of Low Index Single Crystal Faces of LaB_6, CeB_6 and PrB_6*, Vol. 37 (Applied Surface Science, 1989).

[111] D. J. Warner, *Advanced Cathode for Next Generation Electric Propulsion Technology* (U.S. Air Force Institute of Technology, 2008).

[112] J. S. Sovey and S. D. Kovaleski, *Preliminary Results of Field Emission Cathode Tests*, 27th ed. (International Electric Propulsion Conference, 2001).

[113] P. V. Sushko, A. L. Schluger, M. Hirano, and H. Hosono, *From Insulator to Electride: A Theoretical Model of Nanoporous Oxide 12CaO7Al2O3*, Vol. 129 (Journal of the American Chemical Society, 2007).

[114] S. Kim, Y. Toda, K. Hayashi, M. Hirano, and H. Hosono, *Synthesis of a Room Temperature Stable 12CaO7Al2O3 Electride from the Melt and Its Application as an Electron Field Emitter*, Vol. 18 (Chemistry of Materials, 2006).

[115] Y. Toda, S. Kim, K. Hayashi, M. Hirano, T. Kamiya, H. Hosono, T. Haraguchi, and H. Yasuda, *Intense thermal field electron emission from room-temperature stable electride*, Vol. 87 (Applied Physics Letters, 2005).

[116] Y. Toda, S. Matsuishi, K. Hayashi, K. Ueda, T. Kamiya, M. Hirano, and H. Hosono, *ChemInform - Work Function of a Room-Temperature, Stable Electride [Ca24Al28O64] 4+(e-)4.*, Vol. 16 (Advanced Materials, 2004).

[117] R. H. Huang and J. L. Dye, *Low temperature (-80 ^{o}C) thermionic electron emission from alkalides and electrides*, Vol. 166 (Chemical Physics Letters, 1990).

[118] L. P. Rand and J. D. Williams, *Instant Start Electride Hollow Cathode*, 33rd ed. (International Electric Propulsion Conference, 2013).

[119] L. P. Rand, J. D. Williams, J. Blakely, B. Beal, and D. Brown, *C12A7 Electride Hollow Cathode*, 60th ed. (JANNAF Space Propulsion Meeting, 2013).

[120] Y. Toda, H. Yanagi, E. Ikenaga, J. J. Kim, M. Kobata, S. Ueda, T. Kamiya, M. Hirano, K. Kobayashi, and H. Hosono, *Work Function of a Room-Temperature, Stable Electride [Ca24Al28O64]4+(e–)4*, Vol. 19 (Advanced Materials, 2007).

[121] Y. Toda, H. Yanagi, E. Ikenaga, J. J. Kim, M. Kobata, S. Ueda, T. Kamiya, M. Hirano, K. Kobayashi, and H. Hosono, *ChemInform - Work Function of a Room-Temperature, Stable Electride [Ca24Al28O64] 4+(e-)4.*, Vol. 39 (John Wiley and Sons, 2008).

[122] S. Kim, S. Matsuishi, M. Miyakawa, K. Hayashi, M. Hirano, and H. Hosono, *Fabrication of room temperature-stable C12A7 electride: a review*, Vol. 18 (Journal of Materials Science: Materials in Electronics, 2007).

[123] J. E. Medvedeva, E. N. Teasley, and M. D. Hoffman, *Electronic band structure and carrier effective mass in calcium aluminates*, Vol. 76 (Physical Review B, 2007).

[124] Y. Toda, S. Matsuishi, K. Hayashi, K. Ueda, T. Kamya, M. Hirano, and H. Hosono, *Field Emission of Electron Anions Clathrated in Subnanometer-Sized Cages in [Ca24Al28O64]4+(4e-)*, Vol. 16 (Advanced Materials, 2004).

[125] S. Matsuishi, Y. Toda, M. Miyakawa, K. Hayashi, T. Kamiya, M. Hirano, I. Tanaka, and H. Hosono, *Fabrication of room temperature-stable C12A7 electride: a review*, Vol. 301 (American Association for the Advancement of Science, 2003).

[126] Y. Toda, Y. Kubota, M. Hirano, H. Hirayama, and H. Hosono, *Surface of Room-Temperature-Stable Electride [Ca24Al28O64]4+(e-)4: Preparation and Its Characterization by Atomic-Resolution Scanning Tunneling Microscopy*, Vol. 5 (American Chemical Society Nano, 2011).

[127] H. Hosono, S. Kim, M. Miyakawa, S. Matsuishi, and T. Kamiya, *Thin film and bulk fabrication of room-temperature-stable electride C12A7:e- utilizing reduced amorphous 12CaO7Al2O3 (C12A7)*, Vol. 354 (Journal of Non-Crystalline Solids, 2008).

[128] S. Kim, M. Miyakawa, K. Hayashi, T. Sakai, M. Hirano, and H. Hosono, *Simple and Efficient Fabrication of Room Temperature Stable Electride: Melt-Solidification and Glass Ceramics*, Vol. 127 (Journal of the American Chemical Society, 2005).

[129] S. Miyazaki, T. Maruyama, A. Kohno, and M. Hirose, *Photoelectron yield spectroscopy of electronic states at ultrathin SiO2Si interfaces*, Vol. 48 (Microelectronic Engineering, 1999).

[130] R. Schlaf, H. Murata, and Z. H. Kafafi, *Work function measurements on indium tin oxide films*, Vol. 120 (Journal of Electron Spectroscopy and Related Phenomena, 2001).

[131] N. R. S. Caruso and M. S. McDonald, *Thermionic Emission Measurements of 12(CaO)-7(Al2O3) Electride in a Close-Spaced Diode*, 35th ed. (International Electric Propulsion Conference, 2017).

[132] D. M. Goebel and R. M. Watkins, *Compact lanthanum hexaboride hollow cathode*, Vol. 81 (Review of Scientific Instruments, 2010).

[133] J. C. Zheng, L. Zhang, and A. V. Kretin, *High thermal conductivity of hexagonal boron nitride laminates*, Vol. 3 (2D Materials, 2016).

[134] P. Wellmann, *Materialien der Elektronik und Energietechnik: Halbleiter, Graphen, funktionale Materialien* (Springer Vieweg, 2016).

[135] W. A. Hargus, J. S. Lubkeman, K. E. Remy, and A. E. Gonzales, *Investigation of Singly Ionized Iodine Spectroscopy in Support of Electrostatic Propulsion Diagnostics Development* (Air Force Research Laboratory, 2012).

[136] D. Jacobson and D. Manzella, *50 kW class krypton hall thruster performance*, 39th ed. (Joint Propulsion Conference and Exhibit, 2003).

[137] J. A. Linnel and A. D. Gallimore, *Efficiency analysis of a hall thruster operating with krypton and xenon*, Vol. 22 (Journal of Propulsion and Power, 2006).

[138] J. F. Seixal, S. L. Mauro, B. L. Lewis, G. A. Jerman, D. H. Calvert, J. Dananich, K. A. Polzin, and S. R. Peeples, *Propulsion System Development for the Iodine Satellite (iSat) Demonstration Mission*, 34th ed. (International Electric Propulsion Conference, 2015).

[139] L. J. Cheney, *Development of Safety Standards for CubeSat Propulsion Systems* (California Polytechnic State University, 2014).

[140] J. Dankanich, H. Kamhawi, R. C. Hunter, and A. Petro, *The Iodine Satellite* (National Aeronautics and Space Administration, 2015).

[141] J. Dankanich, K. A. Polzin, and D. Calvert, *The Iodine Satellite (iSat) Hall Thruster Demonstration Mission Concept and Development*, 50th ed. (Joint Propulsion Conference, 2014).

[142] S. Mauro, *Thermal Analysis of Iodine Satellite (iSAT) from Preliminary Design Review (PDR) to Critical Design Review (CDR)*, 46th ed. (International Conference on Environmental Systems, 2014).

[143] P. A. Schweitzer, *Corrosion Engineering Handbook*, 2nd ed. (CRC Press, 1996).

[144] J. C. Wren, G. A. Glowa, and J. Merritt, *Corrosion of Stainless Steel by Gaseous I_2*, Vol. 265 (Journal of Nuclear Materials, 1999).

[145] K. Iwamoto and J. Oishf, *The Behavior of Iodine in Adsorption and Desorption by Graphite*, Vol. 5 (Journal of Nuclear Science and Technology, 1968).

[146] G. Y. Lai, *High Temperature Corrosion and Materials Applications* (ASM International, The Materials Information Society, 2007).

[147] M. G. Fontana and R. W. Staehle, *Advances in Corrosion Science and Technology* (Plenum Press, 1976).

[148] M. Bulera and P. Mark, *Chemical Resistance Chart - Hydrogen Gas - Methyl Acrylate* (Quick Cut Gasket & Rubber Corporation, 2017).

[149] A. Voerman, C. Bakelaar, and R. Nusmeier, *Chemical Resistance Chart* (Pro Rotating, 2017).

[150] P. J. McHale, D. Flinterman, and B. Clerx, *Chemical Compatibility Guide* (Graco, 2013).

[151] D. Scheidler and R. Cunningham, *Chemical resistance* (Masterflex Group, 2013).

[152] F. K. Farhangi-Najafi, *PEEK Chemical Compatibility* (CP Lab Safety, 2013).

[153] E. Wendler-Kalsch and H. Gräfen, *Korrosionsschadenkunde* (Springer, 1998).

[154] H. Simmons and A. Whiles, *Corrosion resistance of titanium* (Timet - Titanium Metals Corporation, 1997).

[155] M. W. Crofton and T. D. Hain, *Environmental Considerations for Xenon Electric Propulsion*, 30th ed. (International Electric Propulsion Conference, 2007).

[156] G. Parissenti, N. Koch, D. Pavarin, E. Ahedo, K. Katsonis, F. Scortecci, and M. Pessana, *Non Conventional Propellants for Electric Propulsion Activities* (Space Propulsion, 2010).

[157] R. A. Buerschaper, *Thermal and Electrical Conductivity of Graphite and Carbon at Low Temperatures*, Vol. 15 (Journal of Applied Physics, 1944).

[158] P. Molina-Cabrera, G. Y. Herdrich, M. Z. Lau, and S. X. Fausolas, *Pulsed Plasma Thrusters: a worldwide review and long yearned classification*, 32nd ed. (International Electric Propulsion Conference, 2011).

[159] W. J. Guman and D. M. Nathanson, *Pulsed Plasma Microthruster Propulsion System for Synchronous Orbit Satellite*, Vol. 7 (Journal of Spacecraft Propulsion, 1970).

[160] Y. Brill, A. Eisner, and L. Osborn, *The Flight Application of a Pulsed Plasma Microthruster, The NOVA Satellite*, Vol. 20 (American Institute of Aeronautics and Astronautics, 1982).

[161] N. Alvarez and W. D. Williams, *BmP-220 Micro-Pulsed Plasma Thrusters* (Busek, 2016).

[162] R. Wirz, M. Gale, J. Mueller, and C. Marrese, *Miniature Ion Thrusters for Precision Formation Flying*, 40th ed. (AIAA/ASME/SAE/ASEE Joint Propulsion Conference, 2004).

[163] R. Wirz, *TPF-I Propulsion System for Formation Flying Interferometry* (Jet Propulsion Laboratory, 2005).

[164] M. Berger, M. Rath, and H. Ellerbrock, *RIT Propulsion Systems for All-Electric Telecommunication Satellites*, 33rd ed. (International Electric Propulsion Conference, The George Washington University, 2013).

[165] H. J. Leiter, R. Kukies, and R. Killinger, *RIT-22 Ion Propulsion System: 5,000h Endurance Test Results and Life Prediction*, 43rd ed. (AIAA Joint Propulsion Conference & Exhibit, 2007).

[166] S. W. Janson, *Chemical and Electric Micropropulsion Options for Nanosatellites*, 30th ed. (Joint Propulsion Conference, 1994).

[167] J. R. Brophy, J. E. Polk, J. Blandino, and J. Mueller, *Micromachined Ion Accelerators*, Vol. 20 (Technical Briefs, 1996).

[168] J. A. Dooley and P. R. Lawson, *Technology Plan for the Terrestial Planet Finder* (Jet Propulsion Laboratory, 2005).

[169] R. Wirz, J. Polk, C.Marrese, J. Mueller, J. Escobedo, and P. Sheehan, *Experimental and Computational Investigation of the Performance of a Micro-Ion Thruster*, 38th ed. (Joint Propulsion Conference, 2002).

[170] R. Wirz, D. Goebel, C. Marrese, and J. Mueller, *Development of Cathode Technologies for a Miniature Ion Thruster*, 39th ed. (Joint Propulsion Confere, 2003).

[171] R. Killinger, H. Grayt, R. Kukies, M. Surauer, G. Saccoccia, A. Tomasetto, and R. Dunster, *Artemis Orbit Raising In-Flight Experience with Ion Propulsion*, 38th ed. (AIAA/ASME/ASEE Joint Propulsion Conference and Exhibit, 2002).

[172] G. Saccoccia, *ESA Spacecraft Propulsion Activities*, 4th ed. (Proceedings of the International Spacecraft Propulsion Conference, 2004).

[173] P. Lozano and M. M. Sanchez, *Ionic liquid ion sources: characterization of externally wetted emitters*, Vol. 282 (Journal of Colloid and Interface Science, 2005).

[174] J. Mahoney, A. Yahiku, R. Moore, and J. Perel, *Electrohydrodynamic Ion Source*, Vol. 40 (Journal of Applied Physics, 1969).

[175] J. Perel, *Alkali Metal Ion Sources*, Vol. 115 (Journal of The Electrochemical Society, 1968).

[176] J. Perel, T. Bates, J. Mahoney, R. Moore, and A. Yahiku, *Research on Charged Particle Bipolar Thrustor*, Vol. 5 (American Institute of Aeronautics and Astronautics, 1967).

[177] M. N. Hubermann and S. G. Rosen, *Advanced High-Thrust Colloid Sources*, Vol. 11 (Journal of Spacecraft and Rockets, 1974).

[178] P. W. Kidd and K. H. Shelton, *Life Test (4350 Hours) of an Advanced Colloid Thruster Module*, 10th ed. (Electric Propulsion Conference, 1973).

[179] J. Perel, J. Mahoney, and C. Sujo, *Micro-Electric Propulsion Using Charged Clusters* (Air Force Research Laboratory, 1998).

[180] F. M. Pranayaja, *Progress on Colloid Micro-Thruster Research and Flight Testing*, 13th ed. (Annual AIAA/USU Conference on Small Satellites, 1999).

[181] J. Ziemer, T. Randolph, and G. Franklin, *Colloid Micro-Newton Thrusters for the Space Technology 7 Mission and Beyond* (Jet Propulsion Laboratory, 2016).

[182] V. Hruby, *ST7-DRS Colloid Thruster System Development and Performance Summary*, 44th ed. (AIAA/ASME/SAE/ASEE Joint Propulsion Conference, 2008).

[183] C. Scharlemann and M. Tajmar, *Development of Propulsion Means for Satellites*, 43rd ed. (AIAA/ASME/SAE/ASEE Joint Propulsion Conference, 2007).

[184] D. Bock, A. Kramer, P. Bangert, K. Schilling, and T. M, *NanoFEEP on UWE platform - Formation Flying of CubeSats using Miniaturized Field Emission Electric Propulsion Thrusters*, 34th ed. (International Electric Propulsion Conference, 2015).

[185] M. Tajmar, *Overview of Indium LMIS for the NASA-MSS Mission and its Suitability for an In-FEEP Thruster on LISA*, 32nd ed. (International Electric Propulsion Conference, 2011).

[186] J. Mitterauer, *Prospects of Liquid Metal Ion Thrusters for Electric Propulsion*, 22nd ed. (International Electric Propulsion Conference, 1991).

[187] G. Kornfeld, *Plasmabeschleuniger anordnung* (European Patent Office, 2006).

[188] T. Brandt, R. Groll, F. Jansen, and F. Hey, *Simulation of a down-scaled HEMP-Thruster*, 5th ed. (German-Russian Conference on Electric Propulsion and Their Application, 2014).

[189] A. Keller, P. Köhler, W. Gärtner, B. Lotz, D. Feili, P. Dold, M. Berger, C. Braxmaier, D. Weise, and U. Johann, *Feasibility of a down-scaled HEMP Thruster*, 32nd ed. (Internation Electric Propulsion Conference, 2011).

[190] A. Keller, P. E. Köhler, F. G. Hey, M. Berger, C. Braxmaier, D. Feili, D. Weise, and U. Johann, *Parametric Study of HEMP-Thruster Downscaling to μN Thrust Levels*, Vol. 43 (IEEE Transactions on Plasma Science, 2015).

[191] F. Marchandise, *EPS500 - An innovative and multi-application design* (Electric Propulsion Innovation & Competitiveness Workshop, 2014).

[192] C. Boniface and N. Arcis, *An overview of electric propulsion activities at CNES*, 30th ed. (International Symposium on Space Technology and Science, Japan, 2015).

[193] S. Zurbach, N. Cornu, and P. Lasgorceix, *Performance Evaluation of a 20 kW Hall Effect Thruster*, 32nd ed. (International Electric Propulsion Conference, Wiesbaden, 2011).

[194] J. Huddleson, *QinetiQ Electric Propulsion Technology & Capability* (Electric propulsion innovation & Competitiveness, 2014).

[195] P. Guggenbach, *Electric Propulsion Pointing Mechanisms* (RUAG Space, 2016).

[196] C. Soret, *Boeing selects Safran PPS5000 electric thruster for use on a commercial satellite* (Safran, 2017).

[197] J. J. Delgado, J. A. Baldwin, and R. L. Corey, *Space Systems Loral Electric Propulsion Subsystem: 10 Years of On-Orbit Operation*, 30th ed. (International Symposium on Space Technology and Science, Japan, 2015).

[198] V. Murashko, , A. Koryakin, and A. Nyatin, *State of the Art and Prospects of Electric Propulsion in Russia*, 28th ed. (International Electric Propulsion Conference, 2003).

[199] J. J. Delgado, R. L. Corey, and V. Murashko, *Qualification of the SPT-140 for use on Western Spacecraft*, 50th ed. (AIAA Joint Propulsion Conference, 2014).

[200] D. Manzella, C. Sarmiento, and J. Sankovic, *Performance Evaluation of the SPT-140*, 25th ed. (International Electric Propulsion Conference, 1997).

[201] O. Olshanskaya and A. U. Usanov, *Analysis of the SPT-140 thruster mechanical strength*, 6th ed. (Russian-German Conference on Electric Propulsion and Their Application, 2017).

[202] J. Fisher, A. Wilson, D. King, S. Meyer, and K. de Grys, *The Development and Qualification of a 4.5 kW Hall Thruster Propulsion System for GEO Satellite Applications - Status Update*, 28th ed. (International Electric Propulsion Conference, 2003).

[203] O. Olshanskayaa and A. U. Usanovb, *Alex Mathers and Kristi de Grys and J. Paisley*, 31st ed. (International Electric Propulsion Conference, University of Michigan, 2009).

[204] B. Welander, J. Monheiser, N. Meckel, K. de Grys, and P. Peterson, *Demonstration of the XR-12 Hall Current Thruster*, 33rd ed. (International Electric Propulsion Conference, The George Washington University, 2013).

[205] T. A. Corcoran, E. Drake, and J. R. Henderson, *Dual Mode BPT-4000 Hall Thruster* (Aerojet Rocketdyne, 2003).

[206] W. G. Lichtenstein, J. H. Perry, and M. Turchin, *Leading the Way to Electric Propulsion in Belfast* (Aerojet Rocketdyne, 2014).

[207] C. E. Garner, J. R. Brophy, J. E. Polk, and L. C. Pless, *Cyclic Endurance Test of a SPT-100 Stationary Plasma Thruster*, 30th ed. (AIAA/SAE/ASME/ASEE Joint Propulsion Conference and Exhibit, 1994).

[208] J. M. Sankovic, J. A. Hamley, and T. W. Haag, *Performance evaluation of the Russian SPT-100 thruster at NASA LeRC*, 23rd ed. (International Electric Propulsion Conference, 1993).

[209] S. Cesare and G. Sechi, *Next Generation Gravity Mission*, Vol. 31 (Distributed Space Mission for Earth System Monitoring, 2013).

[210] H. Leiter, D. Block, B. Lotz, D. Feili, and C. Edwards, *Qualification of the miniaturized Ion Thruster RIT μX - Perspectives, Program, Results and Outlook*, 32nd ed. (International Electric Propulsion Conference, 2011).

[211] T. Randolph, V. Kim, H. Kaufman, K. Kozubsky, V. Zhurin, and M. Day, *Facility Effects in Stationary Plasma Thruster Testing*, 23rd ed. (International Electric Propulsion Conference, 1993).

[212] A. Sengupta, J. A. Anderson, C. Garner, J. R. Brophy, K. L. deGroh, B. A. Banks, and T. A. K. Thomas, *Deep Space 1 Flight Spare Ion Thruster 30,000 hours Life Test*, Vol. 25 (The Journal of Propulsion and Power, 2009).

[213] R. Nadalini, Private conversation, Sonaca Space GmbH (May 2017).

[214] J. R. Bertucci and G. R. Beecher, *Introduction to Bayard-Alpert Ionization Gauges* (Granville-Phillips Helix Technology Corporation, 2009).

[215] F. G. Hey, *Development, Integration and Test of a Micro Newton Thrust Balance* (Technische Universität Dresden, 2012).

[216] J. W. Dankanich, M. W. Swiatek, and J. T. Yim, *A Step Towrards Electric Propulsion Testing Standards: Pressure Measurement and Effective Pumping Speeds*, Vol. 50 (American Institute of Aeronautics and Astronautics, 2012).

[217] R. Blott, S. Gabriel, and D. Robinson, *Draft Handbook for Electric Propulsion (EP) Verification by Test* (ESA/ESTEC, 2012).

[218] F. G. Hey, A. Keller, U. Johann, C. Braxmaier, M. Tajmar, E. Fitzsimons, and D. Weise, *Development of a Micro Thruster Test Facility which fulfils the LISA requirements*, 610th ed. (Journal of Physics: Conference Series, 2015).

[219] F. G. Hey, C. Altmann, U. Johann, C. Braxmaier, M. Tajmar, E. Fitzsimons, and D. Weise, *Development of a Highly Sensitive Micro-Newton Thrust Balance: current status and latest results*, 34th ed. (International Electric Propulsion Conference, 2015).

[220] F. G. Hey, M. Vaupel, and C. Braxmaier, *Development of a Highly Sensitive, Highly Stable Micro-Newton Thrust Balance*, 35th ed. (International Electric Propulsion Conference, 2017).

[221] W. Lahmadi, *VSS Stepper Motor - For Applications up to Ultra-high-vacuum* (Phytron, Inc., 2017).

[222] H. P. Harmann, *Untersuchung und Modellierung der Ionenstrahl formung grossflaechiger Ionenquellen mit Hilfe einer beweglichen Faradaysondenzeile* (University of Giessen, 2003).

[223] W. Gaertner, *Design, Konstruction und Test eines praezisen Gegenfeldanalysators zur energetischen Strahlvermessung eines µN RIT Triebwerkes* (University of Giessen, 2010).

[224] P. E. Koehler and B. K. Meyer, *Beam Diagnostics for Mini Ion Engines*, 33rd ed. (International Electric Propulsion Conference, 2013).

[225] C. Böhm and J. Perrin, *Retarding-field analyzer for measurements of ion energy distributions and secondary electron emission coefficients in low-pressure radio frequency discharges*, Vol. 64 (Review of Scientific Instruments, 1993).

[226] M. Schramm, *Development of Thruster Plume Diagnostic Tools for Micro High Efficiency Multistage Plasma Thruster Characterization* (University of Stuttgart, 2014).

[227] F. G. Hey, M. Vaupel, and C. Groll, *Development of a Gridless Retarding Potential Analyser*, 35th ed. (International Electric Propulsion Conference, 2017).

[228] F. G. Hey, *Private conversation* (Airbus DS GmbH, November 2017).

A

TECHNICAL DRAWINGS

This appendix contains the technical drawings of the components that are used in order to test the cathodes. First, the technical drawing of the graphite heater is given in Appendix A.1. Next, the boron nitride spacer is described in Appendix A.2. Subsequently, Appendices A.3 and A.4 describe the top and bottom macor insulator disc respectively. Furthermore, the LaB_6 insert is illustrated in Appendix A.5. Finally, an overview of the cathode assembly can be seen in Appendix A.6.

A.1. GRAPHITE HEATER

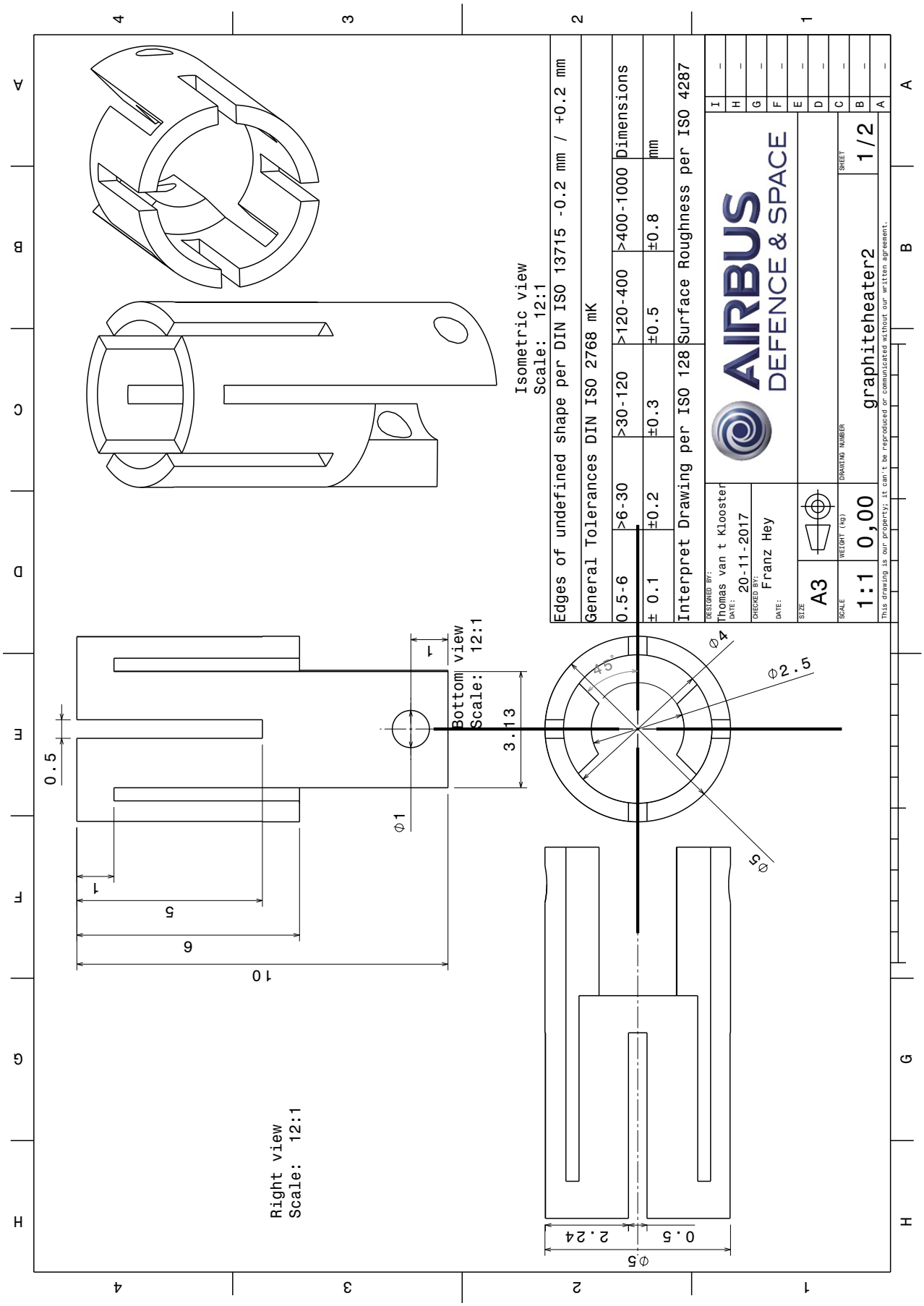

A.2. BORON NITRIDE SPACER

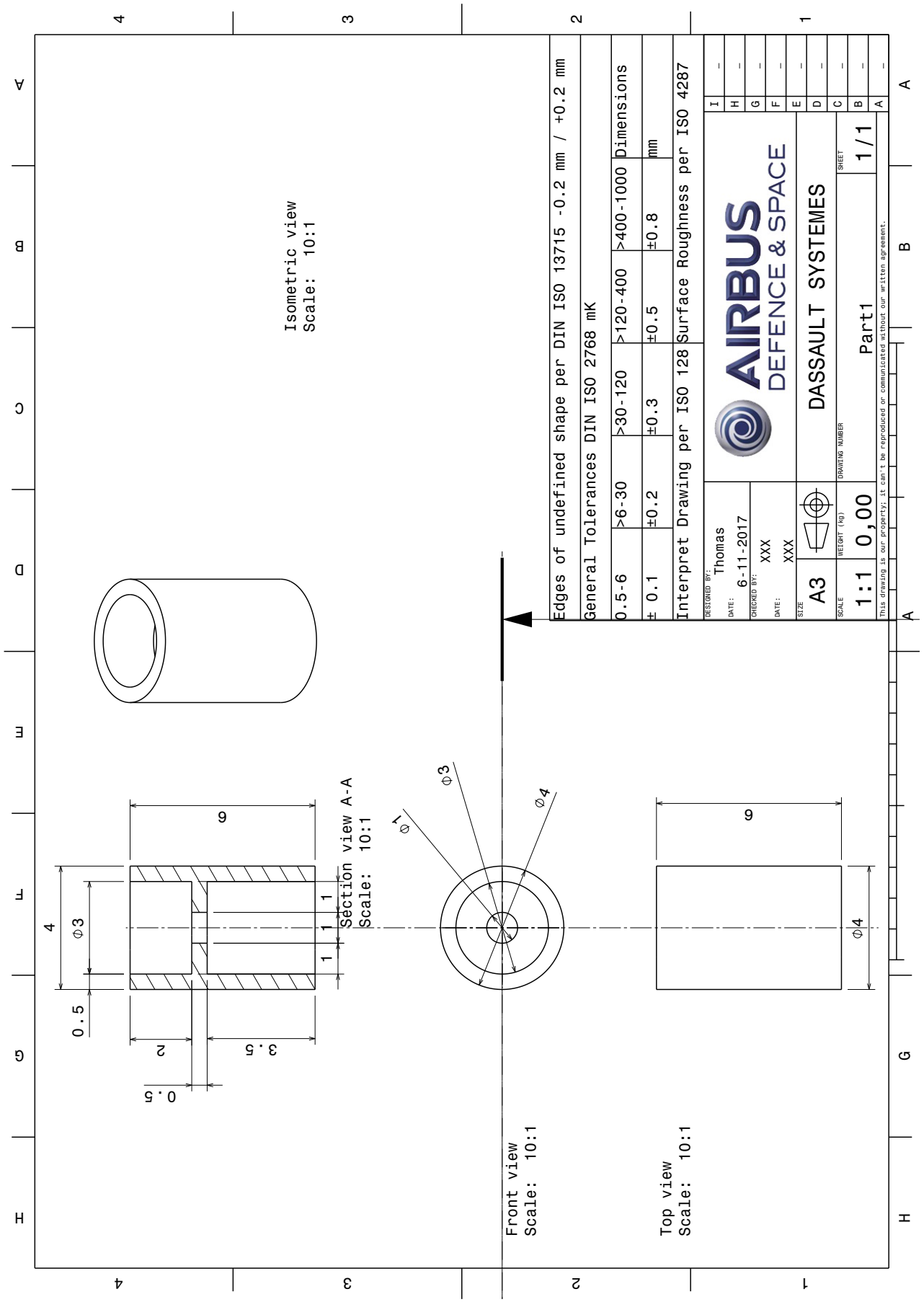

A.3. MACOR TOP INSULATOR DISC

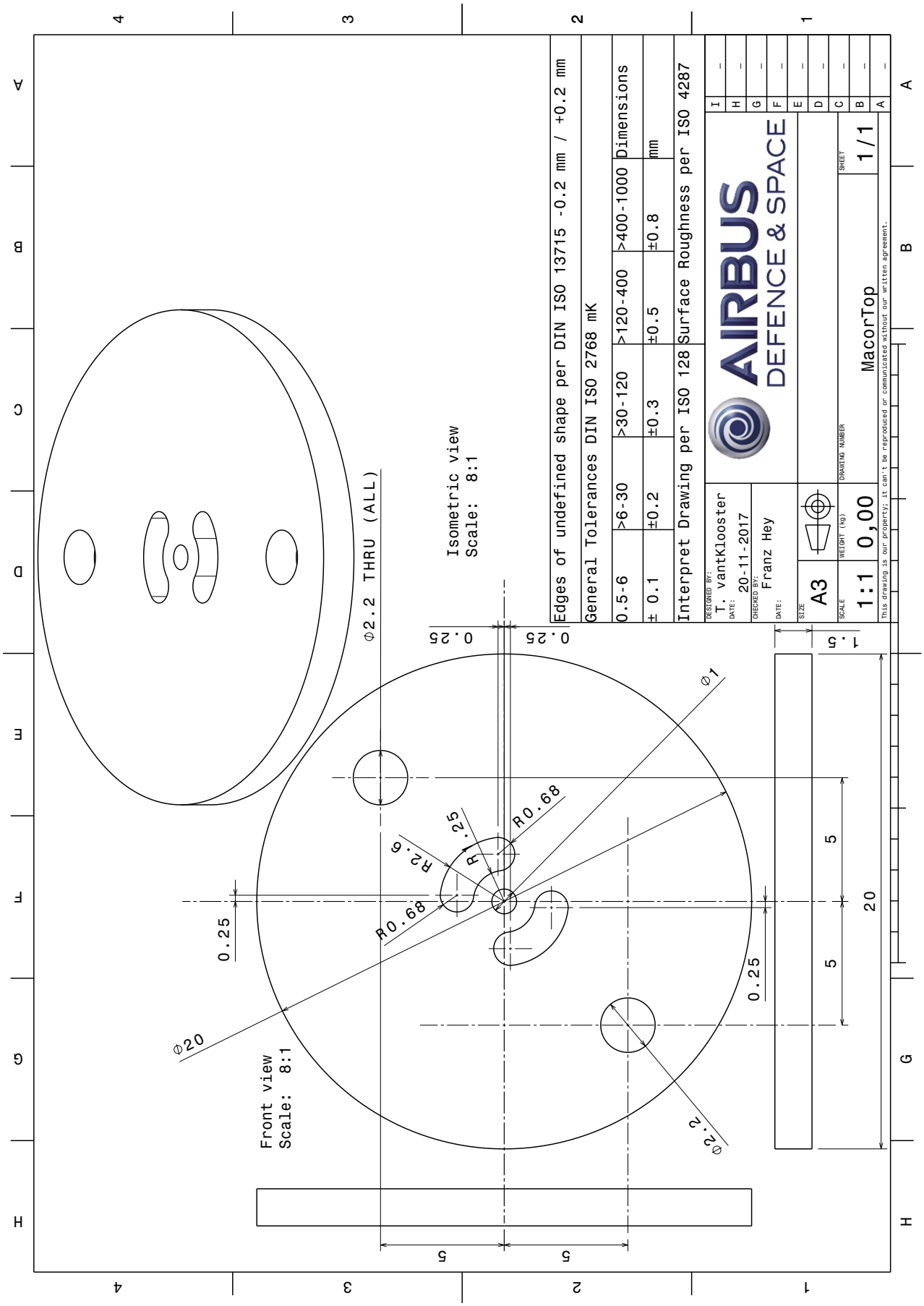

A.4. MACOR BOTTOM INSULATOR DISC

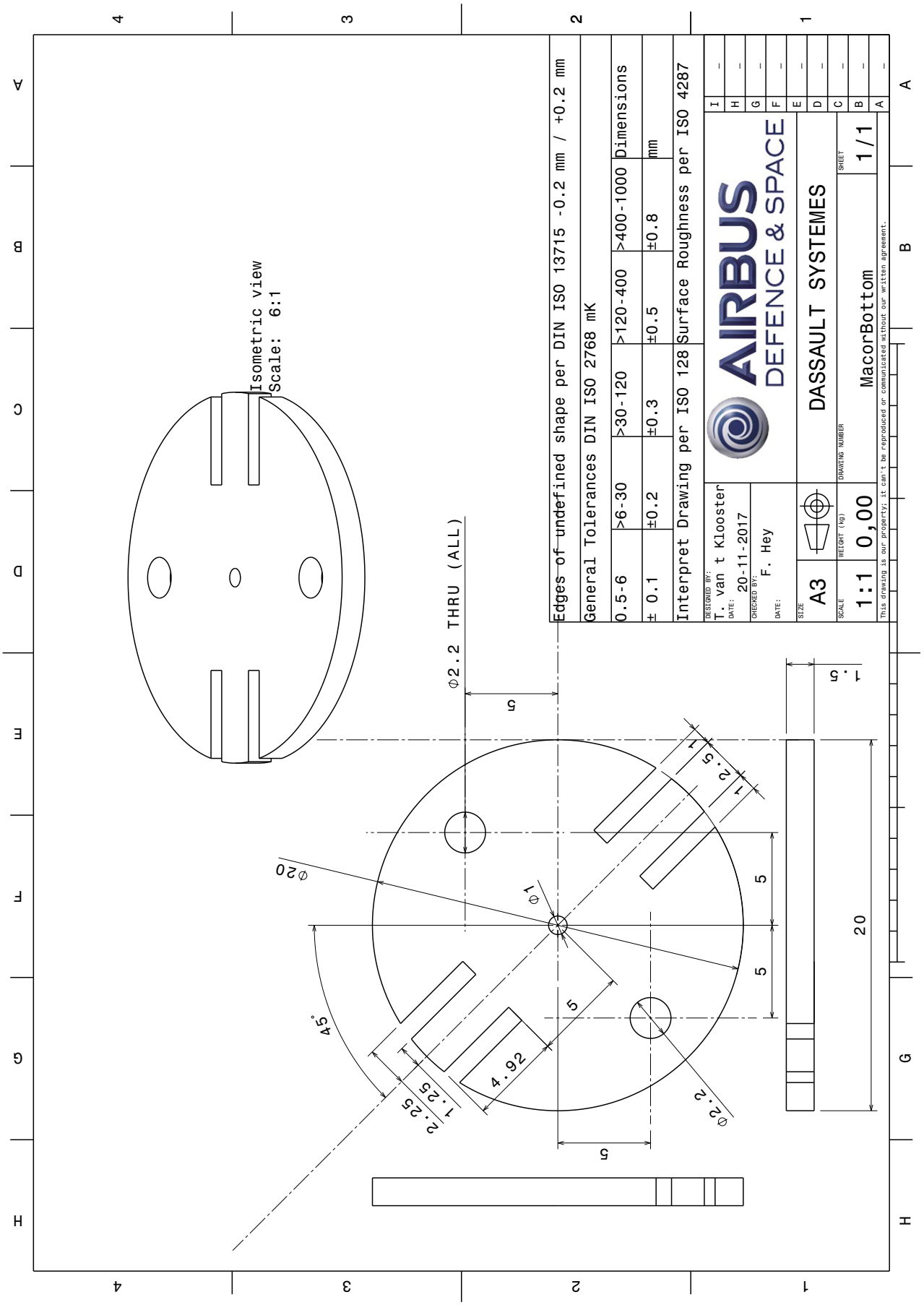

A.5. LaB_6 INSERT

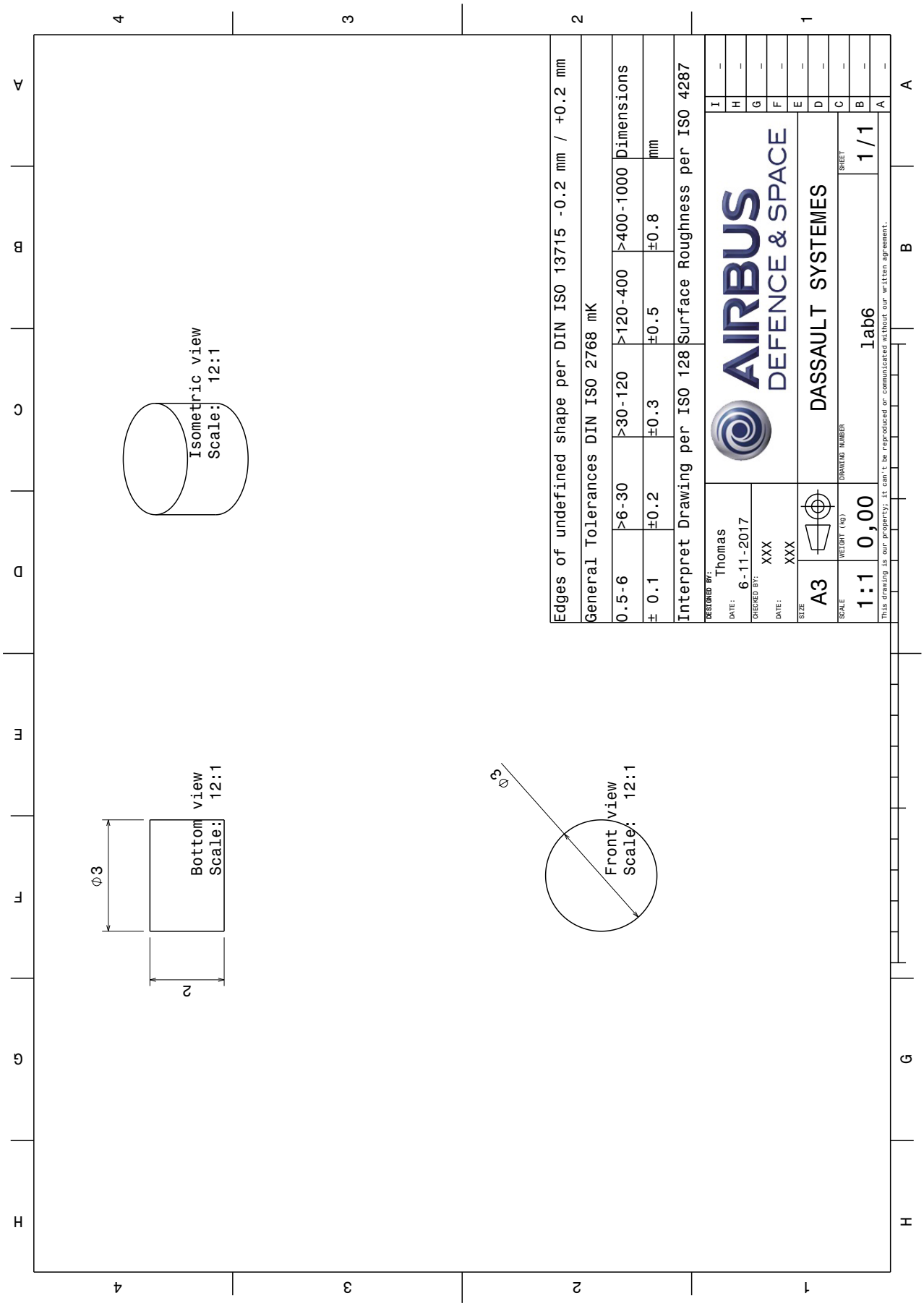

A.6. CATHODE ASSEMBLY

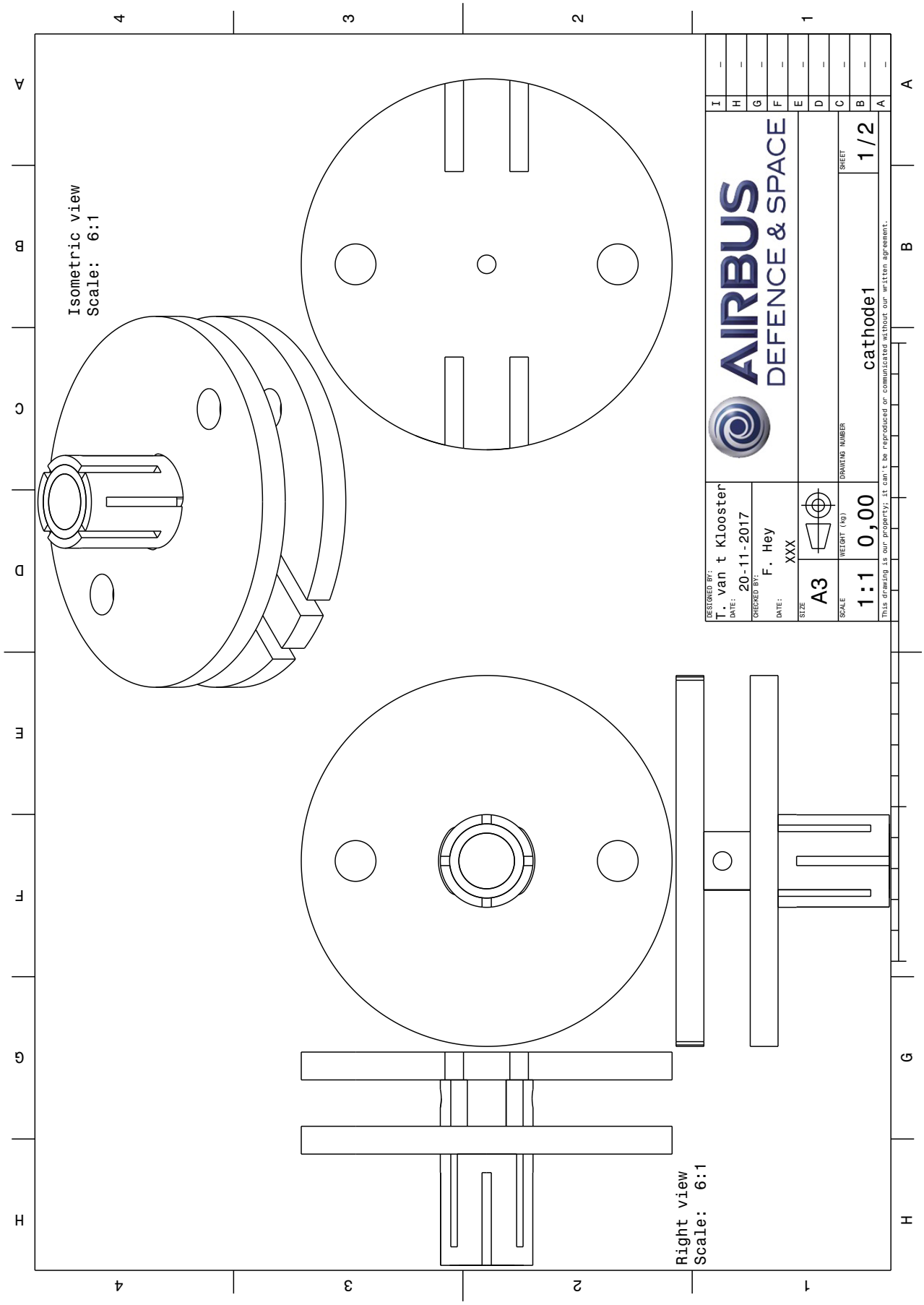

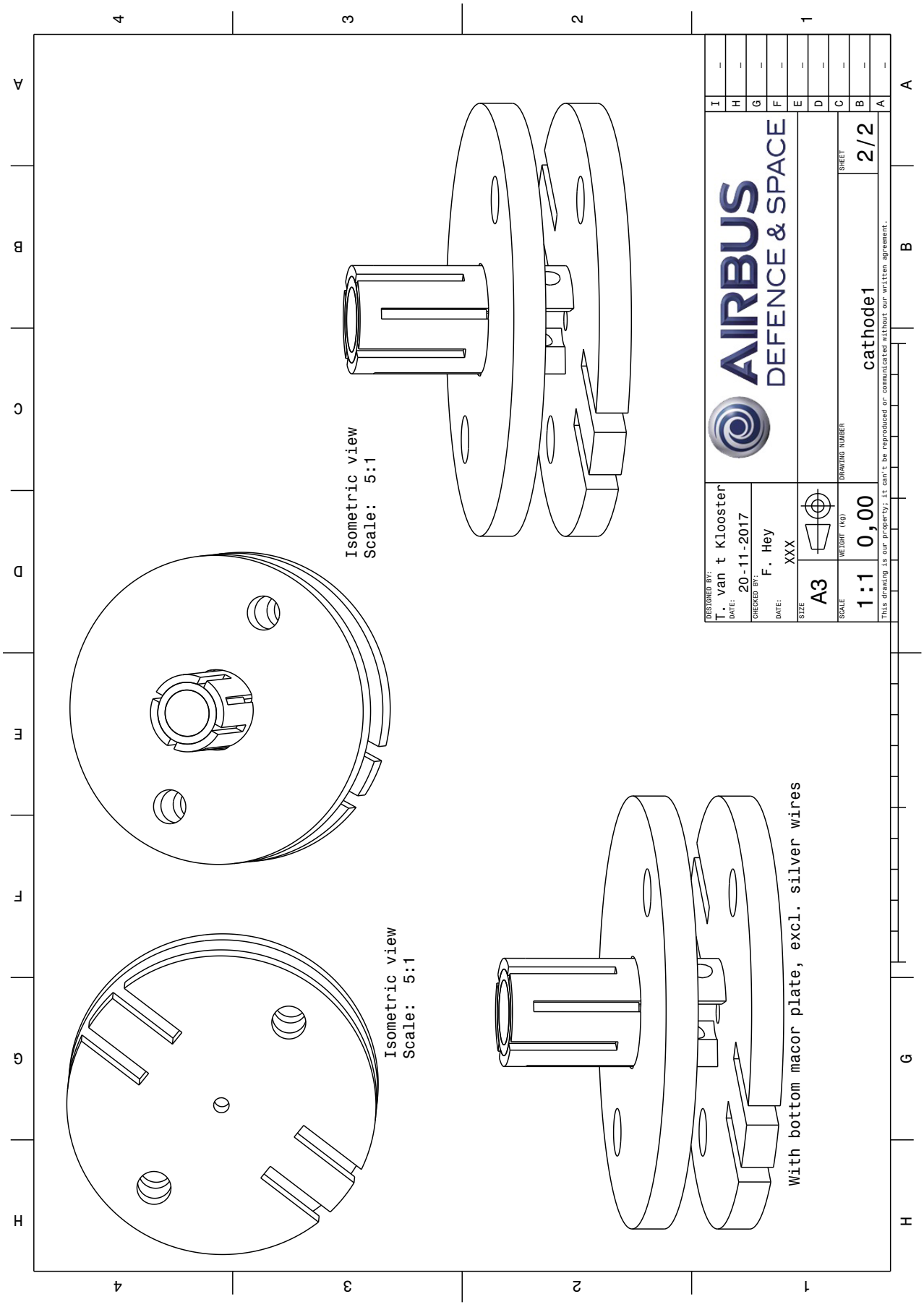
Isometric view
Scale: 5:1
Isometric view
Scale: 5:1
With bottom macor plate, excl. silver wires
AIRBUS
DEFENCE & SPACE
DESIGNED BY: T. van t Klooster
DATE: 20-11-2017
CHECKED BY: F. Hey
DATE: XXX
SIZE A3
SCALE 1:1
WEIGHT (kg) 0,00
DRAWING NUMBER cathode1
SHEET 2/2
This drawing is our property; it can't be reproduced or communicated without our written agreement.